A European Project Supported by the European Commission
within the Sixth Framework Programme for RTD

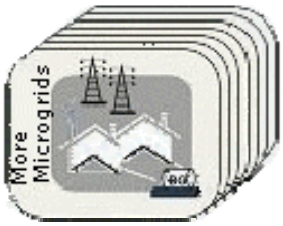

Advanced Architectures and Control Concepts for More Microgrids

Contract No: SES6-019864

WORK PACKAGE G

DG3. Report on the technical, social, economic, and environmental benefits provided by Microgrids on power system operation

Annex 1 - Stochastic Modeling of RES, CHP, and Electricity Markets

November 30th 2009

Final Version
PUBLIC

Coordination:	C. Schwaegerl	christine.schwaegerl@siemens.com
Authors:	L. Tao	liang.tao@siemens.com
	C. Schwaegerl	christine.schwaegerl@siemens.com

Executive summary

Microgrids normally consist of a considerable proportion distributed energy resources (DER) based on renewable energy sources (RES). These renewable units are generally not controllable or dispatchable, which means their energy outcome depends heavily on instantaneous weather conditions and thus can be largely seen as intermittent in nature. This renders deterministic evaluation approaches virtually ineffective in terms of revealing actual system running conditions. Consequently, stochastic modelling of intermittent DER units is necessary for successful analysis of Microgrid systems.

Depending on the complexity of a Microgrid system and requirement on calculation accuracy, two approaches can be adopted for stochastic modelling of intermittent DER units—the analytical approach and the simulation (Monte Carlo) approach. In scope of this report, all modelling efforts are based on the simulation approach due to its capability of retaining temporal features of real-time running data. Modelling is carried out on an annual basis with a time step of one hour, and inter-year difference is discarded so as to predict future DER production from historical data.

Stochastic modelling is performed on a type-to-type basis with different approaches for different DER types — load and CHP units are modelled by the transposition of a deterministic trend curve and a truncated normal disturbance variable; wind turbines are modelled via a basic Markov chain model with slight seasonal considerations; and photovoltaic units are modelled on both annual and daily scales using a combination of Markov chain, statistical decoupling, and Beta distribution variables. All modelling approaches can be described as a two-step procedure: firstly the characteristic parameters are obtained for a given set of historical data, then a simulated production curve can be obtained with the parameters and a certain stochastic model.

Content

Abbreviations

AAT	Approximated Annual Trend Curve
AcP	Accumulated Active Power
AcQ	Accumulated Reactive Power
AOP	Annual Overloading Probability
AR	Autoregressive Method
ARMA	Autoregressive Moving-Average Method
AUoS	Avoided Use of System Charge
AVC	Automatic Voltage Control
BS	Branched Section
C&I	Commercial and Industrial
CDF	Cumulative Distribution Function
CHP	Combined Heat and Power
CNV	Constant Node Voltage
DER	Distributed Energy Resources
DEV	Decoupled Equivalent Variables
DG	Distributed Generation
DSM	Demand Side Management
DSO	Distribution System Operator
EEX	European Energy Exchange AG
EHV	Extra High Voltage
EMP	Equivalent Meshing Power
ETS	Emission Trading System
FA	First After Branch
FACTS	Flexible Alternating -Current Transmission System
FIT	Feed-in Tariff
FLH	Full Load Hours
G/L	Generation / Load
GHG	Green House Gas
HDR	Hard-Dry-Rock
HV	High Voltage
ICV	Instantaneous Coefficient of Variation
IPM	Iterative Power Modification
IPP	Independent Power Producer
IPVM	Iterative Power and Voltage Modification
IVM	Iterative Voltage Modification
LB	Last Before Branch
LD	Loss Reduction Credit (Loss Difference)
LF	Load Flow
LFEA	Load Flow Estimation Algorithm
LNL	Line-Node-Load Element
LR	Loss Ratio
LTSN	Left-Truncated Standard Normal Distribution
LV	Low Voltage
MA	Moving-Average Method
MS	Main Section
MV	Medium Voltage
NPV	Net Present Value
O&M	Operation and Maintenance
ORG	Original Curve
PBTVE	Power-Based Transformer Voltage Estimation
PD	Peak Reduction Credit (Peak Difference)

PDF	Probability Distribution Function
PLF	Probabilistic Load Flow
PR	Peak Ratio
PV	Photovoltaic
RCV	Relative Coefficient of Variation
RDA	Daily Average Value
RES	Renewable Energy Sources
RHV	Relative Hourly Value
RTSN	Right-Truncated Standard Normal Distribution
SCL	Scale Factor
SER	Simulated Error Curve
SHP	Small Hydro Plant
SIM	Simulated Curve
SMO	Smoothed-Out Annual Curve
SPE	Starting Power Estimation
SVE	Starting Voltage Estimation
T&D	Transmission and Distribution
TGC	Tradable Green Certificates
TLTN	Translated Left-Truncated Normal Distribution
TSN	Truncated Standard Normal Distribution
TSO	Transmission System Operator
USC	Use of System and Connection Charges
VNV	Varying Node Voltage
VPP	Virtual Power Plant
WT	Wind Turbine

Chapter 1 Stochastic Modeling and Simulation

1.1 Introduction

In order to assess the performance and reliability of Microgrids, it is generally agreed that traditional deterministic network calculation methods can not yield results accurate enough to reflect real-time running conditions. This is partly caused by the intermittent nature of DG (dispersed generation) / DER (distributed energy resources) units—especially with technologies based on RES (renewable energy sources) such as solar or wind. Further explanations concerning this issue can be found in Annex A of this report.

With accumulated field measurements from local utilities, however, it is possible to build stochastic models that summarize the general statistical features of a DG / DER unit's generation profile. Since simulation of a Microgird generally aims to evaluate system performance over a certain period in future, stochastic modelling makes it possible to predict potential DER behavior with maximum accuracy in spite of the limited availability of historical data. The soundness of network calculations can thus be improved by introducing simulated generation and load curves based on acquired models and parameters.

This chapter is focused on the development of stochastic models and simulation algorithms respectively for normal loads, wind turbines, and PV units; in the end statistical analysis are performed separately to check the validity of simulation results.

Seven probability distribution functions are generally used as the basis of most statistical analysis carried out in this section, namely they are:

1. *Uniform Distribution—for formulation of Markov chain approach (used for modelling of wind turbines and annual PV generation)*

2. *Normal Distribution—for simulation of load / CHP curves*

3. *Truncated Normal Distribution, with variants in forms of:*
   --for simulation of load / CHP curves
   3.1 TSN: Truncated Standard Normal Distribution
   3.2 LTSN: Left-Truncated Standard Normal Distribution
   3.3 RTSN: Right-Truncated Standard Normal Distribution
   3.4 TLTN: Translated Left-Truncated Normal Distribution

4. *Weibull Distribution—for simulation of wind turbines*

5. *Gamma Distribution—for simulation of daily PV generation*

6. *Beta Distribution—for simulation of daily PV generation*

The mathematical descriptions and generation algorithms for these seven types of distribution functions are briefly given and explained in Annex B.

1.2 Evaluation of Analytical Calculation Approach

The evaluation of Microgrid performance under DER penetration will be primarily complicated by the stochastic information in DER generation profiles — to be specific, simultaneous consideration of time-varying load demand and DER output at every node of a network could lead to high requirements on modeling and calculation. In order to perform statistical analysis for such a multitude of time-series data, two general approaches can be adopted: the analytical approach and the simulation approach.

The primary difference between analytical and simulation approaches lies in the way of integrating stochastic information into traditionally deterministic network calculation processes — the analytical approach relies on mathematical models extracted from time-series data to perform probabilistic load flow [16]; while the simulation approach applies Monte Carlo method [17][18] to observe system behavior with a large state space of random variables. In this report, the simulation approach is adopted over the analytical approach in spite of its high computation requirements, and the reason of this choice is explained in this section. In Table 1-1, a brief summary is given for load and DER time-series data used for further calculation efforts.

Serial	Type	Name	Average	Standard Deviation
L1	Load	Household	0,5350	0,2072
L2	Load	Business	0,4823	0,2399
L3	Load	Commercial	0,2393	0,2816
L4	Load	Industrial	0,7365	0,1366
L5	Load	Agricultural	0,4728	0,1934
G6	DER	CHP	-0,5008	0,1559
G7	DER	Wind Turbine	-0,2203	0,2409
G8	DER	Photovoltaic	-0,1461	0,2268

Table 1-1 Summary of Original Time-Series Data for Load and DER Units

In Table 1-1, all 8 categories of time-series data are collected as annual hourly (8760 points per set) per-unit power values (positive for load, negative for DER units) from historical data of some Germany utilities. Statistical description of data is given in terms of average and standard deviation, which is summarized from p.u. (per unit) curves as shown in Figure 1-1.

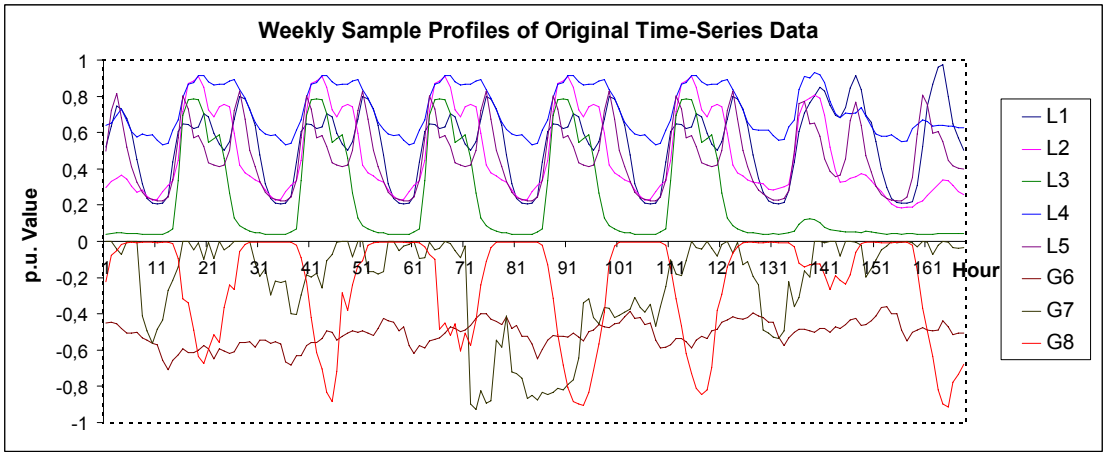

Figure 1-1 Sample Weekly Profiles for Load and DER Data

The p.u. values in Table 1-1 and Figure 1-1 are calculated as the ratio of instantaneous active power consumption or generation over rated power of a load or DER unit. This uniform data format is adopted to extract temporal power flow features from specific network configurations, which makes it possible to evaluate general applicability of different calculation approaches.

Although the influence of DER integration into distribution networks can be found in many aspects, this report will be primarily focused on steady state studies of DER penetration. Consequently, statistical calculations (analytical or simulation) in this section will address the problem of load flow as an example (similar studies can also be performed on other topics such as system reliability).

1.2.1 Transformation of Interdependent Time-Series Data

Probabilistic load flow method was originally developed as an analytical approach for dealing with measurement errors, forecast inaccuracies, unknown variables and outage uncertainties [18] of customer loads; but recently increased DER applications require an adaption of this approach to accommodate more complicated stochastic data from both controllable and uncontrollable (such as wind turbines) distributed generation units [19].

Generally, normal distribution models are adopted for performing probabilistic load flow [16], since load uncertainties and variations can be well represented by variants of normal distribution — however, other probability distribution functions (such as Weibull distribution used for wind turbines) could also be applied to suit specific needs. In following discussions, normal distribution is assumed for describing system data, which can be viewed under a multivariate framework as shown in *Equation 1-1*:

$$\textit{Assume}: \quad \textit{With a Gaussian random vector } \vec{x} = \left[x_1, x_2, \cdots, x_N\right]^T,$$

$$\textit{Its mean vector can be written as } \vec{\mu} = \left[\mu_1, \mu_2, \cdots, \mu_N\right]^T,$$

$$\textit{And a covariance matrix can be defined as } \Sigma = \begin{bmatrix} c_{11} & c_{12} & \cdots & c_{1N} \\ c_{21} & c_{22} & \cdots & c_{2N} \\ \vdots & \vdots & \ddots & \vdots \\ c_{N1} & c_{N2} & \cdots & c_{NN} \end{bmatrix},$$

$$\textit{Then}: \quad \textit{The probability distribution function of } \vec{x} \textit{ can be written as}:$$

$$f_x(\vec{x}) = \frac{1}{(2\pi)^{N/2}|\Sigma|^{1/2}} \cdot \exp\left\{ -\frac{1}{2}\left[\vec{x} - \vec{\mu}\right]^T \Sigma^{-1}\left[\vec{x} - \vec{\mu}\right] \right\}$$

$$\textit{Specially}: \textit{When } N = 2, \textit{the bivariate pdf with } \mu_x = 0 \textit{ and } \mu_y = 0 \textit{ is}:$$

$$f_{xy}(x, y) = \frac{1}{2\pi\sigma_x\sigma_y\sqrt{1-\rho^2}} \cdot \exp\left\{ -\frac{1}{2(1-\rho^2)}\left[\frac{x^2}{{\sigma_x}^2} + \frac{y^2}{{\sigma_y}^2} - \frac{2\rho xy}{\sigma_x\sigma_y} \right] \right\}$$

$$\rho \textit{ as correlation between } x \textit{ and } y: \quad \rho = \frac{\sigma_{xy}}{\sigma_x\,\sigma_y} = \frac{c_{xy}}{\sqrt{c_{xx}\,c_{yy}}}$$

Equation 1-1

It can be seen from *Equation 1-1* that the size of collective state space for stochastic data will largely determine the complexity of mathematical modeling and calculation. However, it should be noted that the random variables considered in *Equation 1-1* are not restricted to time-series data described in this section, as uncertainties in device outage [20] and network operation [17] [21] can also be modeled in similar fashions. Considering the fact that outage of a network or DER device can be viewed as largely independent from the development of energy flow in the time frame, both aspects can be modeled by a multiplied probability equation as given in [22].

Due to the focus of this report on DER intermittency, outages in generation and transmission devices are neglected to simplify calculations; thus the 8-th order load / DER profiles described in Table 1-1 can be easily modeled by a multivariate normal distribution with a state space of corresponding size if the examined time-series data are normally distributed independent variables [16]. However, such a convenient assumption cannot be directly obtained since the examined load / DER profiles are interrelated by multiple complex factors such as weather, time, human activities etc., which can be seen from the correlation between coefficients between each pair of time-series data as shown in Figure 1-2.

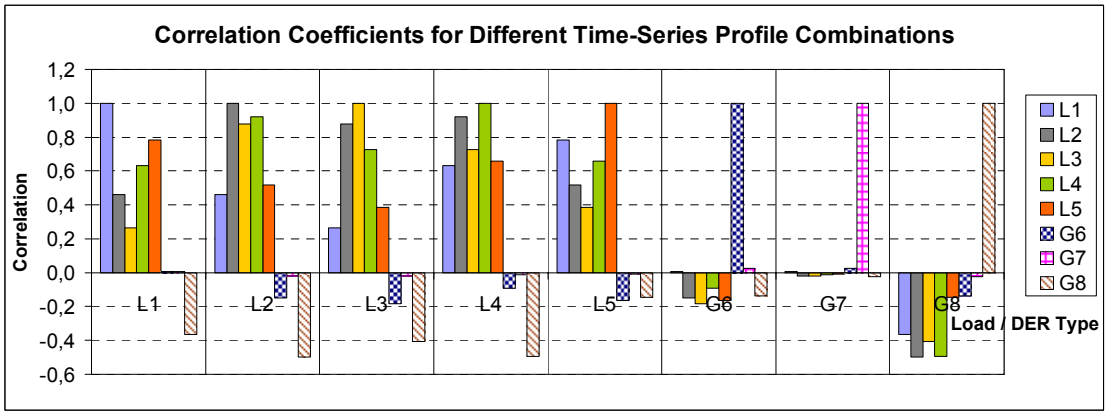

Figure 1-2 Correlation Coefficients for Different Time-Series Profile Combinations

Obviously, it can be seen from Figure 1-2 that almost all load profiles are closely correlated while DER data exhibit differing behaviors from type to type — the profile of wind turbine has very small correlations with all other time-series data, while CHP generation data shows a comparatively larger degree of correlation with loads or PV units and the PV profile is closely interlinked with most load types. Thus it is very likely that a system with a single load type and wind turbine installations can be modeled with two sets of approximately independent time-series data. However, since more complicated scenarios are common in real life, handling of dependent time-series data is necessary on many occasions.

In [21], it is suggested that linearly dependent data can be easily integrated into a probabilistic load flow algorithm when load flow equations are linearized as well. This discovery is further extended to second-order dependence in [22] and [23], both of which have proved the feasibility to calculate probabilistic load flow with time-series data sets whose dependence can be fully described by their 2nd order moments or cumulants. The conclusions of [22] and [23] are achieved by transforming dependent data into uncorrelated vectors through matrix multiplication. In [22], Gram-Schmidt orthogonalization is proposed as the method of transformation, while [23] adopts a relatively simple approach of Cholesky factorization. In this section, Cholesky factorization is used to decouple dependent vectors as shown in *Equation 1-2*.

$$\textit{Assume}: \quad \vec{x} = [\, x_1, x_2, \cdots, x_N \,]^T \ \textit{as a set of dependent vectors},$$
$$\vec{\mu} = [\, \mu_1, \mu_2, \cdots, \mu_N \,]^T \ \textit{as the mean vector of } \vec{x} \textit{ with } \mu_i = E(x_i), 1 \le i \le N$$
$$\textit{And the covariance matrix of } \vec{x} \textit{ is } \Sigma_x = \begin{bmatrix} c_{11} & c_{12} & \cdots & c_{1N} \\ c_{21} & c_{22} & \cdots & c_{2N} \\ \vdots & \vdots & \ddots & \vdots \\ c_{N1} & c_{N2} & \cdots & c_{NN} \end{bmatrix},$$

$$\textit{Then}: \quad \textit{By applying Cholesky factorization to } \Sigma, \textit{ a transition matrix } A \textit{ exists, s.t.}$$
$$\Sigma_x = A \cdot A^T, \quad A \textit{ is a lower triangular matrix, thus}:$$

$$\textit{Let } A = \begin{bmatrix} a_{11} & 0 & \cdots & 0 \\ a_{21} & a_{22} & \cdots & 0 \\ \vdots & \vdots & \ddots & \vdots \\ a_{N1} & a_{N2} & \cdots & a_{NN} \end{bmatrix}, \quad \Rightarrow \begin{cases} a_{ii} = \sqrt{c_{ii} - \sum_{k=1}^{i-1} a_{ik}^{\,2}} \\ a_{ji} = \begin{cases} 0, & \textit{if } i > j \\ \left(c_{ji} - \sum_{k=1}^{i-1} a_{jk} a_{ik} \right) / a_{ii}, & \textit{if } i < j \end{cases} \end{cases}$$

$$\textit{A set of uncorrelated vectors } \vec{y} = [\, y_1, y_2, \cdots, y_N \,]^T \textit{ can be obtained as}:$$
$$\vec{y} = A^{-1} \cdot \left(\vec{x} - \vec{\mu} \right), \quad \textit{such that } \Sigma_y = I_N \ (\textit{unit matrix})$$

$$\textit{Specifically, when } N = 2, \quad A = \begin{bmatrix} \sqrt{c_{11}} & 0 \\ c_{12} / \sqrt{c_{11}} & \sqrt{c_{11} c_{22} - c_{12}^{\,2}} / \sqrt{c_{11}} \end{bmatrix}$$

Equation 1-2

Through the transformation procedure shown in *Equation 1-2*, a linear relationship can be established between original interdependent time-series vectors and a set of uncorrelated (zero covariance) data. However, it should be noted that uncorrelated variables in probabilistic sense are not necessarily independent, while the algorithms suggested by [22] and [23] are based upon the assumption that transformed vectors are both uncorrelated and independent. In order to check the applicability of this assumption on the time-series data used in this report, a CDF (cumulative distribution function) comparison approach [25] in 2-dimensional state space is adopted — i.e., if vector *x* with CDF $f_x(x)$ and *y* with CDF $f_y(y)$ are independent, then their bivariate CDF $f_{xy}(x,y)$ should be equal to the product of their individual CDF expressions $f_x(x)^* f_y(y)$. This can be easily done for any pair of time-series data — for example, CDF plots for transformed vectors of L1 (TL1) and L3 (TL3) in both cases are shown in Figure 1-3.

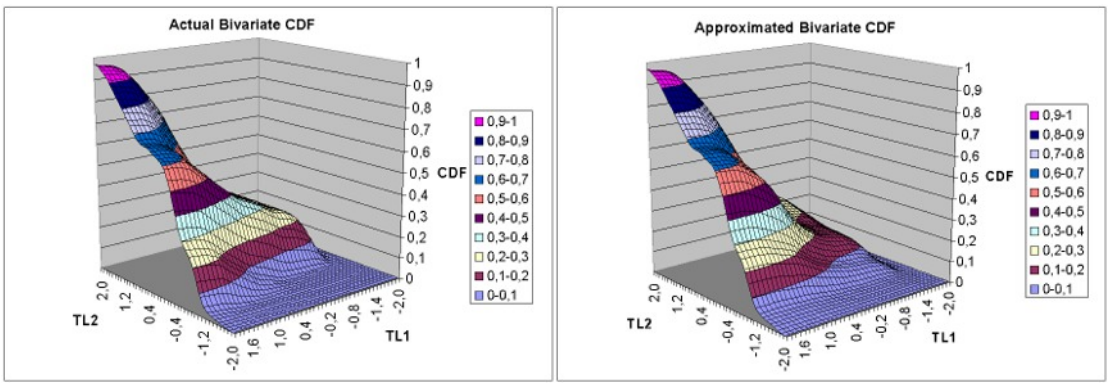

Figure 1-3 Actual and Approximated (Product) Bivariate CDF between TL1 and TL3

Obvious shape differences can be observed from actual (bivariate) and approximated (product of univariate values) CDF curves given in Figure 1-3, which indicates that the studied profiles are not strictly independent. The error caused by the assumption of mutual independence can thus be quantified by the difference between actual and approximated CDF curves.

In order to provide a more general result of comparison, six bivariate scenarios are studied including the TL1&TL2 case already shown in Figure 1-3:

(1) household and business loads (TL1&TL2),
(2) commercial and industrial loads (TL3&TL4),
(3) household load and PV unit (TL1&TG8),
(4) commercial load and wind turbine unit (TL3&TG7),
(5) agricultural load and CHP unit (TL5&TG6),
(6) CHP and PV units (TG6&TG8).

Their CDF error curves in bivariate state space are listed in Figure 1-4.

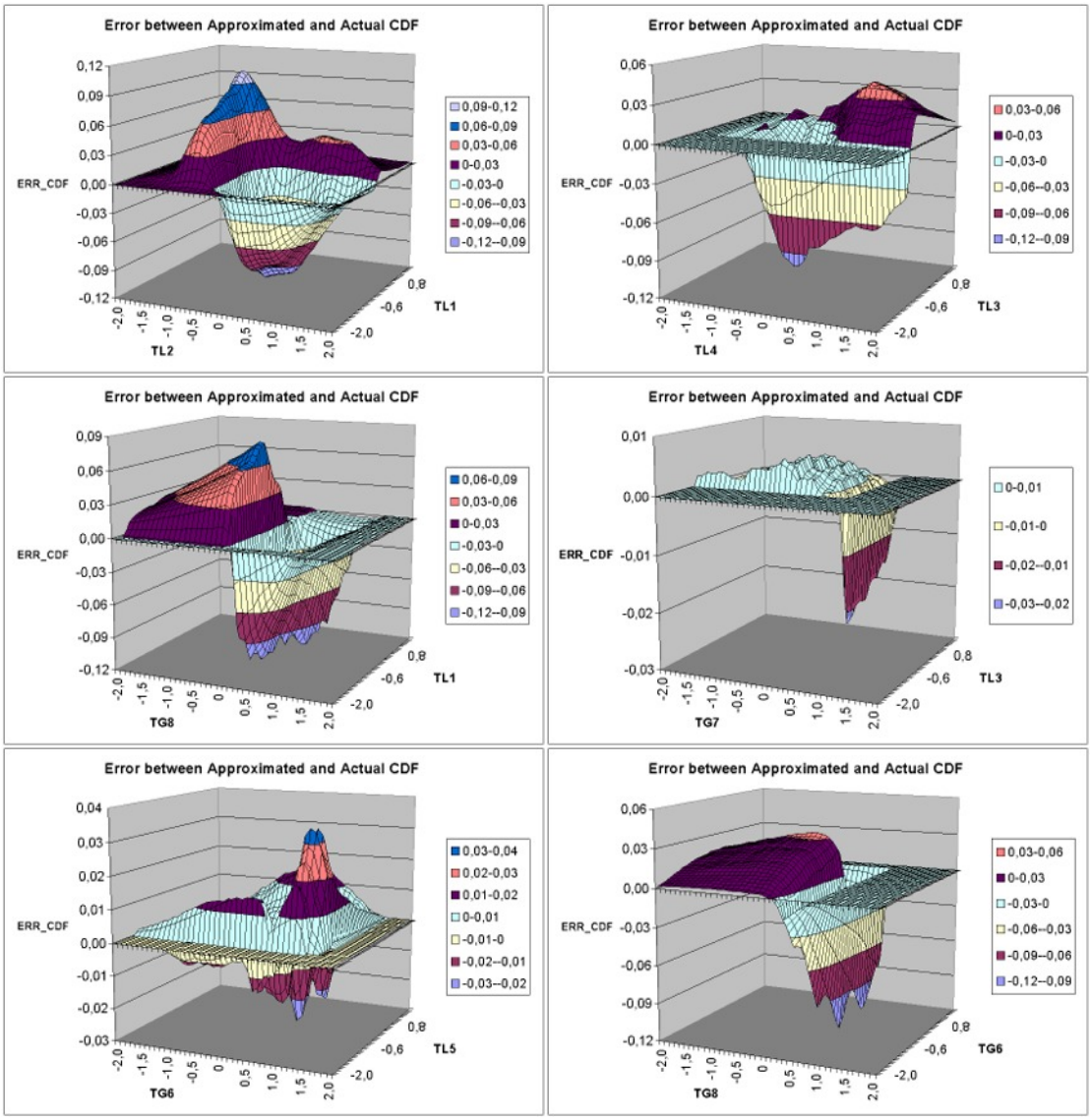

Figure 1-4 Difference between Actual and Approximated (Product) Bivariate CDF's

It can be seen from Figure 1-4 that approximation errors caused by the assumption of independence are not evenly distributed across a bivariate state space, which

means in certain bivariate regions large approximation errors could be expected even though the overall error is relatively small. Thus a bivariate CDF error curve can be characterized by the maximum and average of its absolute values. In Figure 1-4, the average absolute errors of different scenarios range from 0.1% to 2.8%, which appears to be quite insignificant; but two thirds of the scenarios have maximum absolute error values that exceed 10%, which could pose a considerable threat to modeling accuracy.

In order to better illustrate the worst case when absolute error reaches global maximum, actual and approximated bivariate CDF profiles can be captured in an univariate form by fixing one input variable either in horizontal or vertical direction to its value at the point of maximum global error (absolute). Captured CDF curves in both directions can be used for estimating largest potential shape deviation for each single variable caused by mutual independence assumption. In Figure 1-5, the actual (solid line) and approximated (dotted line) univariate CDF curves captured at worst case condition are shown for transformed vectors of all studied scenarios.

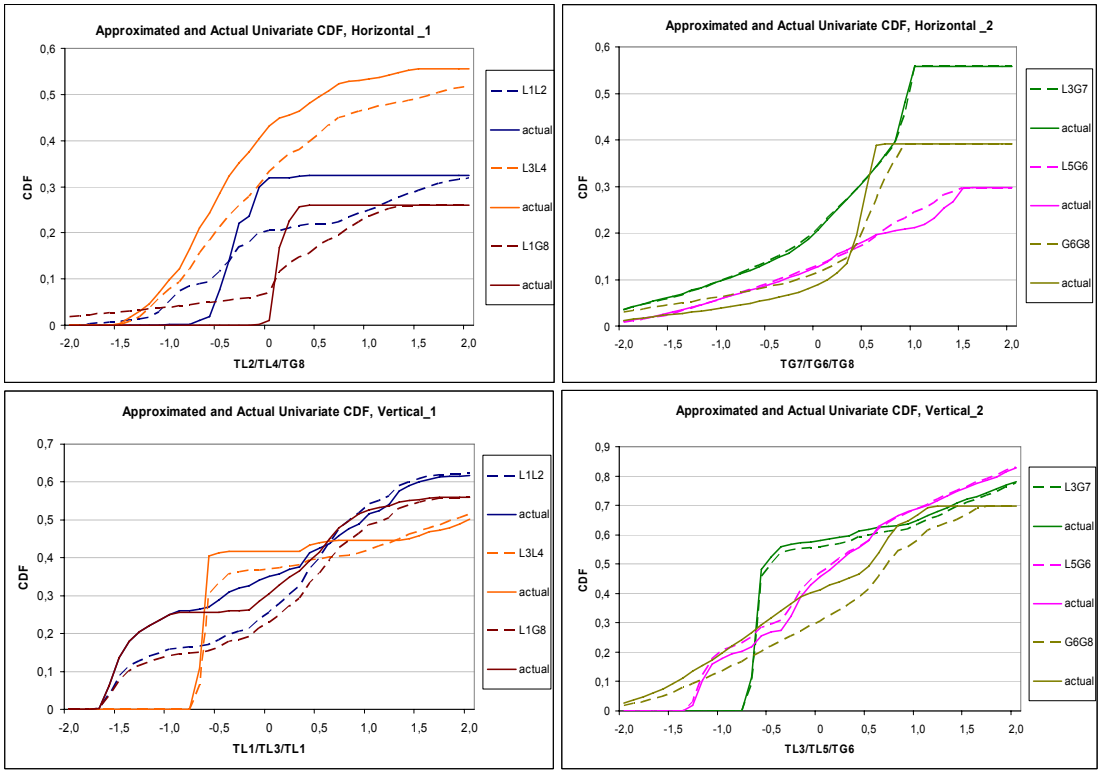

Figure 1-5 Actual and Approximated (Product) Univariate CDF under Maximum Error

Figure 1-5 suggests that except for the scenario of L3&G7 (commercial load and wind turbine combination), all other cases exhibit considerable shape deviations between approximated and actual curves, thus the previous assumption of second-order dependence can be found as inaccurate for most profile combinations. However, the examinations so far have only considered theoretical errors in general (bivariate) and extreme (univariate) cases, which cannot directly reflect the impact of modeling inaccuracy on actual probabilistic load flow (PLF) results. Thus in section 1.2.2, a sample scenario is calculated to reveal the consequences.

1.2.2 Linearized Load Flow under Gram-Charlier Expansion

As already pointed out in section 1.2.1, the potential errors of PLF approach have to be examined under actual calculation results. Thus in order to provide as simple a reference framework as possible, a single-node network with one household load (L1) and a PV unit (G8) is chosen for performing corresponding calculations. Since the PLF approach uses PDF functions as both input and output information of load flow calculation, traditional non-linear load flow formulas cannot be applied directly. Thus in [16] and ensuing [21], [24] etc. linearized load flow solutions are suggested, which make it possible to obtain PDF functions of unknown network variables through linear combinations of input PDF information.

Although many different linear load flow solutions have been developed up to now, their core mechanisms still resemble each other to a large extent. Since the aim of this section is to analyze the potential errors of the analytical approach, the simplest form of linear load flow will suffice—the single node system adopts a dc load flow algorithm assuming zero line loss and thus constant rated voltage at all nodes in the network. With this simplified network, the input variables are the power profiles of the load (PL1) and the DER unit (PG8), and the only output variable is the branch power flow (PB) in the transmission line. The linearized algorithm is shown in *Equation 1-3*

$$\begin{aligned}
&\textit{Assume}: \quad \overrightarrow{P_N} = \left[P_{L1},\, P_{G8} \right]^T \textit{ as nodal input power with mean vector } \overrightarrow{\mu_N} = \left[\mu_{L1},\, \mu_{G8} \right]^T \\
&\qquad P_B \textit{ as branch power flow with linear equation}: \quad P_B = \alpha P_{L1} + \beta P_{G8} \\
&\qquad \textit{Firstly obtain the transition matrix } A \textit{ of } \overrightarrow{P_N} \textit{ from Equation } 1-2: \\
&\qquad A = \begin{bmatrix} \sqrt{c_{11}} & 0 \\ c_{12} / \sqrt{c_{11}} & \sqrt{c_{11} c_{22} - c_{12}^{\,2}} / \sqrt{c_{11}} \end{bmatrix} = \begin{bmatrix} a_{11} & a_{12} \\ a_{21} & a_{22} \end{bmatrix} \\
&\textit{Then}: \quad \textit{A set of uncorrelated vectors } \overrightarrow{T_N} = \left[T_{L1}, T_{G8} \right]^T \textit{ can be obtained as}: \\
&\qquad \overrightarrow{T_N} = A^{-1} \cdot \left(\overrightarrow{P_N} - \overrightarrow{\mu_N} \right) \Leftrightarrow \begin{cases} P_{L1} = \mu_{L1} + \left(a_{11} T_{L1} + a_{12} T_{G8} \right) \\ P_{G8} = \mu_{G8} + \left(a_{21} T_{L1} + a_{22} T_{G8} \right) \end{cases} \\
&\textit{Thus}: \quad P_B = \alpha P_{L1} + \beta P_{G8} = \left(\alpha \mu_{L1} + \beta \mu_{G8} \right) + \left(\alpha a_{11} + \beta a_{21} \right) T_{L1} + \left(\alpha a_{12} + \beta a_{22} \right) T_{G8} \\
&\qquad \textit{With average } \mu_B = E\left(P_B \right) = \alpha \mu_{L1} + \beta \mu_{G8} \\
&\qquad \Rightarrow \begin{cases} P_B - \mu_B = \left[T_{L1}, T_{G8} \right] \cdot \begin{bmatrix} a_{11} & a_{21} \\ a_{12} & a_{22} \end{bmatrix} \cdot \begin{bmatrix} \alpha \\ \beta \end{bmatrix} = \overrightarrow{T_N}^T A^T \left[\alpha,\, \beta \right]^T \\ T_B = P_B - \mu_B,\ \delta = \alpha a_{11} + \beta a_{21},\ \varepsilon = \alpha a_{12} + \beta a_{22} \Rightarrow T_B = \delta T_{L1} + \varepsilon T_{G8} \end{cases}
\end{aligned}$$

Equation 1-3

As can be seen from *Equation 1-3*, the branch power flow PB can be expressed as the linear combination of the uncorrelated vectors TL1, TG8 that are transformed from original time-series data of PL1 and PG8. Consequently, if TL1 and TG8 are independent normal distribution variables, corresponding PB should be normally distributed as well, and its mean and variance can be easily computed from the parameters of TL1 and TG8. However, the assumption of Gaussian property does not always hold true for transformed load or DER profiles, thus mean and variance might be insufficient for describing the characteristics of an unknown type of probability distribution. In order to tackle this modeling issue, the Gram-Charlier expansion method can be used to approximate non-Gaussian variables from the high-order derivatives of a standard Gaussian distribution function as *Equation 1-4*:

$$PDF: \quad F(x) = \Phi(x) + \sum_{i=1}^{\infty} \frac{k_i}{i!} \Phi^{(i)}(x), \quad CDF: \quad f(x) = \varphi(x) + \sum_{i=1}^{\infty} \frac{k_i}{i!} \varphi^{(i)}(x)$$

Equation 1-4

In order to perform numerical calculations with the Gram-Charlier expansion method, the derivatives of a standard normal PDF formula are expressed as the product of Hermite polynomials and the standard normal PDF [24]. In the mean time, all the constant coefficients k_i in *Equation 1-4* can be derived from the moments of examined time-series data. This can be seen from *Equation 1-5*.

$$Since: \quad F(x) = \Phi(x) \cdot \left[1 + \sum_{i=1}^{\infty} \left(\frac{1}{i!} k_i H_i(x) \right) \right],$$

$$F(x) \text{ as unknown PDF}, \quad \Phi(x) \text{ as PDF of standard normal distribution}$$

$$Define: \quad m_i = E\left(x^i\right) \text{ as the } i-th \text{ moment of } x, \text{ then}:$$

$$\begin{cases} k_1 = 0 \\ k_2 = 0 \\ k_3 = m_3 \\ k_4 = m_4 - 3 \\ k_5 = m_5 - 10m_3 \\ k_6 = m_6 - 15m_4 + 30 \\ \cdots\cdots \end{cases} \qquad \begin{cases} H_1(x) = x \\ H_2(x) = x^2 - 1 \\ H_3(x) = x^3 - 3x \\ H_4(x) = x^4 - 6x^2 + 3 \\ H_5(x) = x^5 - 10x^3 + 15x \\ H_6(x) = x^6 - 15x^4 + 45x^2 - 15 \\ \cdots\cdots \end{cases}$$

Equation 1-5

Obviously, *Equation 1-5* suggests that modeling accuracy of Gram-Charlier method should be related to the highest order of *x* in Hermite polynomial or equivalently the highest order of *x*'s moment used for approximation. In order to illustrate this point, the transformed variables TL1 and TG8 are both approximated by 4th order and 8th order Gram-Charlier expansion, with results shown in Figure 1-6.

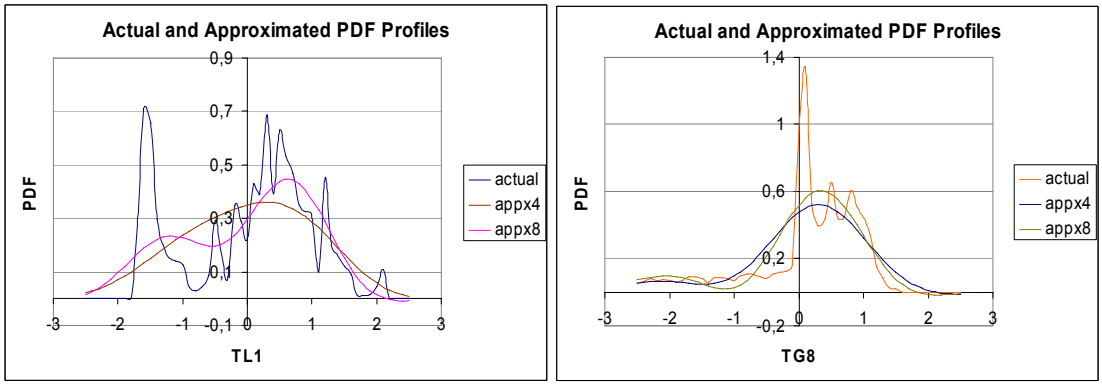

Figure 1-6 Actual and 4th/8th-order Approximations of PDF curves of TL1 and TG8

Interestingly, in Figure 1-6 the actual PDF profiles that are converted from histograms of TL1 and TG8 exhibit rather irregular shapes that appear to be quite difficult to model. Spikes and pit-falls in these summarized profiles could be partly caused by daily and/or seasonal cycles as suggested in [22], thus extraction of these temporal

patterns might potentially reduce irregularities in acquired PDF plots and could serve as a valuable aspect for further research. However, in this simplified study these irregular PDF plots are used nonetheless for evaluation of approximation errors, since inclusion of temporal patterns causes extra complexities in calculation.

By comparing approximated PDF curves to their actual counterparts in Figure 1-6, the approximated curves of TL1 exhibit a considerable degree of improvement under 8th-order Gram-Charlier expansion in comparison to the 4th-order case, while the approximation results of TG8 show relatively small improvements with the increase of expansion order from 4 to 8. In this study, 8th order Gram-Charlier expansion is chosen to simplify calculation procedures, although further increase of this order could potentially reduce the difference between actual and approximated curves.

In order to obtain Gram-Charlier expression for a linear combination of independent random variables, the moments of the combined variable have to be obtained from the moments of all the input variables. This is done via mutual transformations between moments and cumulants, since cumulants of a linearly combined variable can be calculated as linear combinations of each component's cumulants [24], which is shown in *Equation 1-6*.

$$
\begin{aligned}
&\textit{Assume}: \quad x_1, x_2, \cdots, x_N \ \textit{as independent random variables} \\
&\qquad\quad \textit{Let } y = \alpha_1 x_1 + \alpha_2 x_2 + \cdots + \alpha_N x_N \\
&\textit{Define}: \quad g_x(t) = \log\left[E\left(e^{tx}\right)\right] \textit{as the cumulant-generating function of } x, \\
&\qquad\quad \textit{And } i\text{-th cumulant of } x \textit{ can be calculated as } c_i(x) = g_x^{(i)}(0) \\
&\textit{Then}: \quad \begin{cases} c_1(y) = \alpha_1 c_1(x_1) + \alpha_2 c_1(x_2) + \cdots + \alpha_N c_1(x_N) \\ c_2(y) = \alpha_1{}^2 c_2(x_1) + \alpha_2{}^2 c_2(x_2) + \cdots + \alpha_N{}^2 c_2(x_N) \\ \cdots\cdots \\ c_M(y) = \alpha_1{}^M c_M(x_1) + \alpha_2{}^M c_M(x_2) + \cdots + \alpha_N{}^M c_M(x_N) \end{cases}
\end{aligned}
$$

Equation 1-6

Consequently, in order to obtain the moments of an output variable, the moments of input variables should be first converted into cumulants. And then these cumulants are linearly combined to yield the cumulants of output variable. Finally, the acquired cumulants of output variable are converted back into moments, which can be used to construct Gram-Charlier expansion for the approximation of output PDF. The transformation formulas between moments and cumulants are given in *Equation 1-7*.

$$
\begin{aligned}
&\textit{Assume}: \quad x \textit{ as a random vector}, \quad c_i \textit{ as } i\text{-th cumulant of } x, \quad m_i \textit{ as } i\text{-th moment of } x \\
&\textit{Then}: \quad \begin{cases} c_1 = m_1 \\ c_2 = m_2 \\ c_3 = m_3 \\ c_4 = m_4 - 3m_2{}^2 \\ c_5 = m_5 - 10m_2 m_3 \\ c_6 = m_6 - 15m_2 m_4 - 10m_3{}^2 + 30m_2{}^3 \\ \cdots\cdots \end{cases} \quad \begin{cases} m_1 = c_1 \\ m_2 = c_2 \\ m_3 = c_3 \\ m_4 = c_4 + 3c_2{}^2 \\ m_5 = c_5 + 10c_2 c_3 \\ m_6 = c_6 + 15c_2 c_4 + 10c_3{}^2 + 15c_2{}^3 \\ \cdots\cdots \end{cases}
\end{aligned}
$$

Equation 1-7

With studied single-node system, the difference between analytical approach (PLF) and simulation approach (Monte Carlo) can be simply interpreted as the way of obtaining characteristic parameters (moments) of output variable if the Gram-Charlier model is used to summarize statistical data in both cases. The PLF approach first extracts characteristic data from transformed individual input variables, and then relates the characteristic data of output variables to the input characteristics through linearized load flow equations. The Monte Carlo approach, on the other hand, will first construct output variables in the time frame by performing standard load flow for each state of operation, and then summarize the output by collecting characteristic data directly from calculated time-series results. Thus errors stemming from the assumption of second-order input data dependence made in section 1.2.1 can be evaluated by comparing PDF curves of output branch power obtained through both analytical and simulation approaches, as shown in Figure 1-7.

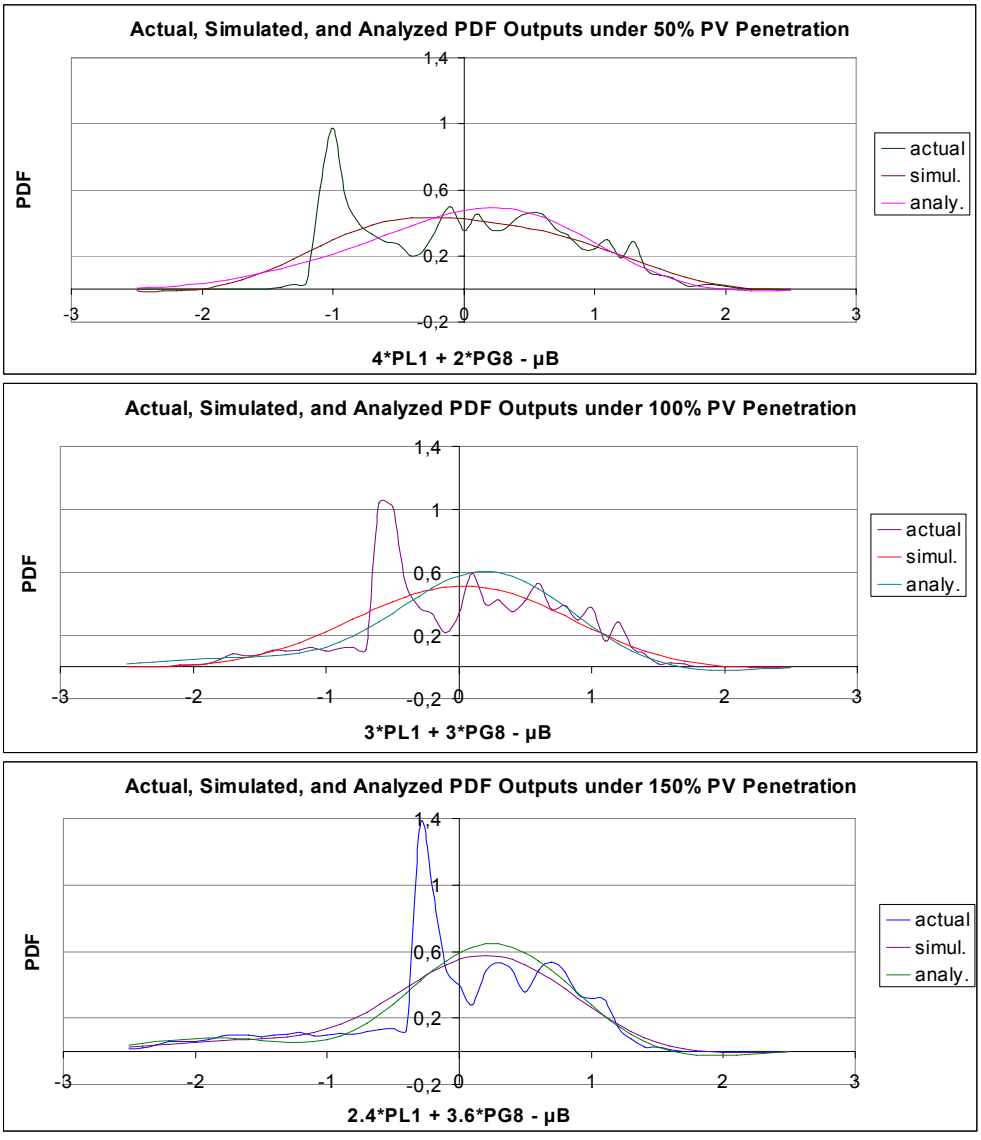

Figure 1-7 Actual and Approximated Output PDF curves for Different Scenarios

In Figure 1-7, the actual PDF curves are constructed from histograms of Monte Carlo simulation results, which represent the raw output data and only serve as reference plots. Comparison should be drawn between modeled PDF outputs under analytical and simulation approaches, which obviously shows differences in curve shapes for

all studied scenarios. Thus in comparison with Monte Carlo simulation, the analytical approach has two inherent deficiencies that inevitably cause errors in calculation results, namely: (1) the input series data have to be independent from 3rd order above, otherwise errors will be found in output PDF curves as shown in Figure 1-7; (2) Even if the first condition is satisfied, the Gram-Charlier expansion still cannot exactly model actual PDF curves with a limited dimension (such as 4th or 8th order).

1.3 The Markov Chain Method

A Markov chain, named after Andrey Markov, refers to a discrete process with Markov property, which can be represented by a series of random variables that satisfy a conditional probability distribution [25]. This concept can also be extended to continuous-time processes when a discrete set of state space values can be extracted from and converted back to the original data.

The Markov chain method has found widespread applications ranging from speech recognition to weather forecast, among which the Markov Chain Monte Carlo (MCMC) method has notably been adopted for rather complicated reliability calculations, such as that of electrical networks.

The application of Markov chain method in this chapter, however, is primarily centered on the simulation of wind or solar power generation outputs—this is due to the partially non-random correlations between consecutive values in a continuous-time sequence of these two physical processes. In this light, simulation results achieved by Markov chain method can thus retain and reflect a relatively large proportion of the characteristics of the original physical processes.

1.3.1 Time Domain Characteristics of a Markov Chain

Assuming that a sequence of random state variables $x_1, x_2 \ldots x_N$ satisfies Markov property, then an immediate future value of x depends only on the current value of x and is totally independent from any past values. This can be expressed in mathematical form as [25]:

$$P\left[x_{n+1} = s(n+1) \mid x_n = s(n)\right] = P\left[x_{n+1} = s(n+1) \mid x_n = s(n), x_{n-1} = s(n-1), \ldots, x_1 = s(1)\right]$$

$$n \in [1, N-1], \quad s(n) \text{ can be any value taken from the finite Set } S \text{ that } x_n \text{ belongs to.}$$

Equation 1-8

A Markov chain is viewed as homogeneous or stationary if its properties do not change over time, namely:

$$P\left[x_{n+1} = s(n+1) \mid x_n = s(n)\right] = P\left[x_{n+k+1} = s(n+k+1) \mid x_{n+k} = s(n+k)\right], \quad n, k \in [1, N-1]$$

Equation 1-9

A time-inhomogeneous—or a non-stationary Markov chain—is generally more difficult to model or simulate, and requires relatively large samples of original data in order to achieve desirable accuracy. In scope of this report, only stationary Markov chains are studied and analyzed in full detail due to the limited availability of original data.

1.3.2 The Markov Transition Matrix

With the discussed series of random state variables $x_1, x_2 \ldots x_N$, if the size of the finite set is defined as M—namely, there are M sets of different values $s_1, s_2 \ldots s_M$ that $x_1, x_2 \ldots x_N$ can take on, then the stochastic properties of the set can be expressed by a *M*M* probability matrix called transition matrix P_T, which is shown in *Equation 1-10* as:

$$P_T = \begin{bmatrix} p_{11} & p_{12} & \cdots & p_{1M} \\ p_{21} & p_{22} & \cdots & p_{2M} \\ \vdots & \vdots & \vdots & \vdots \\ p_{M1} & p_{M2} & \cdots & p_{MM} \end{bmatrix}$$

$$p_{ij} = P(x_{n+1} = s_j \mid x_n = s_i), \quad i, j \in [1, M], \quad n \in [1, N-1]$$

Equation 1-10

By definition of the matrix, it can be seen that the sum of all elements in one row of P_T is 1, which can be mathematically proven by:

$$\sum_{j=1}^{M} p_{ij} = p_{i1} + p_{i2} + \cdots + p_{ij} = \sum_{j=1}^{M} P(x_{n+1} = s_j \mid x_n = s_i) = 1$$
$$i, j \in [1, M], \quad n \in [1, N-1]$$

Equation 1-11

In order to facilitate computational expressions, the transition matrix P_T can also be described by a one-dimensional vector space of L_T, which consists of *M*M* variables $l_1, l_2 \ldots l_{M*M}$ and effectively equals the linearized version of P_T:

$$Lt = [l_1, l_2, \cdots, l_{M \cdot M}],$$
$$l_k = p_{ij}, \quad k = i \cdot M + j, \quad k \in [1, M^2], \quad i, j \in [1, M]$$

Equation 1-12

1.3.3 Typical Algorithm of a Markov Chain Simulation

A simulation algorithm using Markov chain typically consists of two major steps: first, the transition matrix of original data set is obtained for a given state space definition; second, random state space variables are generated according to this transition matrix and later reverted to original data format. A number of different vector space variables are involved in this process, and they can be separately defined as:

1. $X(N) = [x_1, x_2, \cdots x_N]$: *original data set with continuous real values*

2. $S(M) = [s_1, s_2, \cdots s_M]$: *the finite state space of* X

3. $Y(N) = [y_1, y_2, \cdots y_N]$: *converted state data of* X *defined over* S

$$Def: if\ x_i \in \left[\frac{(j-1)\cdot rng}{M}, \frac{j\cdot rng}{M}\right],\quad then\ y_i = s_j$$

$$rng = Max(X) - Min(X),\quad i \in [1, N],\ j \in [1, M]$$

(Note: Even distribution of X over state space S is used here, though there might be variations from this general approach.)

4. $A(M^2) = [a_1, a_2, \cdots a_{M\cdot M}]$: *frequency count for each transition matrix element*

$$Def: for\ each\ a_k, i = \text{int}\left(\frac{k}{M}\right),\ j = k - i\cdot M,\quad then\ a_k\ refers\ to\ the\ total\ count\ of:$$

$$all\ cases\ with\ x_{n+1} = s_j\ AND\ x_n = s_i\ for\ n = 1\ to\ N-1$$

$$k \in [1, M^2],\quad i, j \in [1, M]$$

5. $B(M^2) = [b_1, b_2, \cdots b_{M\cdot M}]$: *linearized transition matrix for original state data*

$$Def: for\ each\ b_k, i = \text{int}\left(\frac{k}{M}\right),\ j = k - i\cdot M,\quad then\ b_k\ can\ be\ defined\ as:$$

$$b_k = P(x_{n+1} = s_j \mid x_n = s_i) = \frac{a_k}{sum_i},\quad sum_i = \sum_{p=i\cdot M+1}^{i\cdot M+10} a_p$$

$$k \in [1, M^2],\quad i, j \in [1, M],\quad n \in [1, N-1]$$

6. $C(M^2 + M) = [c_1, c_2, \cdots b_{M\cdot(M+1)}]$: *cumulative probability vector* (*original*)

$$Def: for\ each\ c_k, i = \text{int}\left(\frac{k-1}{M+1}\right),\ j = k - i\cdot(M+1) - 1$$

$$if\ i = 0, then\ c_k = 0$$

$$if\ i \neq 0, then\ c_k = \sum_{p=i\cdot M+1}^{i\cdot M+j} b_p$$

$$k \in [1, M^2 + M],\quad i, j \in [1, M]$$

Equation 1-13

After obtaining the characteristic vectors *A(M), B(M), C(M^2+M)* of original data, a generation algorithm can be developed to produce a random state set *Y'(N)* that is designed to be statistically equivalent to original state data and yield the same transition matrix as the original. Then by identifying the distribution characteristics of original data in each segmented interval corresponding to each state value, the state vector *Y' (N)* can be used to approximate the continuous-time behavior of test physical process and finally the simulated data set *X'(N)* can be generated and ready to be used for further calculation purposes.

The generation algorithm for *Y' (N)* assuming *s (i) = i-1* is given in Figure 1-8 as a reference.

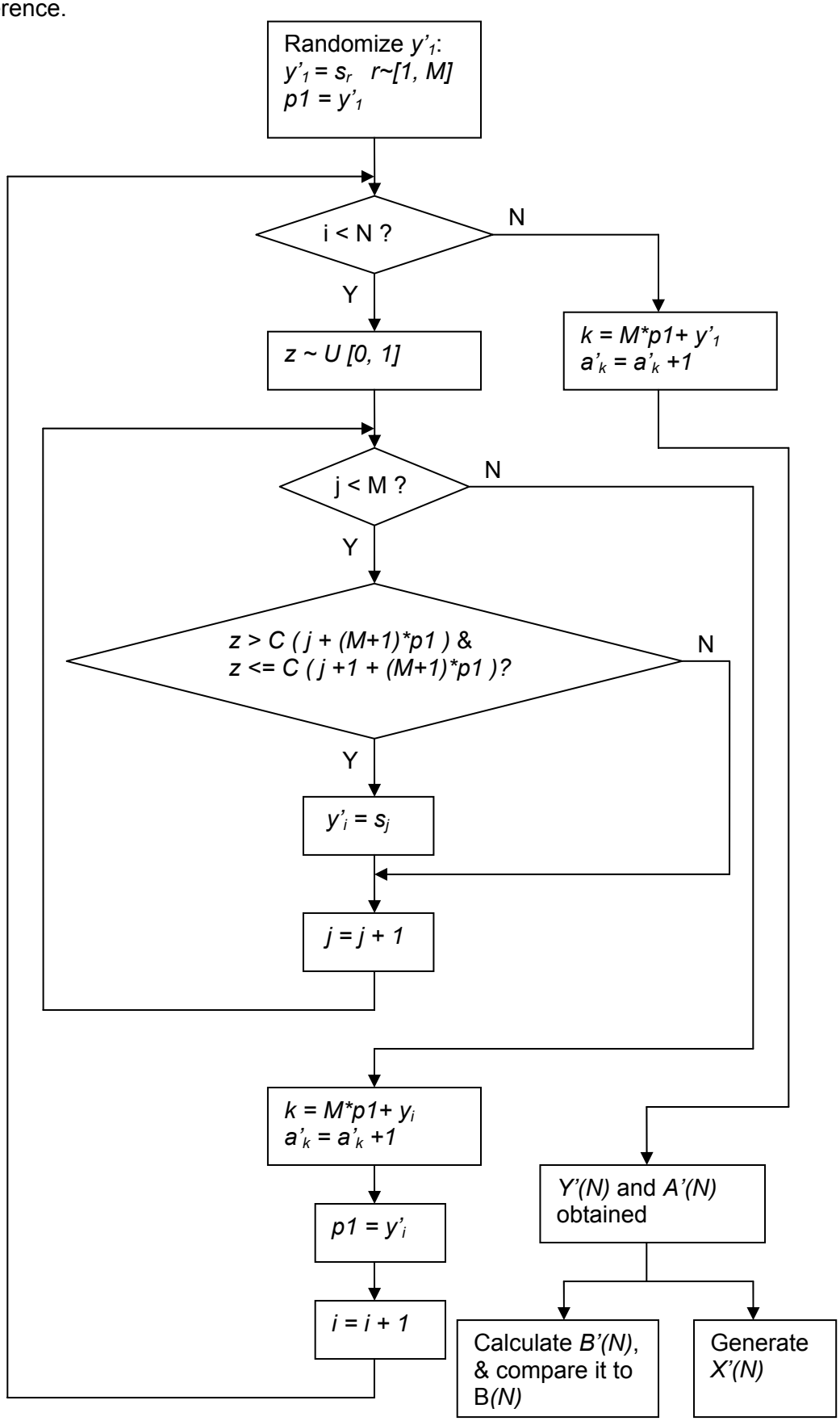

Figure 1-8 Markov Chain State Variable Generation Process

1.3.4 Higher Order Markov Chains

For a Markov chain sequence $x_1, x_2, \ldots, x_N$, if the current value of x depends not only on the immediate past value of x, but also on x value from further past events, then the sequence is defined as a high order Markov chain [28]. Its order K is equal to the number of past events that the current x value depends on—namely:

$$\begin{aligned}
&If\ x_1, x_2, \cdots x_N\ is\ a\ Kth\ order\ Markov\ chain\ sequence, then:\\
&P\left[x_n = s(n) \mid x_{n-1} = s(n-1), x_{n-2} = s(n-2), \cdots, x_{n-K} = s(n-K)\right]\\
&= P\left[x_n = s(n) \mid x_{n-1} = s(n-1), \cdots, x_{n-K} = s(n-K), x_{n-K-1} = s(n-K-1), \cdots, x_1 = s(1)\right]
\end{aligned}$$

$$n \in [K+1, N], \quad s(n)\ can\ be\ any\ value\ taken\ from\ the\ finite\ Set\ S\ that\ x_n\ belongs\ to.$$

Equation 1-14

In order to describe the stochastic property of a higher Markov chain, a single transition matrix is no longer enough due to the increase in order of past events. Thus a Kth order Markov chain with a finite state space of M will need M^{K-1} transition matrices in M*M format in order to identify itself. An example is given below for K=2 and M=3, with 0, 1, 2 as finite states:

The original 1st order Markov chain can be described by only a transition matrix P_1:

$$P_1 = \begin{bmatrix} 0|0 & 1|0 & 2|0 \\ 0|1 & 1|1 & 2|1 \\ 0|2 & 1|2 & 2|2 \end{bmatrix}, \quad i \mid j = P(x_{n+1} = i \mid x_n = j), \quad i, j \in [0,2]$$

Equation 1-15

While a 2nd order Markov chain has to be represented by 3 matrices P_{2a}, P_{2b}, *and* $P2c$ in comparison:

$$P_{2a} = \begin{bmatrix} 0|0|0 & 1|0|0 & 2|0|0 \\ 0|1|0 & 1|1|0 & 2|1|0 \\ 0|2|0 & 1|2|0 & 2|2|0 \end{bmatrix},$$

$$P_{2b} = \begin{bmatrix} 0|0|1 & 1|0|1 & 2|0|1 \\ 0|1|1 & 1|1|1 & 2|1|1 \\ 0|2|1 & 1|2|1 & 2|2|1 \end{bmatrix},$$

$$P_{2c} = \begin{bmatrix} 0|0|2 & 1|0|2 & 2|0|2 \\ 0|1|2 & 1|1|2 & 2|1|2 \\ 0|2|2 & 1|2|2 & 2|2|2 \end{bmatrix},$$

$$i \mid j \mid k = P(x_{n+1} = i \mid x_n = j, x_{n-1} = k), \quad i, j, k \in [0,2]$$

Equation 1-16

If the linearized expression of P is used, then a Kth order Markov chain with a finite state space of M can be described by a one-dimensional vector $L\ (M^{K+1})$ as:

$$L(M^{K+1}) = \left[l_1, l_2, \cdots, l_{M^{K+1}}\right]$$

$$
\begin{aligned}
&\text{for any } l_k,\ k = n + M \cdot p1 + M^2 \cdot p2 + \cdots + M^K \cdot pk \\
&l_k = P(x_i = s_n \mid x_{i-1} = s_{p1},\ x_{i-2} = s_{p2},\ x_{i-3} = s_{p3}, \cdots,\ x_{i-K} = s_{pK}), \\
&k \in \left[1, M^{K+1}\right],\quad n, p1, p2, \cdots pk \in [1, M]
\end{aligned}
$$

Equation 1-17

The generation algorithms for higher order Markov chains are similar to that of first order, and are thus not explained in detail here.

1.4 Decoupling of Multiple Random Variables

When compiling a multi-variant simulation algorithm, it is mostly desirable to have multiple random variables generated independent from each other. Coupling between multiple variables might cause significant barriers to the creation of an efficient algorithm. Thus decoupling of originally interrelated variables becomes necessary under such situations, and efficient conversion and reversion methods are needed in order to achieve maximum computational efficiency. This section will be mainly focused on this topic.

1.4.1 Mathematical Background and Case Analysis

The basic mathematical principle used for decoupling of multiple random variables can be expressed as *Equation 1-18*:

$$
\begin{aligned}
&\textit{Given } N \textit{ sets of random vectors with the same length of } M: \\
&X1(M) = \left[x1_1, x1_2, \cdots x1_M\right] \\
&X2(M) = \left[x2_1, x2_2, \cdots x2_M\right] \\
&\cdots\cdots \\
&XN(M) = \left[xN_1, xN_2, \cdots xN_M\right] \\
&\textit{If it is known that their correlation can be summarized in } K \textit{ sets of linear equations}: \\
&f1(X1, X2, \ldots, XN) \\
&f2(X1, X2, \ldots, XN) \\
&\cdots \\
&fK(X1, X2, \ldots, XN) \\
&\textit{Then the vector group } X1, X2, \ldots XN \textit{ can be statistically replaced by } L = N - K \textit{ vectors}: \\
&Y1(M) = \left[y1_1, y1_2, \cdots y1_M\right] \\
&Y2(M) = \left[y2_1, y2_2, \cdots y2_M\right] \\
&\cdots\cdots \\
&YL(M) = \left[yL_1, yL_2, \cdots yL_M\right] \\
&\textit{Transformation in the opposite direction holds the same conclusion.}
\end{aligned}
$$

Equation 1-18

A simple example with N=3 and K=1 is shown in *Equation 1-19* for reference:

Given random vectors $X1, X2, X3$:

$$X1 \in U(0, 0.4)$$

$$X2 \in U(0.2, 0.4)$$

$$X3 \in U(0.4, 0.6)$$

$$X1 + X2 + X3 = 1$$

Equation 1-19

It can be seen that *X1, X2, X3* cannot be generated as arbitrary random values following the description of their distribution functions—for example, if *X1=0.1, X2=0.3*, then *X3* is fixed as 0.6 rather than being a random variable. Thus the degree of freedom for this state space is 2 instead of 3. Sizing down of variable numbers can be achieved in the following way shown in *Equation 1-20*:

Assume that :

$$\begin{cases} a1 + a2 = 1 \\ a1 = b1 + b2 \\ a2 = b3 \end{cases}$$

$$\Rightarrow b1 + b2 + b3 = 1$$

Let $a1 = Y1, b1 = Y1 \cdot Y2$, *then* :

$$Y1 \cdot Y2 + Y1 \cdot (1 - Y2) + (1 - Y1) = 0$$

By comparing it to the correlation function of $X1, X2, X3$, *it is known that* :

$$\begin{cases} X1 = Y1 \cdot Y2 \\ X2 = Y1 \cdot (1 - Y2) \\ X3 = 1 - Y1 \end{cases}$$

Thus :

$$\begin{cases} Y1 = 1 - X3, \quad 0.4 \le Y1 \le 0.6 \\ Y2 = 1 - \dfrac{X2}{Y1} = \dfrac{X1}{Y1}, \quad 0 \le Y2 \le 1 \end{cases}$$

Equation 1-20

Obviously, regardless of whatever values *Y1* and *Y2* might take on, the corresponding *X1, X2, X3* always sum up to 1.

1.4.2 Sizing-down (Conversion) Process for K = 1 Cases

By extending the upper example to more general cases with any positive integer value of N, the sizing down process for converting *X1, X2,…,XN* into *Y1, Y2,…,YL (L=N-1)* can be expressed as:

$$\begin{cases} a1 + a2 = 1 \\ b1 + b2 + b3 = 1 \\ c1 + c2 + c3 + c4 = 1 \\ \ldots\ldots \end{cases} \quad \begin{cases} a1 = 1 - a2 \\ a1 = b1 + b2,\ b3 = a2 \\ b1 = c1 + c2,\ c3 = b2,\ c4 = b3 \\ \ldots\ldots \end{cases} \quad \begin{cases} a1 = Y1 \\ b1 = Y1 \cdot Y2 \\ c1 = Y1 \cdot Y2 \cdot Y3 \\ \ldots\ldots \end{cases}$$

Equation 1-21

$$If\ X1+X2+\cdots+X(N-1)+XN=1,\quad then\ for\ L=N-1:$$
$$\prod_{p=1}^{L}Yp+(1-YL)\prod_{p=1}^{L-1}Yp+\left(1-Y(L-1)\right)\prod_{p=1}^{L-2}Yp+\ldots+(1-Y3)\prod_{p=1}^{2}Yp+(1-Y2)Y1+(1-Y1)=1$$

Equation 1-22

Thus:

$$\begin{cases} X1=\prod_{p=1}^{L}Yp \\ X2=(1-YL)\prod_{p=1}^{L-1}Yp \\ X3=\left(1-Y(L-1)\right)\prod_{p=1}^{L-2}Yp \\ \cdots \\ X(N-2)=(1-Y3)\prod_{p=1}^{2}Yp \\ X(N-1)=(1-Y2)\cdot Y1 \\ XN=1-Y1 \end{cases} \Rightarrow \begin{cases} Y1=1-XN \\ Y2=1-\dfrac{X(N-1)}{Y1} \\ Y3=1-\dfrac{X(N-2)}{\prod_{p=1}^{2}Yp} \\ \cdots \\ Y(L-1)=1-\dfrac{X(3)}{\prod_{p=1}^{L-2}Yp} \\ YL=1-\dfrac{X(2)}{\prod_{p=1}^{L-1}Yp} \end{cases}$$

Equation 1-23

The obtained variables *Y1, Y2 … YL* are thus independent from each other and can be analyzed separately to identify their stochastic features.

1.4.3 Sizing-up (Reversion) Process for K = 1 Cases

In simulation practice, a set of approximated variables *Y'1, Y'2 … Y'L* are generated with close statistical features to *Y1, Y2 … YL*, and a sizing-up process is necessary to revert them into N sets of *X'1, X'2 … X'N* as finally usable simulation data. In order to improve computational efficiency, *Equation 1-24* can be used instead of the original ones for deducing X from Y:

$$\begin{cases} X'1=\prod_{p=1}^{L}Y'p \\ X'2=X'1\cdot\left(\dfrac{1}{Y'L}-1\right) \\ X'3=X'2\cdot\left(\dfrac{1}{Y'(L-1)}-1\right)\div\left(1-Y'(L)\right) \\ \cdots \\ X'(N-1)=X'(N-2)\cdot\left(\dfrac{1}{Y'2}-1\right)\div\left(1-Y'3\right) \\ X'N=X'(N-1)\cdot\left(\dfrac{1}{Y'1}-1\right)\div\left(1-Y'2\right) \end{cases}$$

Equation 1-24

1.4.4 Additional Note

The conversion and reversion methods discussed in this section apply only to a specific case of *K=1* situation; thus cases with multiple binding equations — i.e., higher K values or even non-linear features are left open for further studies.

1.5 Simulation of Load Curves

Load curves can be identified as the accumulated stochastic behavior of multiple loads at distribution level—although the curve of a single load can appear totally random, the sum of multiple loads will have a relatively constant curve shape in the time domain [29]. This is determined, of course, by the scale of loads a curve actually represents; and notably, a daily load curve will appear differently for different times of year. Stochastic modeling of load curves thus involves identification of the types of daily curves, generation of annual curve according to the daily features, and finally application of variations according to the scaling of loads.

1.5.1 Types and Features of Daily Load Curves

Daily load curves can be categorized according to three different criteria, namely they are:

(1) Nature of load: household, commercial & industrial, agricultural, etc.

This criterion can be used to determine the type of a load curve—for example, Figure 1-9 and Figure 1-10 show the typical daily load curves of a household customer and an agricultural customer on winter Sundays:

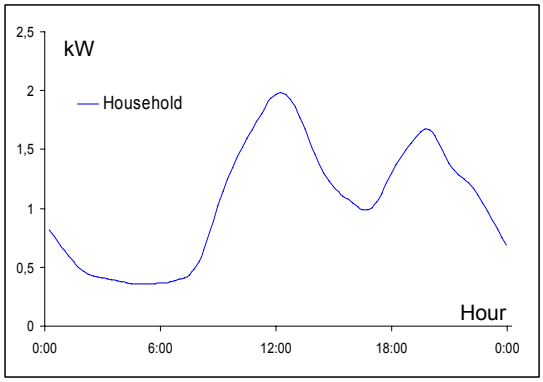

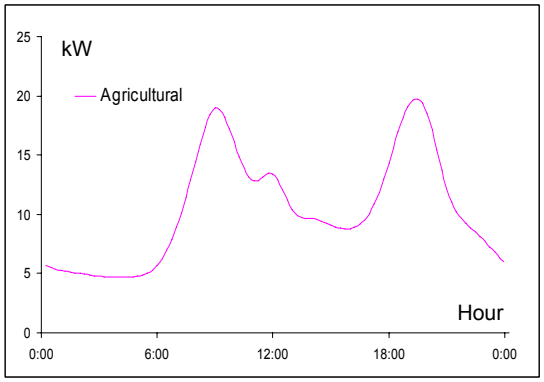

Figure 1-9 Typical Household Load

Figure 1-10 Typical Agricultural Load

(2) Day of week: working day (Monday—Friday), Saturday, or Sunday.

Daily load curves vary very little from Monday to Friday, but take on quite different shapes on weekends. This type of variation is most obvious for commercial and industrial (C&I) customers but not quite visible for agricultural customers. Two daily load curves of household and agricultural customers are shown in Figure 1-11 and Figure 1-12 as an example.

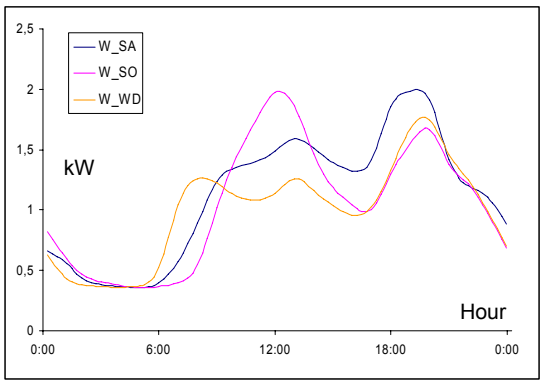

Figure 1-11 Household, Weekly Variation

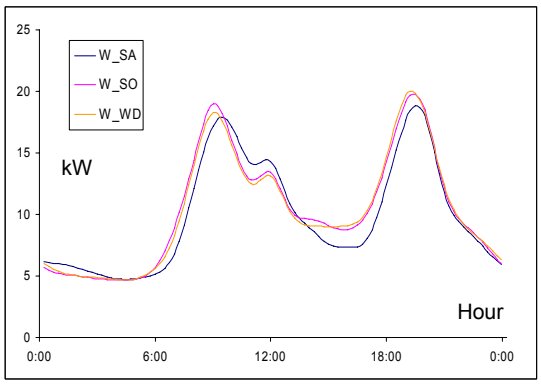

Figure 1-12 Agricultural, Weekly Variation

(3) Season of year: summer, winter, and others (spring or autumn);

Seasonal changes are generally reflected in load curves due to the increase of heating loads in winter and/or air conditioning loads in summer. Geographical as well as meteorological factors also have influence on the seasonal changes of daily load curves. This type of variation is illustrated in Figure 1-13 and Figure 1-14.

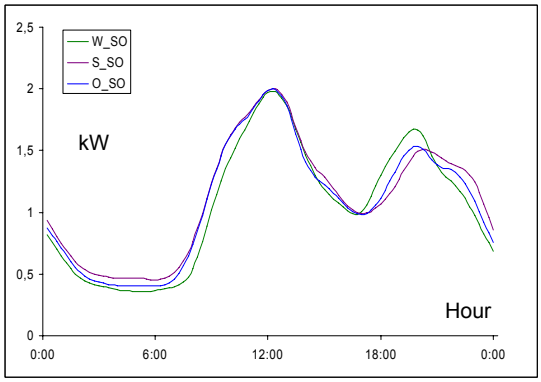

Figure 1-13 Household Seasonal Change

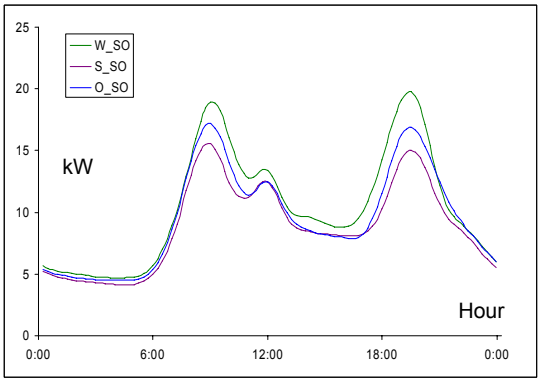

Figure 1-14 Agricultural Seasonal Change

Thus for a given type of load (household, C&I, agricultural, etc.), the following Table 1-2 can be used to label the 9 types of daily load curves applicable to it:

	Working Day (WD)	Saturday (SA)	Sunday (SU)
Summer (S)	**S_WD**	**S_SA**	**S_SU**
Winter (W)	**W_WD**	**W_SA**	**W_SU**
Others (O)	**O_WD**	**O_SA**	**O_SU**

Table 1-2 Types of Daily Load Curves

1.5.2 Generation of Annual Curves

In order to generate annual load curves, typical weekly load curves have to be obtained first as a basis for calculation [30]. Figure 1-15 (listed from Sunday to Saturday) shows the spring/autumn characteristics of a commercial customer:

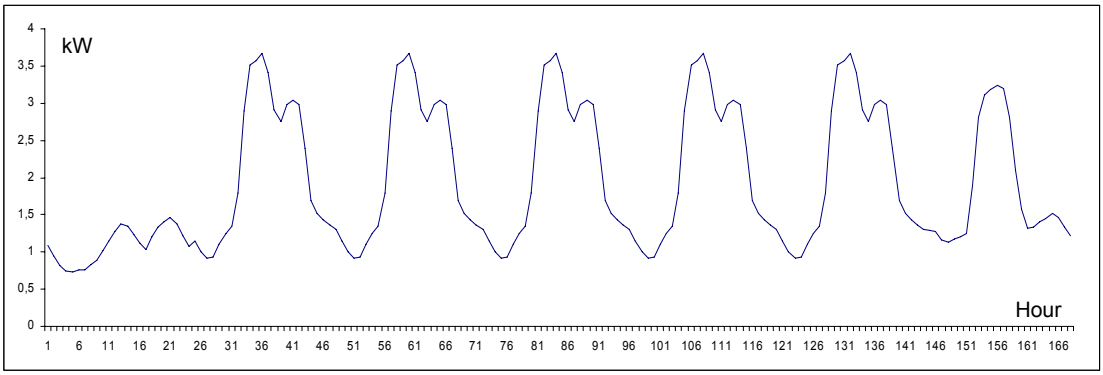

Figure 1-15 Spring/Autumn Weekly Load Curve of a Commercial Customer

By shifting the position of working days and weekends, seven possible combinations can be selected to generate different weekly profiles, thus making it possible to generate annual curves for different calendar years—it should be noted that holidays are not considered in creation of annual load curves in this report.

The 365 days of a year are therefore grouped into 52 weeks with one day left as a single unit. In order to reflect seasonal change in the annual curve, the 3rd, 16th, 29th, and 42nd weeks are respectively considered as the typical winter, spring, summer, and autumn weeks, which means they use exact typical daily curves.

To obtain load curves for all the weeks in between these typical points, the transition daily curves from winter to spring (OmW) as well as from summer to autumn (SmO) are calculated first:

$$x\_OmW = x\_O - x\_W$$
$$x\_SmO = x\_S - x\_O$$

Equation 1-25

This calculation procedure is illustrated in Figure 1-16 and Figure 1-17.

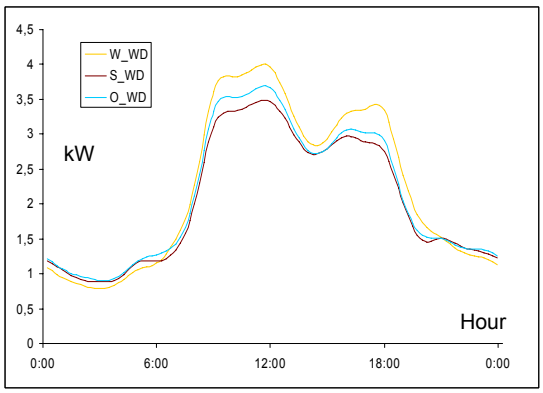

Figure 1-16 W, S, and O; Sunday

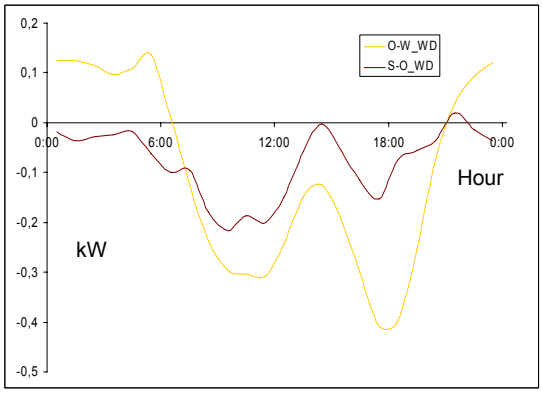

Figure 1-17 OmW and SmO; Sunday

Similar to the generation of weekly spring/autumn profile, the transition curves can also be expressed in weekly form, which is shown in Figure 1-18.

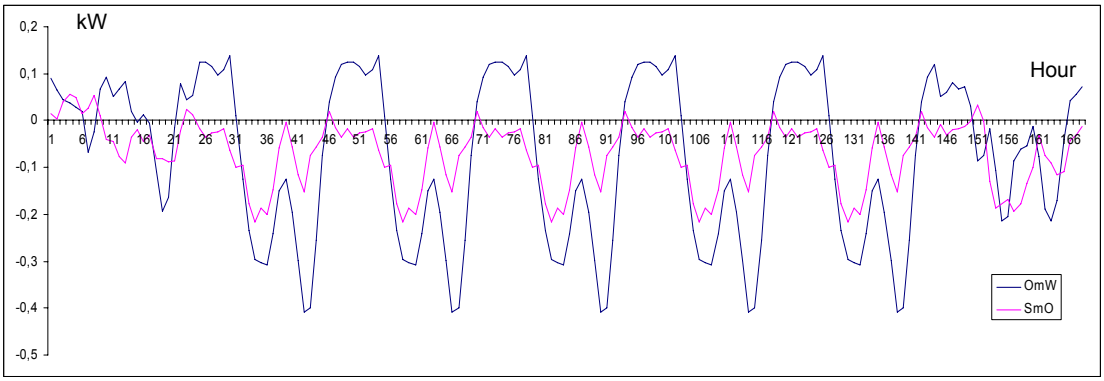

Figure 1-18 Weekly Transition Curves (OmW and SmO) of a Commercial Customer

As a result, the annual curve can be generated according to Figure 1-27:

$$\textit{Assume } n \textit{ as serial of } \textit{week}:$$

$$\begin{cases} x\_A = x\_O - x\_OmW\dfrac{n+10}{13}, & 1 \le n \le 3 \\ x\_A = x\_O + x\_OmW\dfrac{n-16}{13}, & 3 < n \le 16 \\ x\_A = x\_O + x\_SmO\dfrac{n-16}{13}, & 16 < n \le 29 \\ x\_A = x\_O - x\_SmO\dfrac{n-42}{13}, & 29 < n \le 42 \\ x\_A = x\_O - x\_OmW\dfrac{n-42}{13}, & 42 < n \le 52 \end{cases}$$

Equation 1-26

The generated annual load curve is shown in Figure 1-19.

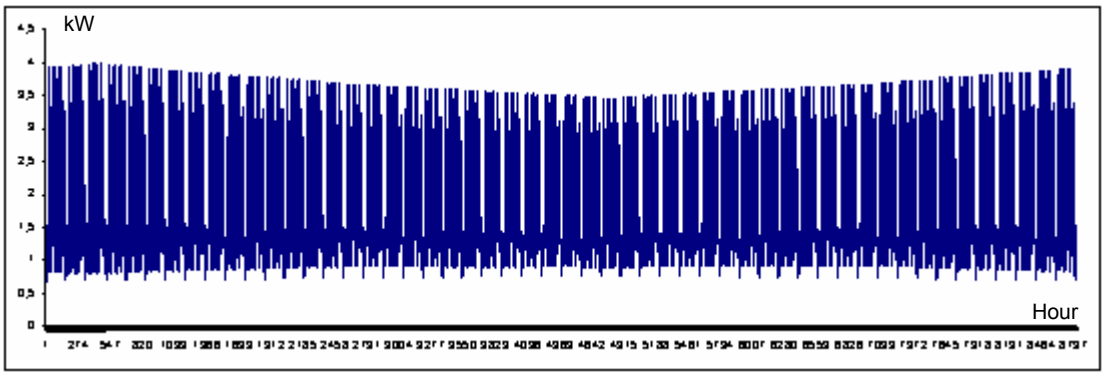

Figure 1-19 Initial Annual Load Curve of a Commercial Customer

1.5.3 Curve Modification by Load Scale

The simulation procedure for load curves explained so far has been entirely deterministic and contains no random information, in order to reflect the impact of scale of loads—i.e. the number of actual individual loads—represented by a curve, normally-distributed disturbance should be applied accordingly [31]. The disturbance can be evaluated by the relative coefficient of variation *RCV* calculated from modified and unmodified load curves:

$$Let\ N = 8760;$$

$$Assume\ x1, x2, \cdots xN\ as\ original\ annual\ load;\ y1, y2, \cdots yN\ as\ adjusted\ annual\ load;$$

$$disturbance\ di = yi - xi, 1 \le i \le N$$

$$RCV = \frac{\sigma}{\mu} = \sqrt{\frac{\sum_{i=1}^{N} di^2}{N-1}} \div \frac{\sum_{i=1}^{N} xi}{N} = \sqrt{E(d^2)\frac{N}{N-1}} \div E(x)$$

Equation 1-27

If we define a scale factor SCL as the number of actual loads represented by a load curve, then by knowing the value of RCV_0 for a given SCL_0, the *RCV* of any load scale can be obtained as:

$$RCV = RCV_0\sqrt{\frac{SCL_0}{SCL}} \Leftrightarrow RCV\sqrt{SCL} = Const$$

$$Let\ RS = \frac{SCL_0}{SCL},.\ then\ RCV = RCV_0\sqrt{RS}$$

Equation 1-28

In order to keep the value of RCV constant, the applied disturbance *d1, d2 … dN* should satisfy the requirement in *Equation 1-29*:

$$di \in N\left(0, RCV \cdot E(x)\right) \Leftrightarrow di \in N\left(0, \sigma\right), \quad 1 \le i \le N$$

Equation 1-29

Equation 1-29 implies that the same standard deviation value *RCV*E(x)* is applied throughout the whole annual range regardless of the value of *x*—this might, however, lead to a situation where *y1,y2,…,yN* have either negative values or overly large values exceeding rated load when RCV is too large. In order to maintain physical validity of simulation, these negative or over-large values have to be tossed away.

In order to achieve truncations at both upper and lower boundaries of instantaneous load demand, double-truncated normal distribution could be used to model the disturbance. However, since it is difficult to determine both left- and right-truncation points from knowledge of mean and standard deviation, translated left-truncated normal (TLTN) distribution could be applied at both ends to achieve similar effects. For each *xi* value, an instantaneous coefficient of variation *ICV(i)* can be obtained as:

$$ICV(i) = \begin{cases} RCV\dfrac{E(x)}{xi} = \dfrac{\sigma}{xi} & if\ xi < 0.5 \cdot x_{rated}, \\ RCV\dfrac{E(x)}{1-xi} = \dfrac{\sigma}{1-xi} & if\ xi \ge 0.5 \cdot x_{rated}, \end{cases} \quad 1 \le i \le N$$

Equation 1-30

Study shows that the value of coefficient of variation falls into the range of [0.2, 0.97] when truncation point moves from -5 to 5; thus ICV values smaller than 0.2 are corresponded with truncation point -5, which literally equals normal distribution without truncation for *N ≤ 10^4*, while ICV values greater than 0.97 are corresponded with truncation point 5 in the same light.

However, due to considerations of computational efficiency, it is obviously not advisable to apply toss-away method to normally distributed variables as the truncation point takes on relatively large values in the positive half-axis. In order to tackle this issue, an exponential rejection sampling method could be used to approximate truncated normal behavior when truncation point moves beyond 2 (this threshold can be further decreased to 0.45 to speed up computations [32]). The basic algorithm of exponential rejection method for approximating a left-truncated standard normal distribution is described in *Equation 1-31*.

$$\begin{aligned}
&\textit{Assume normal distribution } X \textit{ is left-truncated at value } a, \textit{ and } a \geq 2;\\
&\textit{Then equivalent exponential distribution } Y \textit{ can be obtained via}:\\
&\textit{Do}\\
&\quad \textit{Sample unifromly distributed } u \in U\left[0,1\right]\\
&\quad \textit{Sample exponentially distributed } v \in EXP\left[a\right]\\
&\textit{Loop} \quad \textit{While} \quad u > \exp\left(-\frac{1}{2}\cdot v^2\right)\\
&\Rightarrow \quad y = v + a \;\; \textit{will be statistically equivalent to } x
\end{aligned}$$

Equation 1-31

It should be noted that upper ICV boundary of 0.97 imposes an inherent limitation to TLTN simulation—in fact, the value of this instantaneous coefficient of variation is technically limited to a maximum of 1 due to the nature of exponential approximation (in which mean value equals standard deviation). This makes it difficult to achieve high variations when instantaneous load demand from the deterministic model is close to zero or rated value. Consequently, as the proportion of ICV values greater than 0.97 increases in total, final *RCV* and *E(x)* errors would increase accordingly. As a result, the performance of TLTN algorithm is most satisfactory when:

$$\begin{aligned}
&ICV\left(Min\left(Min(x), Min(1-x)\right)\right) = ICV\left(Min(x, 1-x)\right) = RCV\,\frac{E(x)}{Min(x,1-x)} \leq 0.97\\
&\Rightarrow \quad RCV \leq 0.97\,\frac{Min(x,1-x)}{E(x)} \quad \Leftrightarrow \quad Max(RCV) = 0.97\,\frac{Min(x,1-x)}{E(x)}
\end{aligned}$$

Equation 1-32

Since left-truncation point *a(i)* can be obtained through approximation function $a(i) = appx\_f1\left(ICV(i)\right)$ [1], for any series of load profile data with per-unit values ranging between 0 and 1, the disturbance component *di* for an instantaneous load

[1] *appx_f1(x) = -5 + 10 * Exp(-1.197 * (Abs(x - 0.97)) ^ 0.5 / (x - 0.2) ^ 0.25) + Mod(x)*
*Mod(x) = -0.5838 / ((x - 0.1941) * 28.6533 + 1 / (x - 0.1941) / 28.6533) + 0.102 If x ≤ 0.3918*
*Mod(x) = -1.165 / ((0.969 - x) * 7.194 + 1 / (0.969 - x) / 7.194) + 0.28 If 0.436 ≤ x ≤ 0.933*
*Mod(x) = 0.433 / 0.033 * (x - 0.933) If 0.933 ≤ x ≤ 0.966*
*Mod(x) = 0.433 - 0.233 / 0.004 * (x - 0.966) If 0.966 ≤ x ≤ 0.97*

demand *xi* can be modeled by a left-truncated normal distribution with zero mean and known values of left boundary as well as coefficient of variation. Obviously, this error component can be derived from a left-truncated standard normal (LTSN) distribution via a series of translational and proportional operations. Thus the general procedure of load curve modification can be summarized as Figure 1-20.

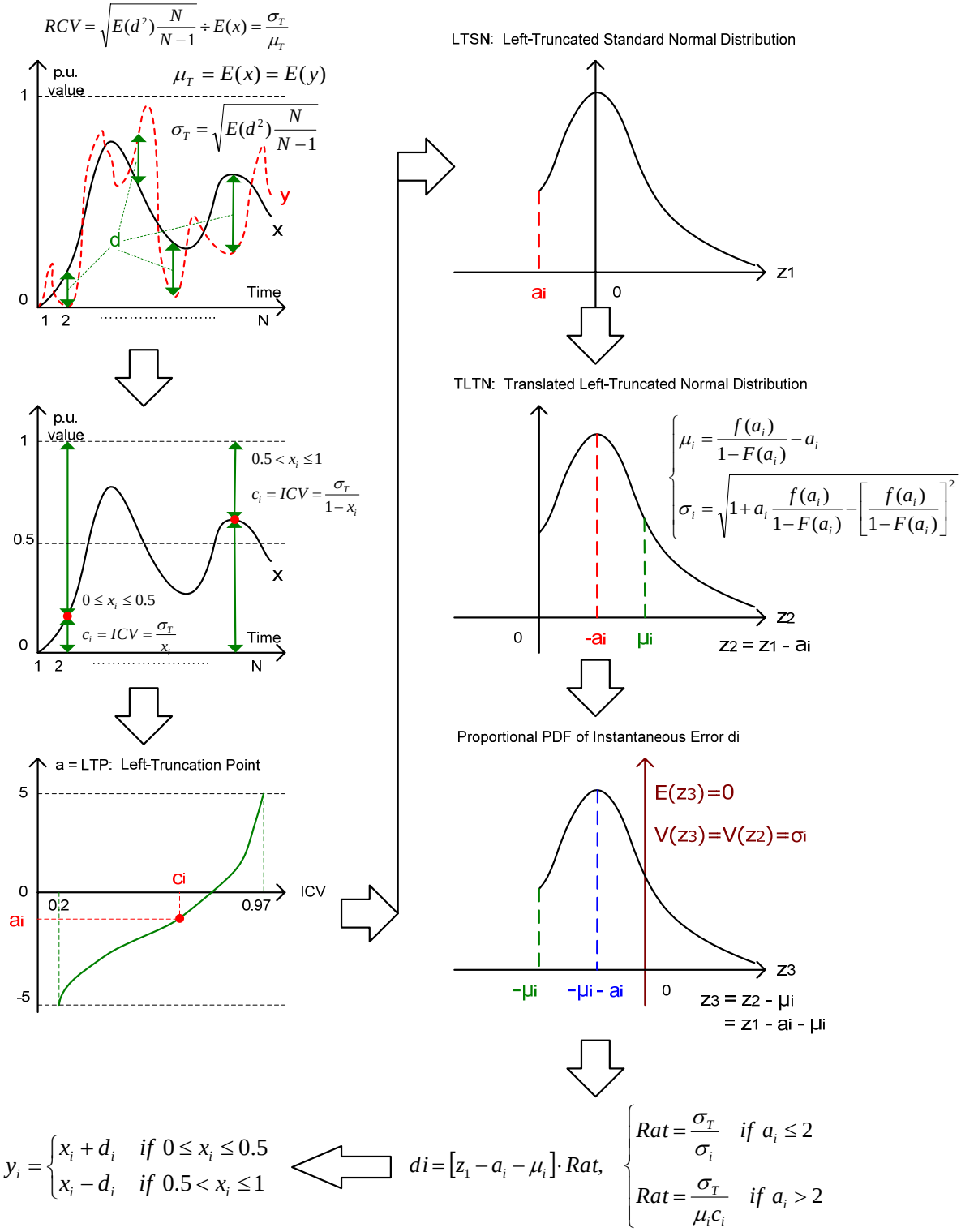

Figure 1-20 Calculation Procedure for Load Curve Modification

As shown in Figure 1-20, the expected average and standard deviation of derived TLTN distribution can be calculated as in *Equation 1-33*.

$$\begin{cases} \overline{\mu}(i) = \dfrac{f(a(i))}{1-F(a(i))} - a(i) \\ \overline{\sigma}(i) = \sqrt{1 + a(i)\dfrac{f(a(i))}{1-F(a(i))} - \left[\dfrac{f(a(i))}{1-F(a(i))}\right]^2} \end{cases}$$

Equation 1-33

With a generated LTSN variable truncated at *a (i)*, the corresponding disturbance *di* for *xi* can be thus obtained from *Equation 1-34*:

$$if\ \ z(i) \in LTSN\ (a(i)), then: \quad di = \left[z(i) - a(i) - \overline{\mu}(i)\right] \cdot \frac{RCV \cdot E(x)}{\overline{\sigma}(i)}$$

Equation 1-34

Figure 1-21 and Figure 1-22 respectively show the weekly and annual load curves after modification for SCL_0 = 1000, *SCL* = 10 (*RS* = 100), RCV_0 = 2%, *RCV* = 20%:

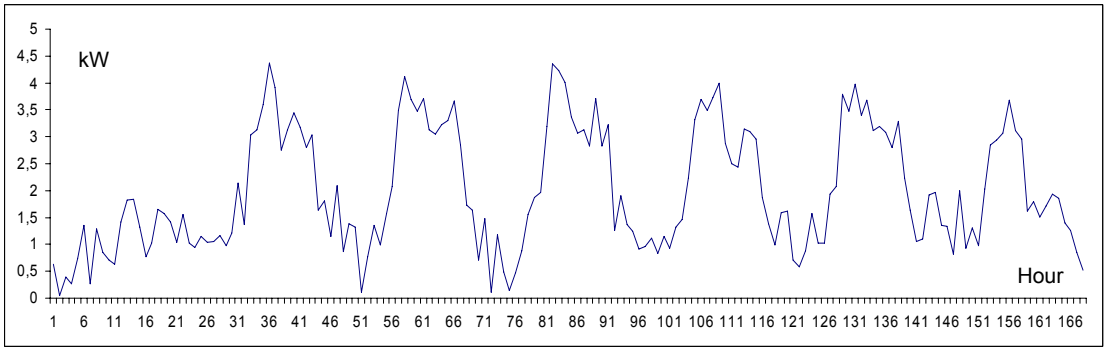

Figure 1-21 Modified Weekly Load Curve of a Commercial Customer

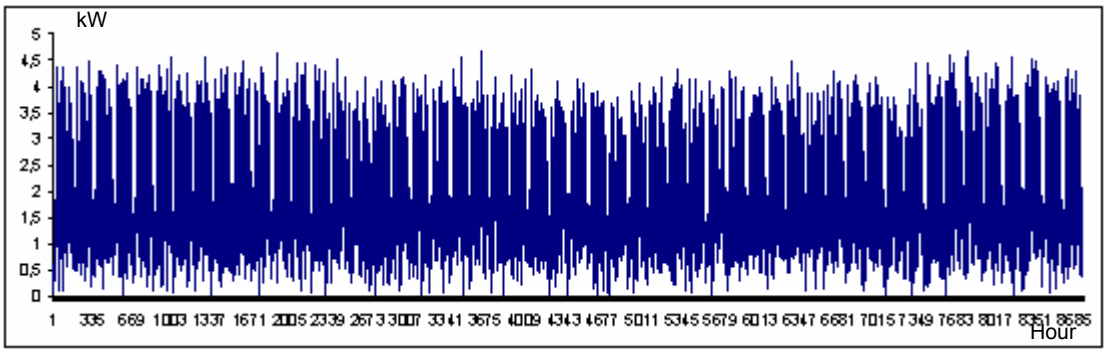

Figure 1-22 Modified Annual Load Curve of a Commercial Customer

With applied load modification approach, two major issues should be noted: (1) since left-truncation instead of double-truncation is deployed to simulate instantaneous error, the right side of truncated normal distribution could theoretically reach infinity, thus modified p.u. instantaneous load demand could (albeit seldom) reach beyond [0, 1], which has to be tossed away; (2) Modeling error will increase as RCV grows larger, in which case either total average or total deviation has to be sacrificed to keep the other value as close to expectation as possible.

1.6 Simulation of a Wind Turbine's Generation Curve

In order to simulate the behavior of wind turbine generation as reasonably as possible, both physical and statistical properties of wind power have to be taken into account. This section gives a brief introduction into both aspects and offers three simulation algorithms as potential alternatives, which are subsequently analyzed, compared and selected.

1.6.1 General Laws on the Variation of Wind Energy

1.6.1.1 The 1/7th Power Law

The 1/7th power law indicates that, given two different altitudes H1 and H2 in a certain location, the corresponding wind speeds V1 and V2 at these two altitudes satisfy *Equation 1-35* [7]:

$$\left(\frac{V1}{V2}\right)=\left(\frac{H1}{H2}\right)^{\frac{1}{7}}$$

Equation 1-35

The correlation is also shown in Figure 1-23.

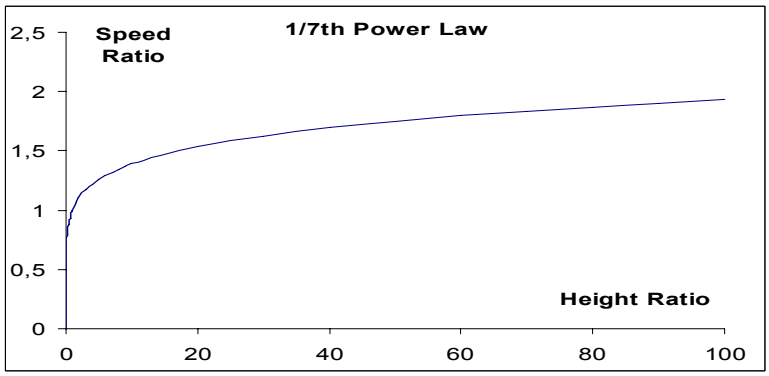

Figure 1-23 the 1/7th Power Law for Wind

This property of wind reveals that, generally speaking, the higher a wind turbine is installed at, the more wind energy it could tap on to convert into electricity—namely, the available wind energy is proportional to the 3/7th root of turbine altitude (which is explained further in section 2.6.1.2). Therefore, such a correlation serves as the basic motive for engineers to design wind turbines installations as high as technological and economical conditions permit.

1.6.1.2 Wind Speed and Wind Power Density

As mentioned in section 2.6.1.1, available wind energy increases with increasing wind speed. Their relationship can be explained by *Equation 1-36* [7]:

$$PD = \frac{P}{S} = \frac{1}{2}\rho \cdot V^3, \quad PD - Power\ Density\ (W/m^2), V - Wind\ SpeedPD\ (m/s)$$
$$P - Power\ (W), S - Area\ (m^2), \rho - Air\ Density\ (kg/m^3)$$

Equation 1-36

The value of air density *ρ* depends on a number of environmental variables—namely altitude H and temperature t. It can be determined by *Equation 1-37* [7]:

$$\rho = \frac{M \cdot p_0}{R \cdot (t + T_0)} \cdot \left(1 + \frac{L \cdot H}{T_0}\right)^{-\frac{g \cdot M}{R \cdot L}}, \quad R, M, L, T_0, p_0, g = Const\ (attached\ in\ Appendix)$$

Equation 1-37

Figure 1-24 and Figure 1-25 respectively show the correlations between wind power density and wind speed at H = 10m and H = 50m:

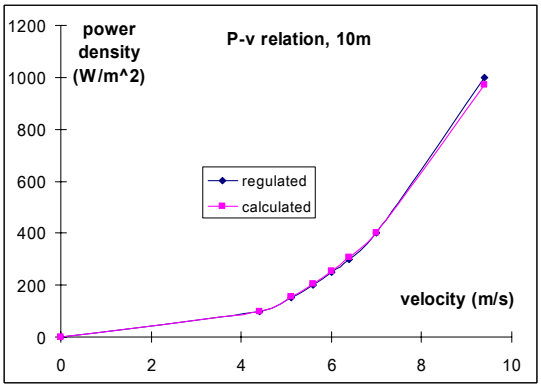

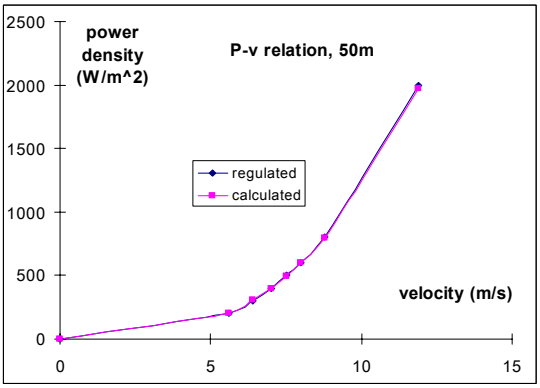

Figure 1-24 PD-V Curve, H=10m

Figure 1-25 PD-V Curve, H=50m

It should be noted, however, that in practice wind speeds are generally hourly or quarterly average values *E (V)* calculated from a group of measured data *V1, V2 … VN* following Weibull distribution [34]. In this case, the equation *PD = 0.5* ρ*V*^{3} can not be applied directly since the average of *V1*^{3}*, V2*^{3}*… VN*^{3} does not equal *E (V)* ^{3}. An extra coefficient *K* (which is taken as 1.91 in this report) has to be multiplied to make the equation usable, namely [7]:

$$E(V^3) = K \cdot E(V)^3 \Rightarrow \quad E(PD) = \frac{1}{2}\rho \cdot K \cdot E(V)^3$$

Equation 1-38

1.6.1.3 The Conversion Efficiency of a Wind Turbine

The conversion efficiency reflects a wind turbine's ability to convert available wind power into electricity, its relationship with wind speed is shown in Figure 1-26 [7]:

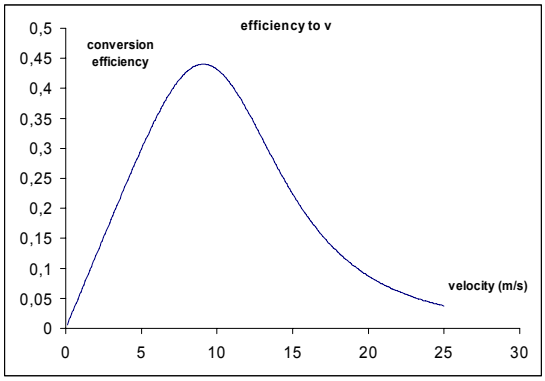

Figure 1-26 Efficiency-Speed Curve

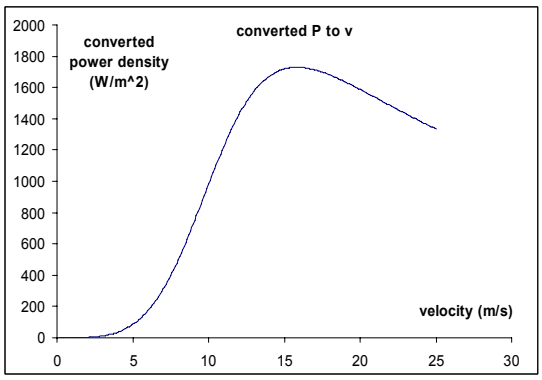

Figure 1-27 PD Output-Speed Curve

It can be seen that conversion efficiency (calculated from η = *appx_f3 (v)*, function attached in appendix) reaches its maximum when wind speed is about 9 m/s. This efficiency factor η can be combined with the equation obtained at the end of section 2.6.1.2 to model the actual power output of a wind turbine in relation to wind speed. This is shown in Figure 1-27 and can be expressed mathematically as:

$$\overline{P\_out} = \frac{1}{2}\rho \cdot K \cdot \eta \cdot E(V)^3 \cdot \pi \cdot R^2, \quad R - radius\ of\ \ rotor$$

Equation 1-39

Figure 1-27 also shows that total energy output reaches maximum when wind speed is around 16 m/s.

1.6.2 Relative Time Dependency of Wind Energy Output

In order to determine the time dependency of wind energy, measured annual data can be examined respectively under daily, weekly, monthly, and seasonal scales to determine whether or not the energy output has time-related behaviors. The plots under these different scales (attached in Appendix) show greatest tendency at daily and seasonal levels. Therefore only these two cases are discussed in this section.

1.6.2.1 Short-term (Daily) Time Dependency

Figure 1-28 and Figure 1-29 respectively show the hourly values in a day averaged over 365 days in a year, and the daily values in a year averaged over 24 hours in a day.

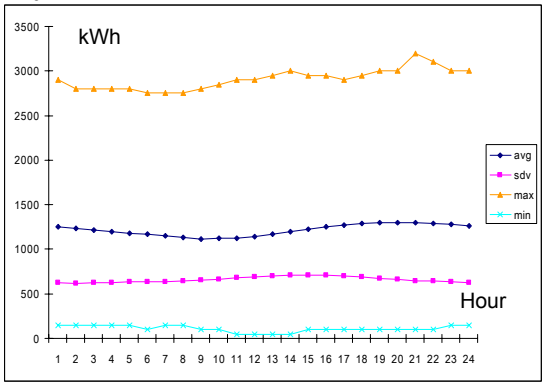

Figure 1-28 Hourly Averages for a Day

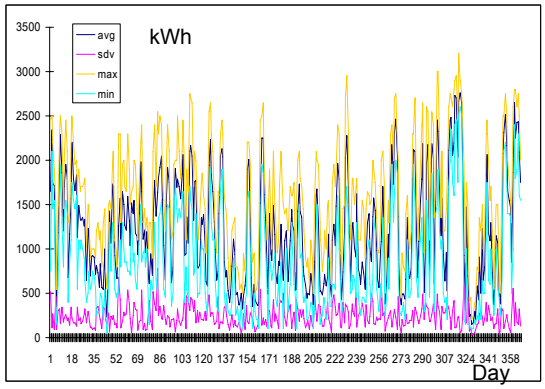

Figure 1-29 Daily Averages for a Year

Figure 1-28 discloses that the average, standard deviation, maximum and minimum values of hourly energy output in a day vary only slightly from hour to hour, thus making it obvious that the hourly turbine output in a day has no strong dependency on which hour it is attached to. Therefore, no obvious daily cycles can be observed for the generation data of a wind turbine. Figure 1-29, on the other hand, reveals that daily average energy outputs can be seen as almost random over a year, which means each day can be viewed as almost identical in stochastic sense. Therefore, it can be concluded that the energy output of a wind turbine has no significant short-term time dependency—at least not at daily levels.

1.6.2.2 Long-term (Seasonal) Time Dependency

Energy output of a wind turbine, when examined under a seasonal scale, shows quite different behaviors from daily cases. Figure 1-30 and Figure 1-31 summarize this phenomenon by listing the relative seasonal average and standard deviation values of five different cases—one turbine site in Germany, one in Spain, and three consecutive annual data sets of a US site in Wisconsin Madison [7].

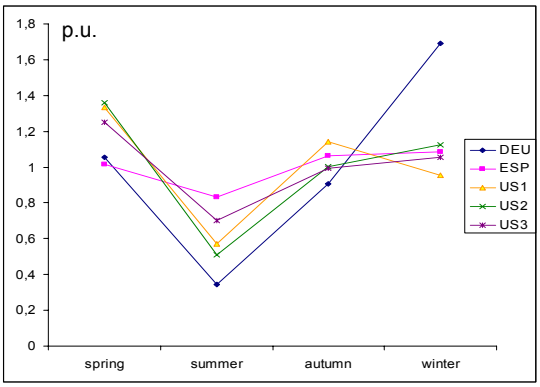

Figure 1-30 Seasonal Relative Average

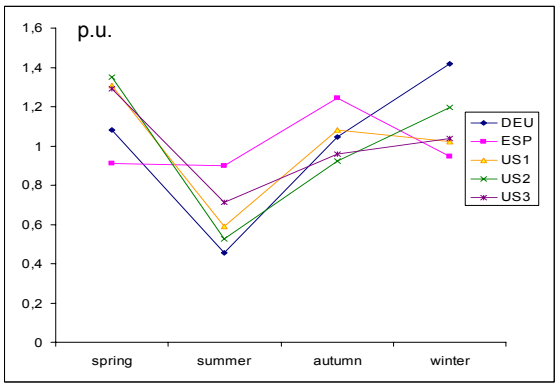

Figure 1-31 Seasonal Standard Deviation

Since all regions listed above are located in the northern hemisphere, the definition of seasons obeys the same meteorological rule as shown in Table 1-3:

Spring	Summer	Autumn	Winter
Mar., Apr., May.	Jun., Jul., Aug.	Sept., Oct., Nov.	Dec., Jan., Feb.

Table 1-3 Definition of Seasons in Northern Hemisphere

Figure 1-30 reveals that for all studied cases, summer average always proves to be the minimum value among all seasons. The maximum value, however, appears in winter for two European cases and spring for all US cases. The other two seasons left in between max and min (spring and autumn for Europe, autumn and winter for US) may switch position with each other according to the multi-year US data. Finally, standard deviation generally follows the change of seasonal average with only one exception of the Spanish winter case.

1.6.3 Simulation Methods: Description and Comparison

1.6.3.1 Simulation by Weibull Distribution

The simplest way to simulate the annual data of a wind turbine is to generate a series of Weibull random variables that share the same shape and scale parameters as the original series [35]. Figure 1-32 and Figure 1-33 show the comparison of PDF and CDF curves of original and simulated data:

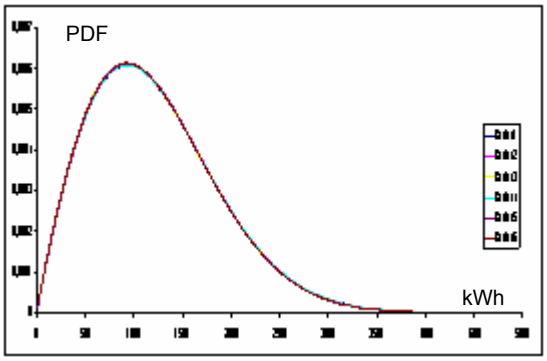

Figure 1-32 PDF of Weibull Simulation

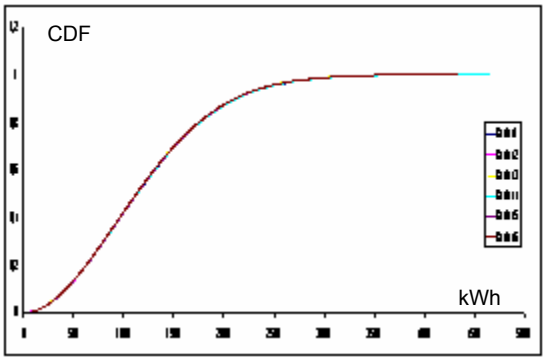

Figure 1-33 CDF of Weibull Simulation

Methods for parameter estimation and generation of Weibull random numbers are explained in section 2.2.4. This simulation approach assumes, however, that no correlation exists between neighboring data points, which ignores the relatively continuous nature of wind power, thus the simulated data can only be viewed as a statistical approximation rather than a physical one.

1.6.3.2 Simulation by Immediate Variation and Truncation (IVT)

In order to tackle the continuity issue of turbine output, a variable δ can be introduced to describe the immediate variation between two neighboring data points:

$$\delta_i = \frac{x_{i+1} - x_i}{E(x)}, \quad 1 \le i \le N-1$$

Equation 1-40

The statistical feature of δ is shown in Figure 1-34:

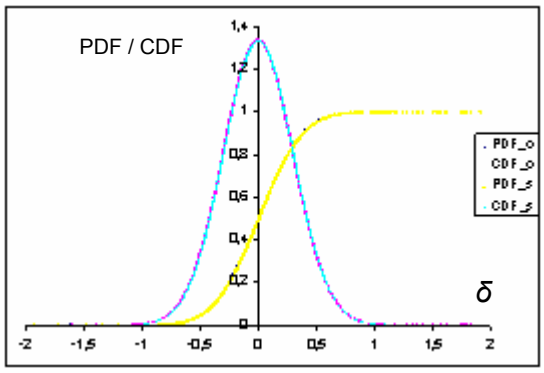

Figure 1-34 PDF and CDF of δ

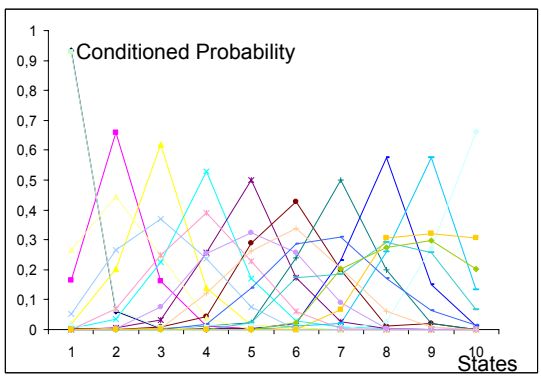

Figure 1-35 Markov Evaluation of IVT

By identifying the parameters of δ under normal distribution, a simple algorithm can be built to simulate turbine energy output: given a random starting value of x, the next data point is calculated as $x + \delta$—if $x + \delta$ value falls out of the given max-min range, the value is tossed out and calculation is repeated until boundary conditions are met. This algorithm yields more physically reasonable results than Weibull simulation; but since δ has been assumed to be independent from the value of x_i, simulated data will prove inaccurate when evaluated under Markov criteria (shown in Figure 1-35).

1.6.3.3 Simulation by the Markov Chain Method

For simulation of wind data, both 1st order [36] and 2nd order [28] Markov chains can be used (description of algorithm can be found in section 2.3), the comparison of original and simulated state parameters of the 1st order case is listed in Figure 1-36 and Figure 1-37 as a reference.

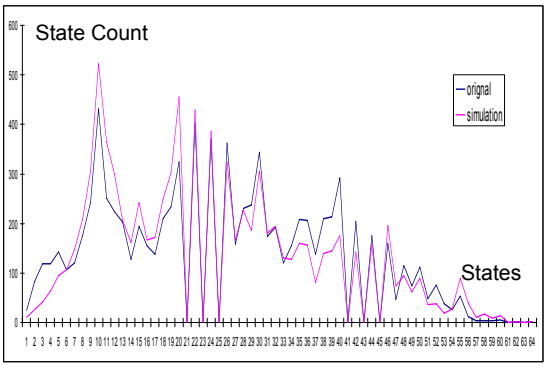

Figure 1-36 Markov State Counts

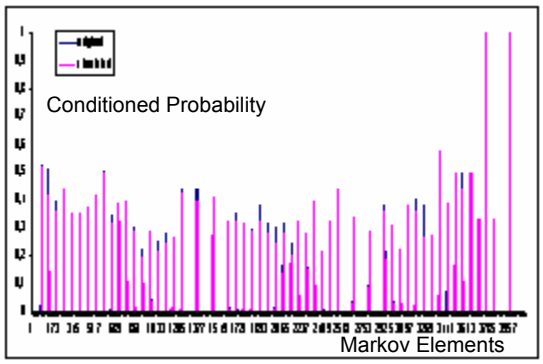

Figure 1-37 Linearized Markov Matrix

1.6.3.4 Comparison of Different Simulated Methods

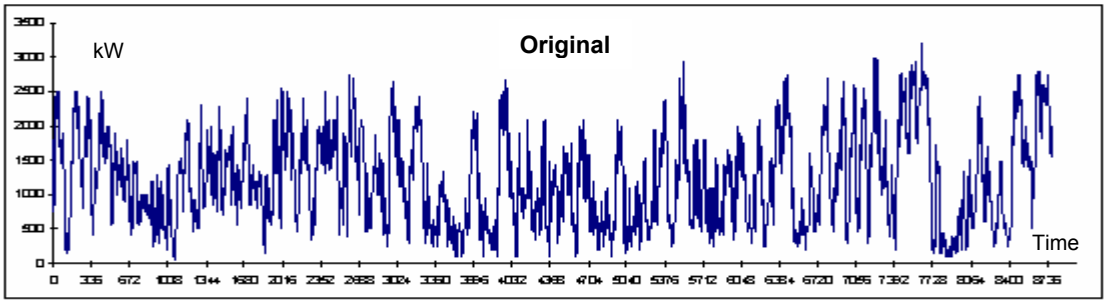

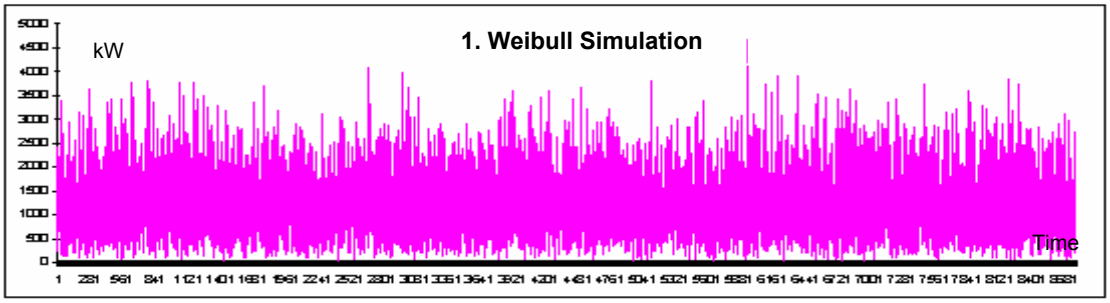

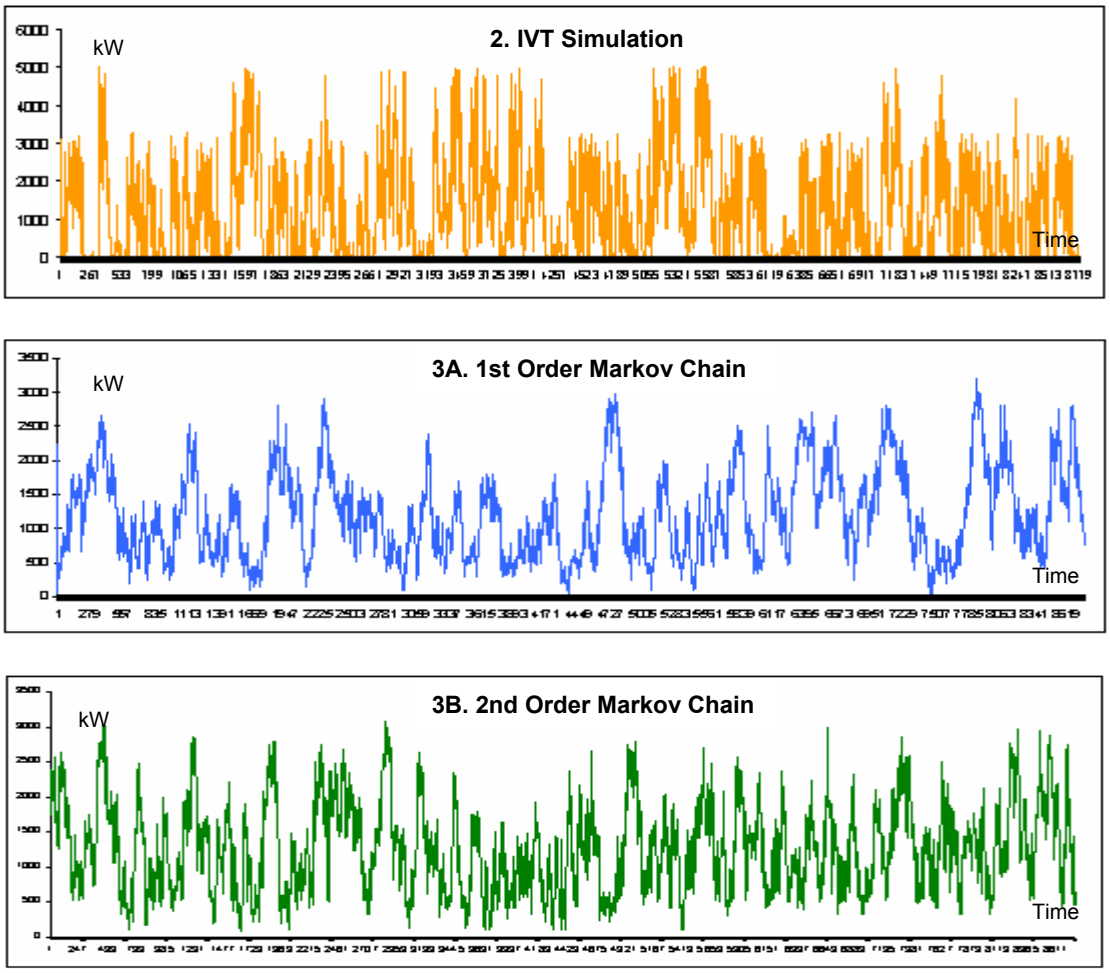

Figure 1-38 Comparisons of Simulated Annual Curves

Figure 1-38 shows that 2nd order Markov chain method yields the physically closest approximation to original curve, while Weibull distribution method tends to generate results that almost evenly permeate the whole value range and IVT method loses a large proportion of the shape characteristics of original data. The difference between 1st order and 2nd order Markov chains are relatively small, thus 1st order Markov simulation can be considered as a possible alternative when computational capability is unable to meet the requirements of 2nd or even higher order Markov chain calculations.

1.6.4 Conclusion

The 2nd order Markov chain method is adopted as finally used solution. However, generated data has to be checked against the seasonal requirements first — after manual selection or relocation of seasonal data groups, the processed data can be eventually used for simulation purposes.

The accuracy of Markov chain simulation is primarily determined by the size S of discrete state space used for calculation. As long as sample scales for each state value do not drop below a certain threshold (which reduces the statistical significance of the corresponding state value), an increase of S will mostly lead to higher simulation accuracy. However, the computational time for an *N-th* order Markov chain algorithm is proportional to S^{N+1}, thus larger S values will inevitably lead to drastic

increase of computational efforts for higher order Markov chain algorithms. Currently the 1st order Markov chain simulations use $S = 64$, while 2nd order Markov chain simulations assume $S = 33$.

It should be noted that the Markov parameters obtained from original data might have slight changes from year to year [7], which is shown in Figure 1-39. Decrease of S could reduce this difference, but then simulation accuracy will be compromised correspondingly. If sufficient annual data in consecutive years is available, then analysis could be done to disclose how the parameters change over different years. Due to obvious limitations on data availability, this possibility is not discussed in this report.

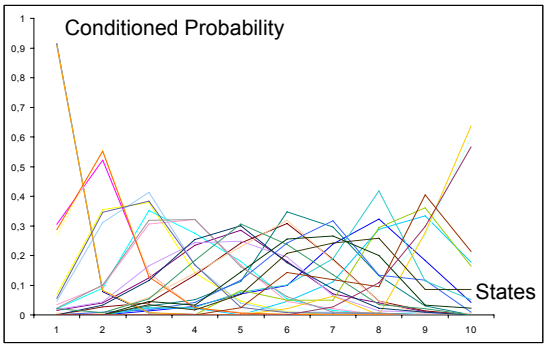

Figure 1-39 Variation/A of Markov Matrix

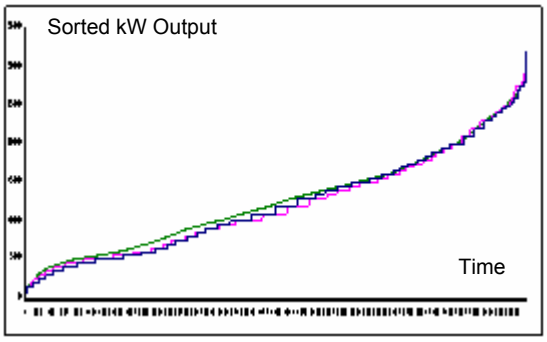

Figure 1-40 Continuous WT Gen. Curves

Finally, the original and simulated (using 1st and 2nd order Markov chain methods) continuous generation curves of a wind turbine are shown in Figure 1-40 (which can also been seen as rotated CDF curves), obviously the simulated data can be seen as equivalent to original in both statistical and physical senses.

1.7 Simulation of a Photovoltaic Module's Generation Curve

The energy output of a PV module is similar to that of a wind turbine in the sense that both exhibit random behavior for determining the instantaneous value of a specific point of time; however, the generation curve of a PV module is more strictly time-dependent than a wind turbine's curve, which makes stochastic simulation relatively difficult due to the existence of multiple physical requirements [37]. Combination of different approaches is therefore necessary to generate physically reasonable results that are simultaneously equivalent to original data in statistical sense. This section is primarily focused on revelation of the physical trends of a PV generation curve as well as the introduction of a two-stage simulation algorithm, which is presented in full detail.

1.7.1 Solar Irradiance and Energy Output of a PV Cell

The generation curve of a PV module is mainly determined by the amount of solar irradiance received at the site of installation. The irradiance level depends on a wide range of factors including geographical (such as altitude and latitude), meteorological (such as temperature and cloudiness), and temporal (such as daily and seasonal changes) ones etc. [7]; some of these factors—mainly geographical—are more directly linked to the general shape of a PV generation curve, while others primarily

influence the instantaneous behavior of energy output. The impacts of the first type of time-invariant factors are generally not covered in this report due to limitations on scope of study, which leaves meteorological and temporal influences as main tests of discussion—this section will first deal with the meteorological aspect.

Since not all influencing meteorological variables can be measured or estimated to model the instantaneous power of a PV module, they can be considered as invisible system input data that are to be evaluated by the output energy curve using a statistical model. This report views the aggregated meteorological data as one time-dependent random variable, thus simplifies the requirements on modeling. Due to the instantaneous nature of meteorological influence, the PV system is examined under its smallest periodic cycle—the daily cycle.

In order to explain the significance of meteorological influence, two typical daily PV generation curves are shown in Figure 1-41 and Figure 1-42 as examples, which are respectively measured under sunny irradiation (SI) and diffuse irradiation (DI) conditions.

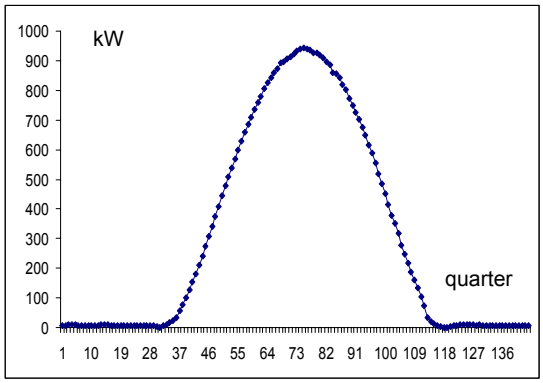

Figure 1-41 PV Daily, Sunny Irradiation

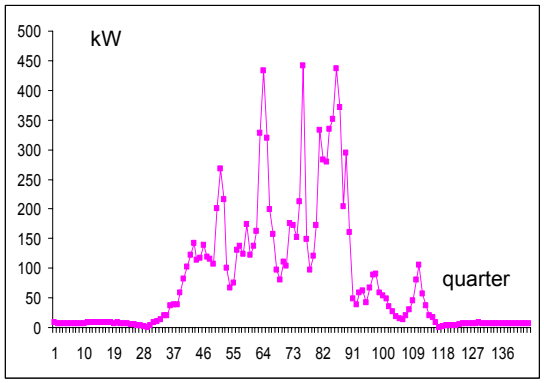

Figure 1-42 PV Daily, Diffuse Irradiation

Obviously, weather conditions can manipulate the shape of a daily PV generation curve to a relatively large extent, which makes it difficult to define a standard daily curve as universal model. This explains why hour-to-hour analysis is necessary for simulation of daily values (detailed in section 2.7.3.2).

1.7.2 Relative Time Dependency of Solar Energy Output

Aside from meteorological influence, temporal factors play quite a significant role in shaping the generation curve of a PV module. In comparison to the behavior of a wind turbine, PV curves show double periodicity in both short-term (daily) and long-term (annual) time scales [38]. This can be seen from Figure 1-43 and Figure 1-44, which give the average, standard deviation, maximum, and minimum values of a day-to-day annual curve (Figure 1-43) and a quarter-to-quarter daily curve (Figure 1-44).

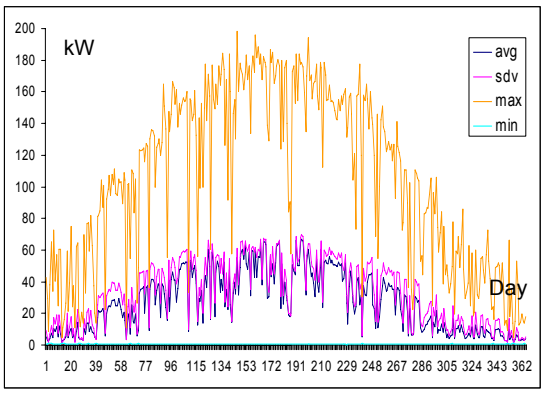

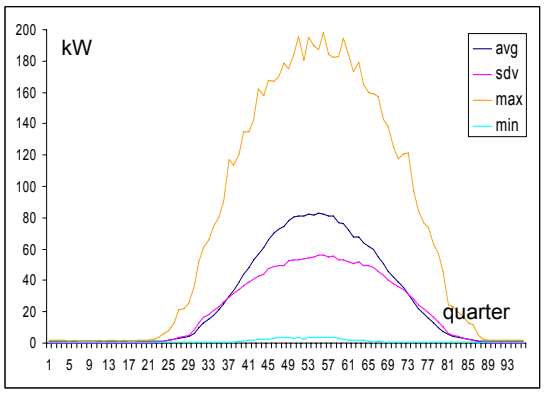

Figure 1-43 Annual PV Generation Trend Figure 1-44 Daily PV Generation Trend

The annual trend discloses that energy output rises to peak in the first half of year and falls to minimum in the second half despite strong oscillations. The actual rates of slope for rising and falling might depend on the location of PV module and vary from year to year [8].

The daily trend, on the other hand, appears to be a relatively continuous, bell-shaped curve with maximum output at noon and close-to zero minimum values during night. However, the averaged trend is a summary of curves under both sunny irradiation and diffuse irradiation conditions, thus the actual generation curve of a specific day might vary significantly from the averaged one [39]. In addition, the starting and ending hours of solar irradiation in a day (determined by daily length of night) change over different months and seasons of a year, therefore the shape of a daily curve is also related to the value of average energy output of that day—this phenomenon leads to a significant improvement of simulation effect, which is detailed in 2.7.3.2.

1.7.3 Simulation of PV Generation Using a Two-stage Method

1.7.3.1 Stage 1: Simulation of Daily Average Values in a Year

As already mentioned in section 2.7.2, the day-to-day annual PV generation curve can be seen as the combined result of an approximated annual trend (AAT) curve and an error (ERR) component with certain stochastic features. In order to obtain the approximated annual trend curve, the following algorithm in *Equation 1-41* can be applied to smooth out the originally oscillating plot:

$$\textit{Assume } x(1), x(2), \cdots x(365) \textit{ as original day-to-day annual data, Let}:$$

$$\begin{cases} y_1(1)=\dfrac{\sum_{i=1}^{3}x(i)}{2},\ y_1(2)=\dfrac{\sum_{i=1}^{3}x(i)}{3},\ \cdots,\ y_1(364)=\dfrac{\sum_{i=1}^{3}x(i+362)}{3},\ y_1(365)=\dfrac{\sum_{i=1}^{2}x(i+363)}{2} \\ y_2(1)=\dfrac{\sum_{i=1}^{3}y_1(i)}{2},\ y_2(2)=\dfrac{\sum_{i=1}^{3}y_1(i)}{3},\ \cdots,\ y_2(364)=\dfrac{\sum_{i=1}^{3}y_1(i+362)}{3},\ y_2(365)=\dfrac{\sum_{i=1}^{2}y_1(i+363)}{2} \\ \cdots \\ y_N(1)=\dfrac{\sum_{i=1}^{3}y_{N-1}(i)}{2},\ y_N(2)=\dfrac{\sum_{i=1}^{3}y_{N-1}(i)}{3},\ \cdots,\ y_N(364)=\dfrac{\sum_{i=1}^{3}y_{N-1}(i+362)}{3},\ y_N(365)=\dfrac{\sum_{i=1}^{2}y_{N-1}(i+363)}{2} \end{cases}$$

Equation 1-41

The algorithm, in effect, yields the following result:

$$y_N(i) = \frac{y_{N-1}(i-1)+y_{N-1}(i)+y_{N-1}(i+1)}{3}$$
$$= \frac{y_{N-2}(i-2)+2y_{N-2}(i-1)+3y_{N-2}(i)+2y_{N-2}(i+1)+y_{N-2}(i+2)}{9}$$
$$= \frac{y_{N-3}(i-3)+3y_{N-3}(i-2)+6y_{N-3}(i-1)+7y_{N-3}(i)+6y_{N-3}(i+1)+3y_{N-3}(i+2)+y_{N-3}(i+3)}{27}$$
$$\ldots$$

Equation 1-42

After *N = 180* cycles, the smoothed-out annual (SMO) curve will become steady and ready for approximation. By applying least square estimation approach, the general trend curve can be obtained as a polynomial function of the day of year: *x_AAT = appx_f4 (D)*. Consequently, the error component can be extracted from the difference of original (ORG) curve and approximated annual trend (AAT) curve: *x_ERR =ext (x_ORG, x_AAT)*. Figure 1-45 and Figure 1-46 respectively show the procedure and result of this algorithm:

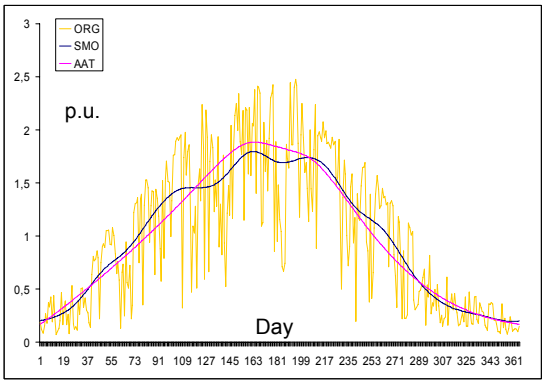

Figure 1-45 ORG, SMO, AAT Curves

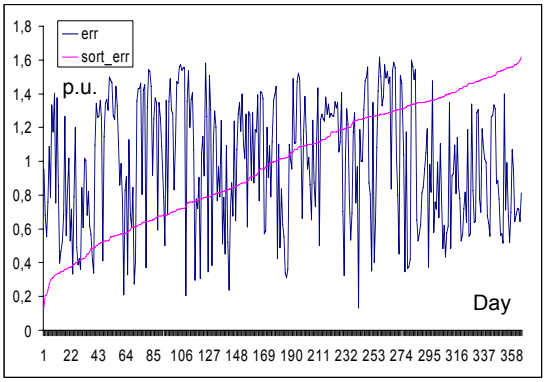

Figure 1-46 ERR and Sorted ERR Curves

By proper selection of extraction function *ext*, the ERR component can be statistically decoupled from the corresponding values of AAT curve. Thus 1st order Markov chain method can be directly applied to the ERR component, which yields a simulated error (SER) curve that can be combined with AAT data to generate final annual simulation (SIM) result: *x_SIM = cmb (x_SER, x_AAT)*—the combination function *cmb* can be seen as the inverse function of *ext* (the expressions of both functions are attached in appendix). The original and simulated day-to-day annual data in both unsorted and sorted orders are presented in Figure 1-47 and Figure 1-48:

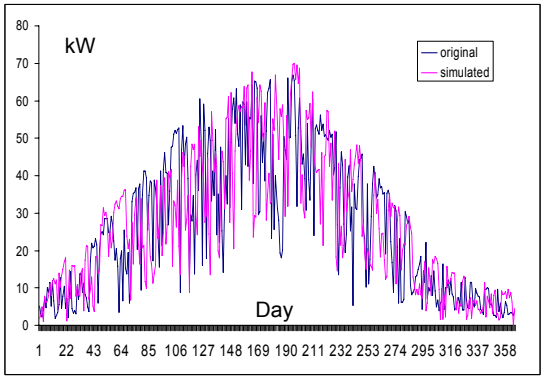

Figure 1-47 Annual ORG & SIM Curves

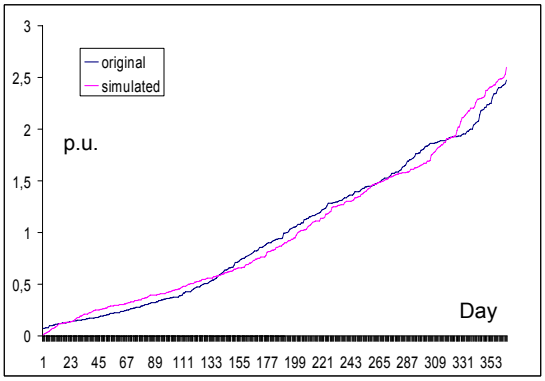

Figure 1-48 Sorted ORG & SIM Curves

Figure 1-48 reveals that relatively large deviations occur at higher daily average values, while at the lower end requirements on minimum daily average—if applicable—might be difficult to be met without further modifications to the currently-used algorithm.

1.7.3.2 Stage 2: Simulation of Hourly Values in One Day

As already mentioned in section 2.7.2, the trend curve approximation method (used in section 2.7.3.1) can not be applied to the daily case since the uncertainty of starting and ending hours of irradiation in a day makes it difficult to use a standard curve for all times of year. Therefore the simulation for relative hourly values (RHV, hourly energy output divided by daily total) in a day is based on the statistical analysis of each separate hour. Figure 1-49 shows the accumulated daily RHV curves of half a year. Obviously the starting hour of solar irradiation varies from 6 to 9, while the ending hour changes from 19 to 22.

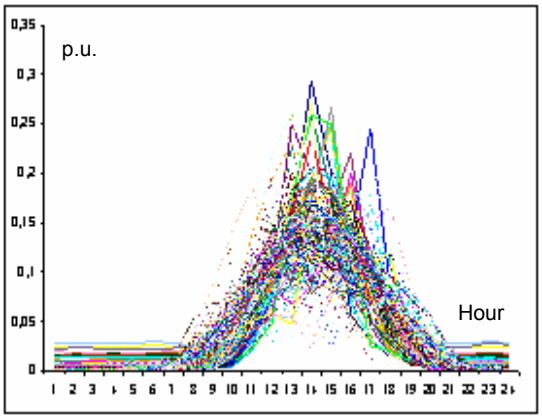

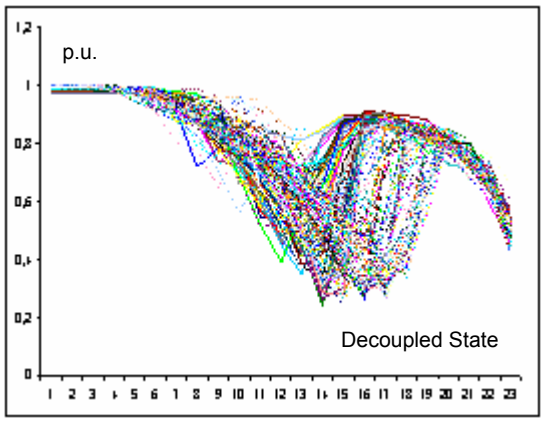

Figure 1-49 Daily RHV Curves (1/2 Year) Figure 1-50 Daily DEV Curves (1/2 Year)

However, direct stochastic modeling of the 24 RHV data series in a day lead to an obvious problem: if all the RHV simulation data are generated independent from each other, no mechanism will ensure the sum of all 24 values will, by definition of RHV, equal 1. Naturally this requirement reflects the coupling of 24 RHV variables, thus in order to make independent stochastic modeling and simulation possible for different RHV's, the decoupling algorithm introduced in section 2.4 should be applied to convert the 24 RHV variables into a set of 23 decoupled equivalent variables (DEV). Typical daily DEV curves of half a year are shown in Figure 1-50.

With obtained DEV data, a case-to-case analysis can be performed to study the stochastic behavior of each DEV to identify the type of distribution it belongs to as well as the characterizing parameters that can be used to describe the DEV's behavior. However, this method still cannot tackle the problem of daily irradiation duration, which varies according to relative daily average (RDA, daily average value divided by total annual average) energy output. Therefore, it is necessary to sort and group obtained DEV data according to corresponding RDA levels before performing stochastic analysis and simulation. Currently six RDA levels are used for segmenting DEV data into 6*23 = 138 groups, they are defined respectively as:

Level 1: RDA < 0.27 Irradiation Interval = 9:00 – 19:00 (approximately)

Level 2: 0.27 ≤ RDA < 0.65 Irradiation Interval = 8:00 – 20:00 (approximately)

Level 3: 0.65 ≤ RDA < 1.2 Irradiation Interval = 7:30 – 20:30 (approximately)

Level 4: 1.2 ≤ RDA < 1.73 Irradiation Interval = 7:00 – 21:00 (approximately)

Level 5: 1.73 ≤ RDA < 2.18 Irradiation Interval = 6:30 – 21:30 (approximately)

Level 6: RDA ≥ 2.18 Irradiation Interval = 6:00 – 22:00 (approximately)

The Daily RHV curves under RDA levels 1 and 6 are shown respectively in Figure 1-51 and Figure 1-52. It can be seen that both the interval of daily irradiation and the shape of daily RHV curves are affected by RDA level, thus different segments of one original DEV series could have quite different stochastic behaviors from each other.

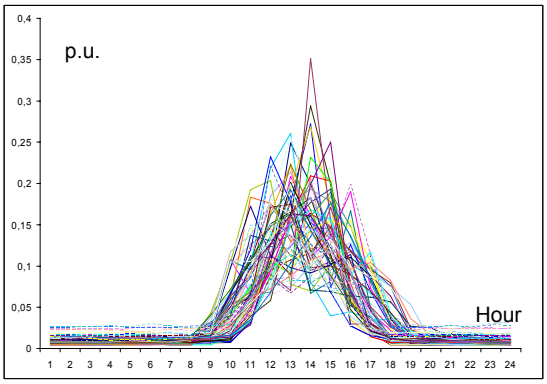

Figure 1-51 Daily RHV at RDA Level 1

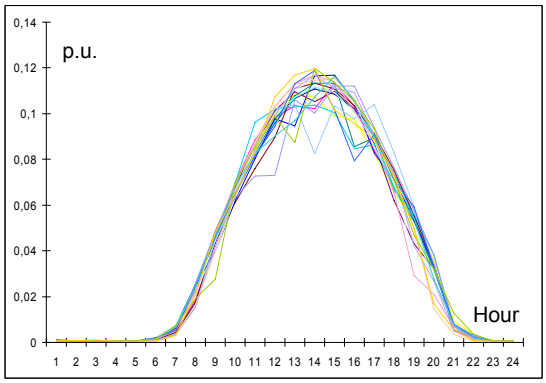

Figure 1-52 Daily RHV at RDA Level 6

It should be noted, however, that neither the number of RDA steps nor the specific RDA boundary values for each level have to be fixed at what is described above—the location of PV module and availability of operational data can cause variations in both. Case-specific analysis should be carried out to adjust RDA level descriptions to the actual running environment.

The segmented 6*23 groups of DEV data can thus be analyzed separately for determining their statistical features. Study reveals that a majority of the data exhibits Beta distribution characteristics, thus for each group of data two shape factors α and β are calculated from average and standard deviation, which yields 2*138 characterizing parameters that can be used to describe the statistical properties of DEV values.

Simulation procedure for DEV can thus be performed by creating Beta distribution variables (algorithm introduced in section 2.2.6 and 2.2.5) that use α and β values selected from the 2*6*23 characterizing parameters of original DEV data. Both RDA level (1—6) and serial of DEV (1—23) serve as the selection criteria of α and β, and a total number of 365*23 = 8395 DEV data entries should be created by utilizing the annual simulation data (obtained in section 2.7.3.1).

Due to the limitation of calculation capacity, the current algorithm for generating Beta distribution variables become less efficient when the value of α and β reaches beyond 5000. Thus when α and β values exceed this boundary, uniform distribution

variables are generated instead in given max-min ranges to approximate original Beta distribution variables.

Figure 1-53 to Figure 1-56 show the original and simulated curves of the 7th and 17th DEV data over 365 days of a year. It can be seen that simulation results for DEV with smaller deviations (such as DEV 7) generally turn out to be more similar to original than those with larger DEV variations (such as DEV 17).

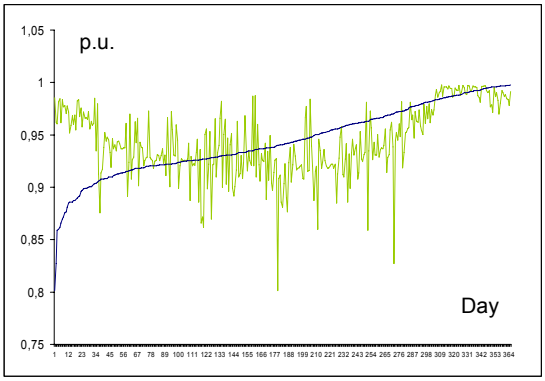

Figure 1-53 Original Curves, DEV 7

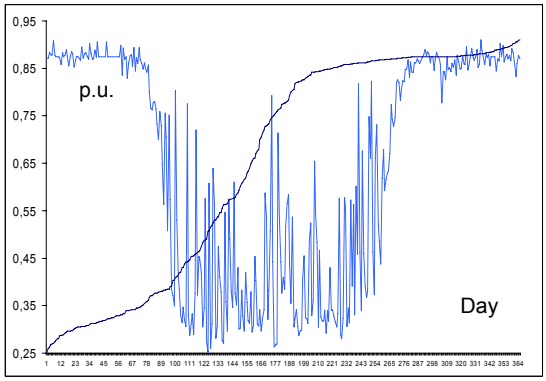

Figure 1-54 Original Curves, DEV 17

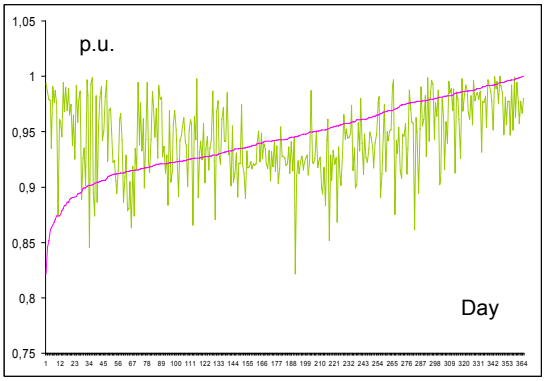

Figure 1-55 Simulated Curves, DEV 7

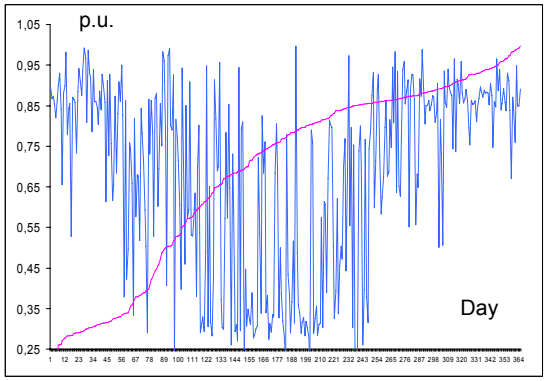

Figure 1-56 Simulated Curves, DEV 17

The sorted original and simulated curves of DEV 7 and DEV 17 are compared in Figure 1-57 and Figure 1-58. Obviously the simulation result of DEV 7 also proves to more consistent with original than that of DEV 17 does after sorting.

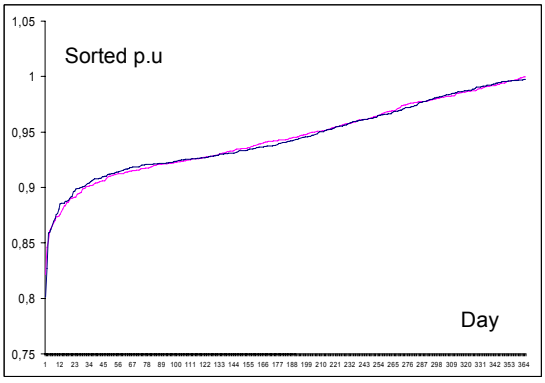

Figure 1-57 Sorted ORG & SIM, DEV 7

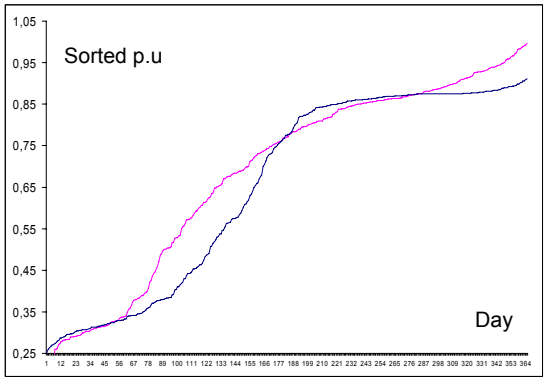

Figure 1-58 Sorted ORG & SIM, DEV 17

After obtaining simulated DEV series, the sizing-up algorithm introduced in section 2.4.3 can be used to calculate corresponding RHV data. Following Figure 1-59 to Figure 1-62 shows the original and simulated curves of 24*RHV at 9:00 am and 12:00 am over 365 days in a year:

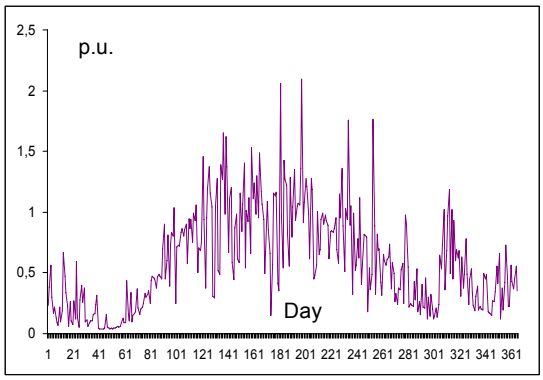

Figure 1-59 Original Curve, 24*RHV 9

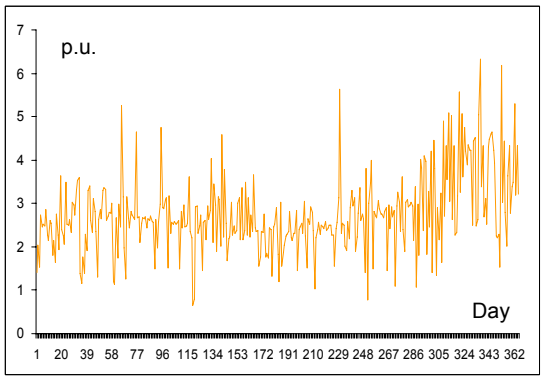

Figure 1-60 Original Curve, 24*RHV 12

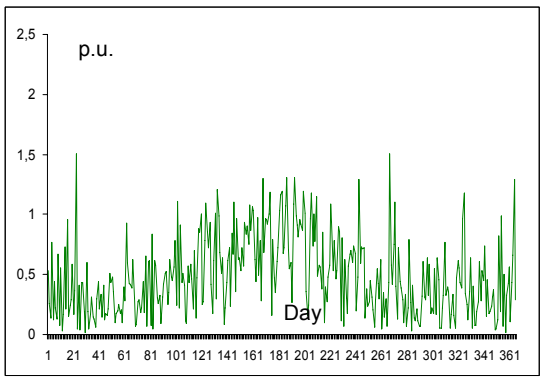

Figure 1-61 Simulated Curve, 24*RHV 9

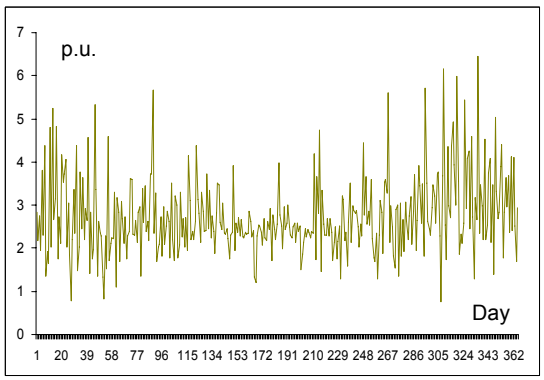

Figure 1-62 Simulated Curve, 24*RHV 12

Comparison shows that simulated data around daily peak output (12:00 am) appears to be closer to original in terms of curve shape when compared with data of lower energy levels (9:00 am). Figure 1-63 and Figure 1-64 showing the sorted data of original and simulated 24*RHV series at 9:00 am and 12:00 am also support this conclusion:

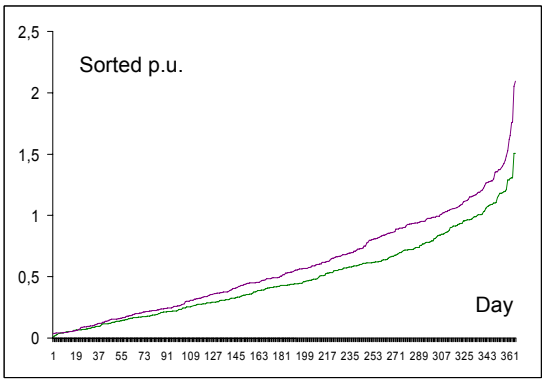

Figure 1-63 Sorted ORG and SIM, RHV9

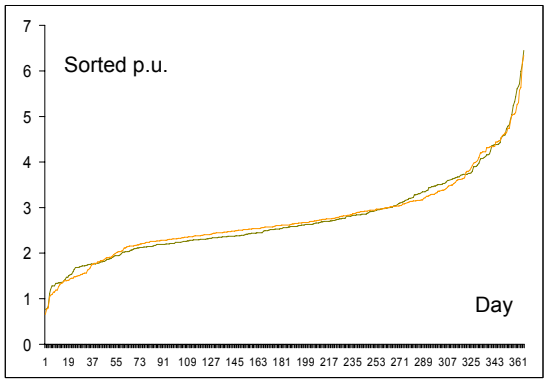

Figure 1-64 Sorted ORG and SIM, RHV12

In Figure 1-65 to Figure 1-68, ten daily curves showing 24*RHV are respectively sampled from original and simulated data. Five of the samples are taken in January, while the other five are taken in June. Obviously Lower RDA levels (1 or 2) can be expected from the first five samples (Figure 1-65 and Figure 1-67); while higher RDA levels (5 or 6) apply to the later (Figure 1-66 and Figure 1-68). Relatively consistent behaviors can be seen between original and simulated curves in terms of solar irradiation interval and general curve shapes, which should be largely attributed to the adoption of RDA segmentation method.

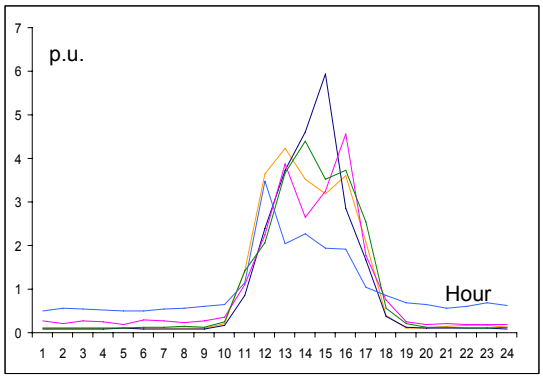

Figure 1-65 Original, Day 19-23, Jan

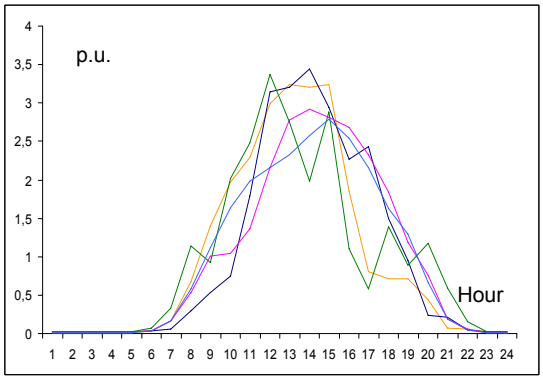

Figure 1-66 Original, Day 153-157, Jun

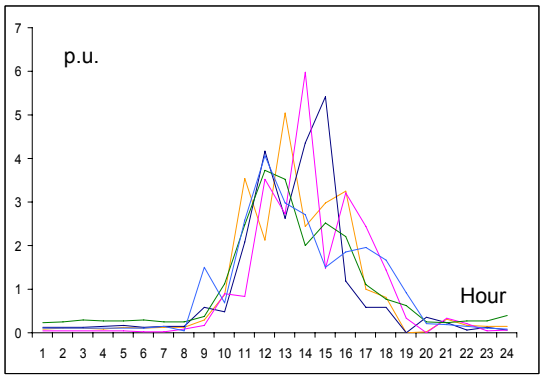

Figure 1-67 Simulated, Day 19-23, Jan

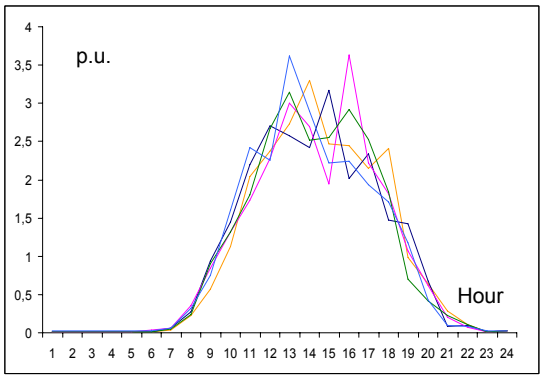

Figure 1-68 Simulated, Day 153-157, Jun

1.7.3.3 Evaluation of Final Annual Generation Curve

The final hour-to-hour annual generation curve can be obtained by multiplying the daily average values generated from stage 1 of algorithm with 24 times the value of corresponding hourly RHV generated from stage 2. Figure 1-69 to Figure 1-71 respectively represent the original hour-to-hour annual curve, the simulated curve without using RDA segmentation algorithm, and the simulated curve under RDA segmentation.

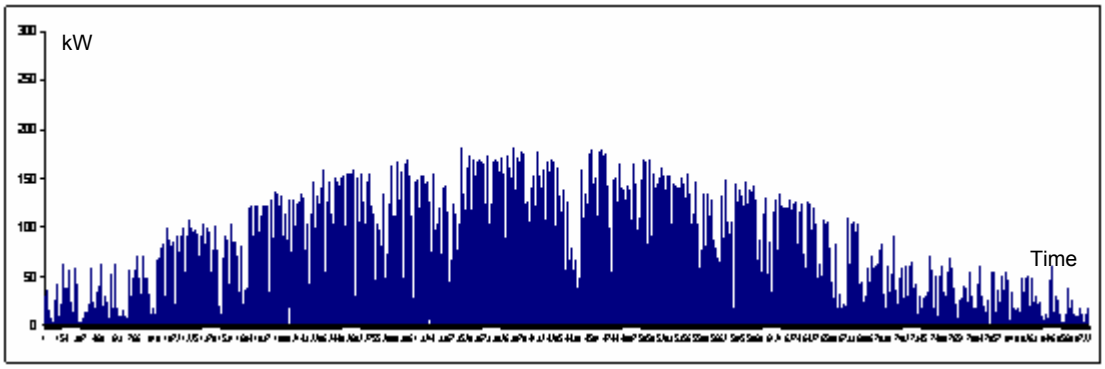

Figure 1-69 Original Annual PV Generation Curve

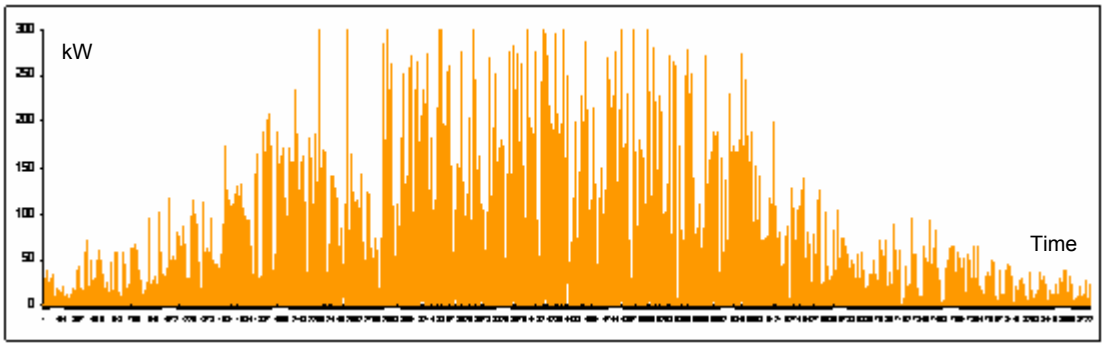

Figure 1-70 Simulated Annual Generation Curve without RDA Segmentation

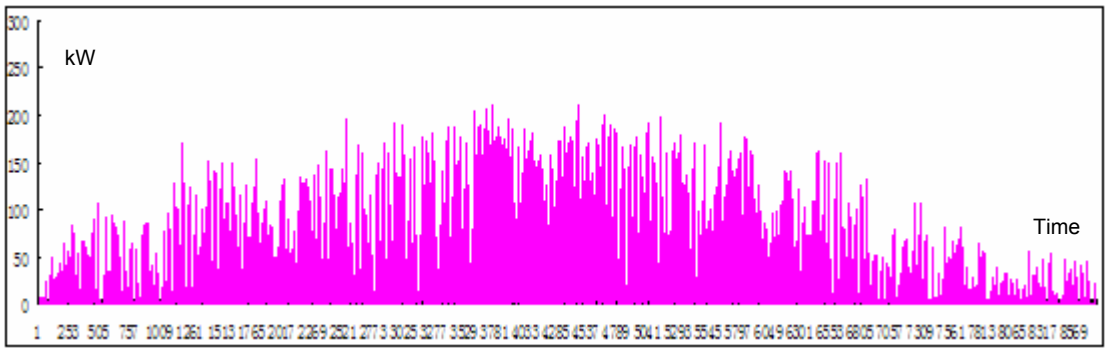

Figure 1-71 Simulated Annual Generation Curve under RDA Segmentation

It can be seen that RDA segmentation effectively reduces random overreaching of hourly energy output values beyond physical maximum rating of the PV module, which evidences a further advantage apart from solving the daily irradiation duration problem in section 2.7.3.2.

The continuous generation curves of original and simulated data (under RDA segmentation) are shown in Figure 1-72, it can be seen that deviations occur mainly at both ends of curves, while the other parts of data show relatively good matches.

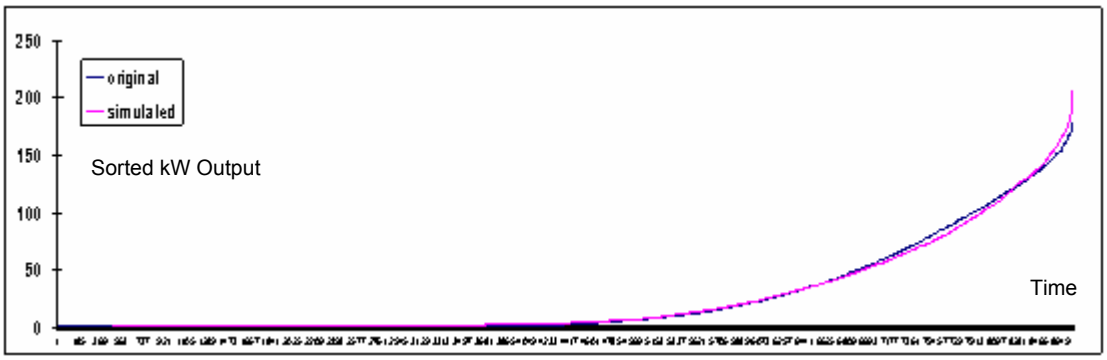

Figure 1-72 Original and Simulated Continuous Annual Generation Curves

Original and simulated data both show truncated behavior when evaluated as normal distribution variables, their PDF and CDF curves are shown in Figure 1-73 and Figure 1-74 as a reference.

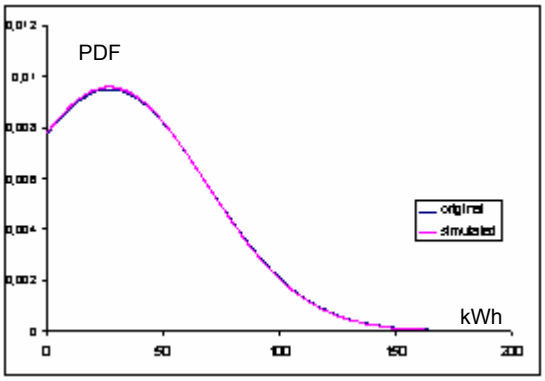

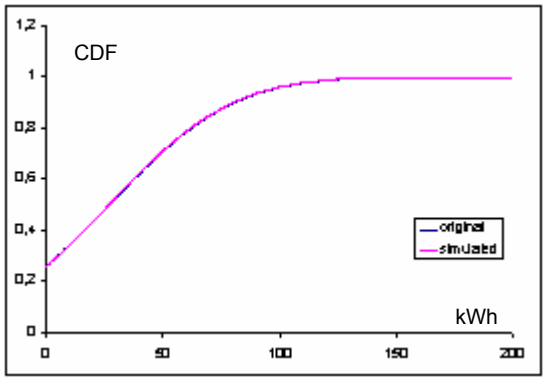

Figure 1-73 Original and Simulated, PDF Figure 1-74 Original and Simulated, CDF

1.7.4 Additional Notes

The currently used algorithm assumes all DEV values to be Beta distributed, which in effect lead to relatively large errors for some of the variables (such as DEV 17 shown in Figure 1-54, Figure 1-56, and Figure 1-58). Introduction of different distribution functions for different DEV data groups might lead to further improvements in this aspect.

1.8 Simulation Considerations for CHP Units

Simulation of CHP units can be basically performed with a similar approach as what was used for load curves with a special regard for seasonal variations—to be specific, CHP generation during summer time can be modeled as weekly variations with a strong day-night cycle property, while winter production behavior of CHP can be seen as a general stochastic process with no obvious schedules to follow. This can be seen Figure 1-75 and Figure 1-76, in which original and smoothed-out (SMO) generation curves of a sample week in summer and winter are respectively compared with error terms. Obviously, summer production exhibit a much higher degree of scheduled characteristics than winter production, which means separate simulation approaches should be used for these two periods.

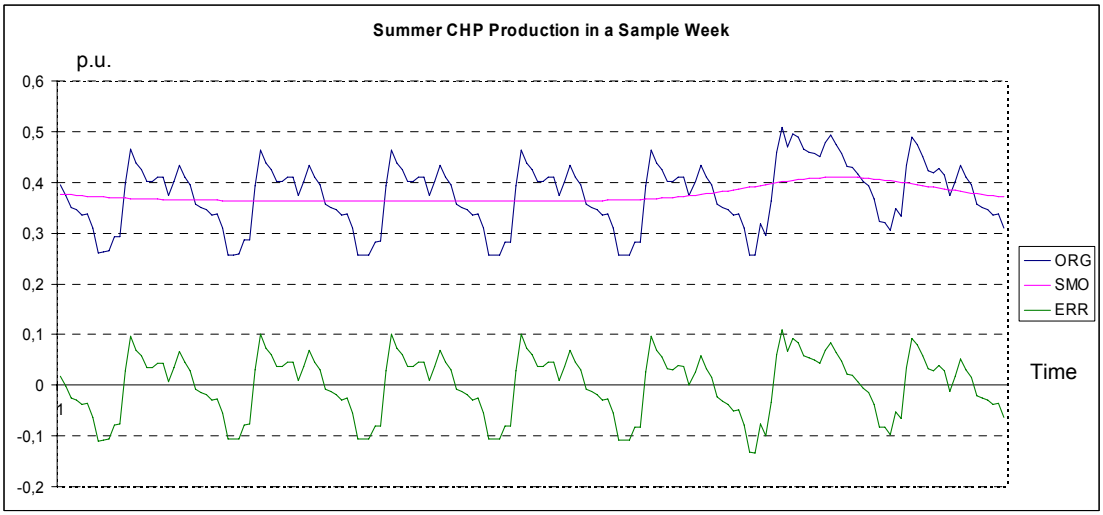

Figure 1-75 Summer CHP Production in a Sample Week

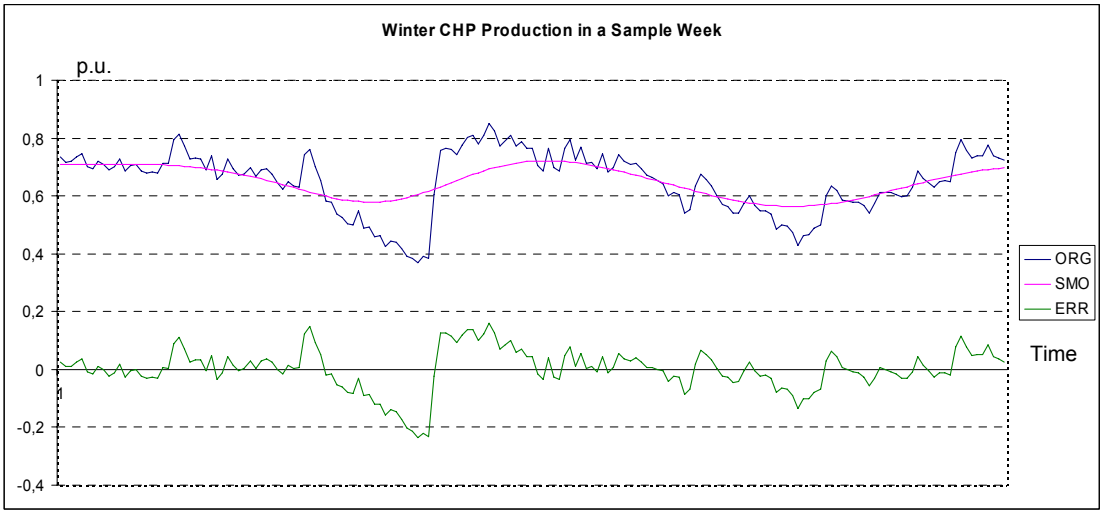

Figure 1-76 Winter CHP Production in a Sample Week

By applying scheduled simulation approach to summer time and normally-distributed variations to SMO-based winter curve, CHP generation can be modeled with an annual result shown in Figure 1-77.

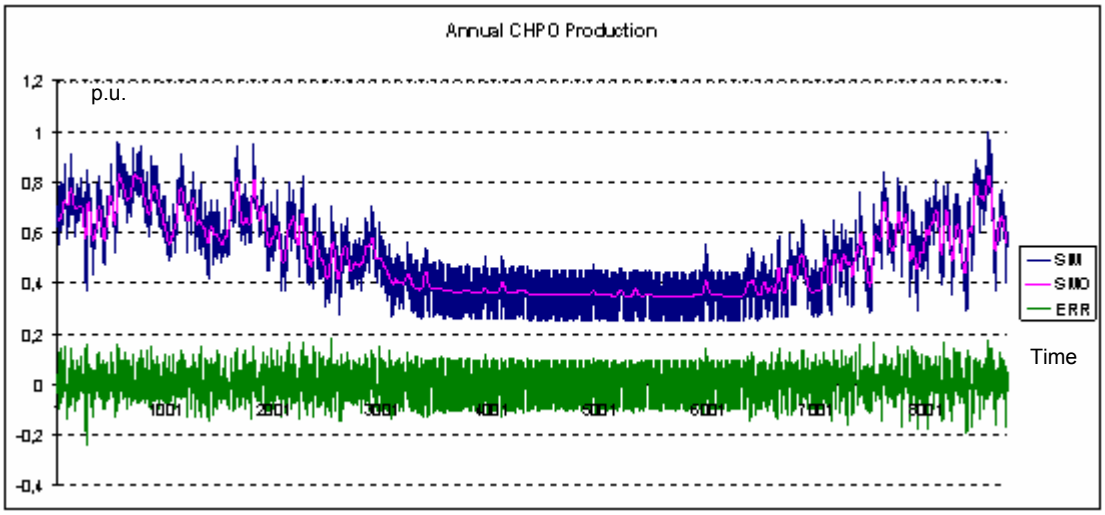

Figure 1-77 Annual CHP Production Curve with SMO and ERR versions.

CHP production curve in this section is modeled under a heat-driven principle. Electricity-driven CHP units could exhibit a very different behavior as they follow the demand patterns of different types of electric loads.

1.9 Summary

Stochastic modeling of yearly profiles of load, wind turbines, photovoltaic arrays, and CHP units are introduced in this chapter with their respective mathematical backgrounds. It was necessary to generate yearly profiles due to strong daily, weekly and seasonal variations in the independent profiles of load and different generation units each with different impact on the network. Applicable simulation technologies are explained for each of them, and optimum algorithms are selected through statistical and physical evaluations. Some of the simulation methods introduced in this chapter follow the currently most widely used procedures (such as Markov chain method), while some others introduce new conceptions (such as RHV decoupling and RDA segmentation) or modify existing practices to suit more demanding situations (such as adding truncated normal variations to load curves and CHP production profiles). Although the validity and accuracy of simulated data are limited somehow to the specific geographical or meteorological conditions of a certain period, the simulation result should be sufficiently reasonable to be used in most electrical distribution networks.

Chapter 2 Contemporary DER Technologies

Contemporary DER applications take on a wide variety of forms depending on the type of primary energy utilized for generation of electricity and the method of energy conversion used for each individual technology, thus categorization of DER can be done under both criteria. In the following sections, three major types of DER applications—wind turbine, photovoltaic (PV), and combined heat and power (CHP) are listed and examined, while several other geographically restricted alternatives are briefly introduced in the end.

2.1 Wind Turbine

Wind power, given its reasonable economic competitiveness and relatively good applicability, is currently viewed as one of the most important renewable energy sources worldwide. For regions with long coastal lines or continuous mountain ridges, wind power is especially favourable due to the plenitude of wind farm sites. Countries like Germany and Spain are investing heavily on wind farms, both on-shore and off-shore, to dramatically increase the share of wind-generated electricity in foreseeable future. Thus wind turbine, the core-technology of modern wind power utilization, is receiving rising attention and scrutiny.

A typical wind turbine of today appears to be a three-bladed, horizontal-axis fan mounted on a supporting tower of up to 120 meters in height. The blades are normally made of glass-reinforced plastics and have a maximum length of 50 meters [3]. The use of three (instead of another number) blades can minimize noise and wearing losses [7], and it offers a most mechanically stable and aesthetically comfortable configuration [3]. With the help of supporting tower, a wind turbine can harvest stronger wind at a higher altitude following the *1/7th power law*, which states that wind speed rises proportionally to the seventh root of altitude [7].

Modern wind turbines are normally rated from a few kilowatts up to 6MW [3], and they can be used both in single form or grouped at a wind farm. For large-scale on-shore or off-shore wind farms, interconnection to distribution grid is neither technically wise nor economically rewarding, thus such applications are not considered as DER and not included for discussion in this article.

The design of wind turbines has undergone several drastic changes since the late 1970's: rotor blades are made flexible in order to adopt a 'lift principle' quadrupling the efficiency of the traditionally used 'resistance principle' [3]; stall-controlled constant speed turbines are gradually outmatched by the more efficient pitch-controlled turbines with variable rotor speed [2]; and the improving performance of power electronic devices are making both synchronous and asynchronous generators more adapted to volatile wind conditions [6].

Currently the average investment cost of wind turbine installations amounts to 800-900 Euro/kW, and average generation cost amounts to 5-12 €ct/kWh [3]. The general trend of cost development over the last two decades has shown a gradual decrease, although the recent evolution into higher hub heights and larger rotor diameters has lead turbines to be equipped with a relatively smaller generator, which actually increases the investment cost per kW while reducing the generation cost per kWh [6].

In order to achieve the generally expected life duration of 20 to 30 years, a wind turbine also requires constant maintenance and repair, the average cost incurred from this aspect could consist up to 20-25% of total electricity price per kWh [6].

Despite the rapid growth of wind turbine installations, many problems persist and still need to be tackled—among them the most striking one is undoubtedly the difficulty of generation forecast due to the intermittent and random nature of wind power. Limited knowledge of wind variation pattern is recognized as directly useable, and probabilistic method is needed to model the wind power input to turbine [7].

Debates against wind turbines are also raised on issues of land occupation, noise emission, inadvertent killing of birds and bats, as well as possible aesthetic intrusions to some residents' eyes [3]. Solution to these problems requires careful selection of site and more understanding and support from the general public population.

2.2 Photovoltaic (PV)

Solar radiation reaches earth surface with maximum peak irradiation (or insolation) of 1,020 W/m^2 at the equator, but the irradiation value of a given region varies with time and climate, resulting in a long-term average of (250 ± 125) W/m^2 for relatively sunny locations [8]. Current utilization of this solar energy for purpose of generating electricity can be divided into two major categories: photovoltaic and solar thermal technologies. Since solar thermal applications are currently limited to certain regions, it will be discussed later in section 1.2.4, and this section will only address issues on photovoltaics.

A photovoltaic (PV) cell—or a solar cell—is a semiconductor (usually made of silicon) device that converts photons into electricity through the so-called *photovoltaic effect* [8]. Normally multiple PV cells are arranged as an array or module to raise output voltage and enhance load-carrying capacity. For purpose of grid connection, a DC\AC inverter is connected in sequence to the array to create a PV system that can be identified as a DER unit. Commercial PV modules generally have ratings ranging from 5W to 300W [6], and the installed power of a PV system can be as small as several watts or reach up to more than 10 MW [8].

Since the late 1980's, PV technology has evolved from the first-generation silicon wafer type into the second generation of thin-film silicon technology, this development has lead to a drastic cost reduction of PV modules. However, the efficiency of currently produced commercial thin-film PV cells is relatively low in comparison to the old silicon wafer type. Thus extensive research is currently conducted on the so-called third generation of PV cells using the advanced thin-film technology, which promises cost-effective PV modules with estimated efficiencies even higher than 30% [6].

PV systems have several significant advantages over other DER options:

1. Low maintenance requirement over around 30 years of service duration;
2. High scalability, as the efficiency of a PV system is independent of its size [2];
3. Easy site selection, normal roofs and facades will do [3];
4. Daily and seasonal peaks of generation profile coincides with load profile [9];
5. No noise or gas emission at all during operation;

However, the drawbacks of PV systems are also extremely obvious:

1. High investment cost;
2. Sensitivity to minor changes of irradiation level [8];
3. Relatively low efficiency (14%-16%) of energy conversion [8];
4. Zero power production during night time, discontinuous generation curve;
5. Inability to provide spinning reserve, poor dynamic characteristics [6];

After two decades of steady cost reduction, nowadays the price of PV-generated electricity generally ranges from 0.40 €/kWh to 0.75 €/kWh (Europe) or from 25 Cent/kWh to 35 Cent/kWh (North America), depending on size and type of PV system [3]. The installation cost of PV systems varies from application to application, but roughly falls into the range of 4-20 €/W [6]. Although these figures do not resemble an apparently economic solution, PV systems are actually financially favourable for a number of situations such as the electrification of islands and remote regions.

Noticeably PV systems have been receiving significant government subsidies in many countries—such as the '100,000-roof' project supported by the German federal government that led to a 400% increase of PV capacity in the country between 2000 and 2002 [3]. Therefore, the application of PV systems is expanding steadily to many established electricity markets, bringing about unprecedented changes for operation and net metering of local utilities.

2.3 Combined Heat and Power (CHP)

Combined Heat and Power (CHP), also called co-generation, refers to an energy conversion process, where electrical power and useful heat are generated in a single, integrated system [6]. By locating a CHP plant close to its heat consumers, energy savings of up to 40% can be achieved in comparison to separate generations of heat and electricity. The produced heat can serve for either district-heating or process-heating of industrial applications.

According to its primary purpose of operation, CHP can be divided into heat-controlled and power-controlled plants. The heat-controlled CHP aims to provide a stable supply of heating that follows varying load as close as possible, thus in terms of electricity production it can not be used for load dispatch. The power-controlled CHP, however, generates electricity as primary product and heat only as by-product; thus this type of CHP is identified as a fully controllable and dispatchable generation unit for electrical grids. Generally the heat-controlled CHP is considered to be the more efficient option and has a larger number of applications, and the heat-to-power ratio of CHP plants can vary from 1.8:1 to 6.9:1 depending on type and size of operation [2].

The size of a CHP plant falls into an extremely broad range: from several kilowatts to over 100 MW. It should be noted, however, that a CHP plant does not necessarily make a DER unit, since many large CHP plants—especially those constructed in early years—are not interconnected to distribution grids.

It can be seen that CHP actually corresponds neither to a single technology for electricity generation nor to a specific type of primary energy source—the concept of CHP therefore encompasses many different DER applications. If the type of fuel source is taken as a criterion of categorization, CHP plants can be found in the following fields:

1. Traditional fossil fuels, namely natural gas and petroleum;

2. Biomass—original source could be wood, grain, plants containing sugar or oil, organic leftovers, and bio-waste—used mainly in a combustion manner [3].
3. Biofuel: mainly referred to rapeseed oil and biodiesel extracted from natural products [3].
4. Landfill gas and CBM (Coal Bed Methane)
5. Geothermal or solar thermal energies (discussed later in 1.2.4)
6. Hydrogen (for fuel cells)

Another option is to differentiate CHP plants by the type of generation technology used for energy conversion; the following list shows the result in this perspective:

1. *Steam Turbine*:
   Normally driven by the steam generated by a boiler to produce electricity, and the low-pressure steam extracted from turbine can be used for further heating purpose; mostly used in heat-controlled CHP plants.

2. *Gas Turbine*:
   Also called combustion turbine, driven by high pressure, high temperature gas obtained from the combustion of gas or liquid fuel, exhaust gas after combustion can be used to produce steam for heating appliances.

3. *Microturbine*:
   A relatively newly-developed gas combustion technology evolved from the automobile turbo charger principle with turbine, compressor, and generator mounted on single or split shaft; usually with high speed and small size [2].

4. *Reciprocating Engine*:
   Requires fuel, air and ignition source to operate in reciprocating cycles to produce electricity and heat, can be operated on a wide variety of liquid and gaseous fuels.

5. *Stirling Engine*:
   Operated on a close thermodynamic cycle (Carnot cycle), requires external heat input to function with approximately 30% heat utilization for electricity generation, waste heat picked by cooling liquid can be used for CHP.

6. *Fuel Cell*:
   Fuel cells rely on electrochemical processes to convert the chemical energy of hydrogen into water and DC power without direct combustion of a fuel source, with heat as by-product of chemical reaction. Currently commercial fuel cells include AFC, PEMFC, PAFC, MCFC, and SOFC [3].

The production costs for heat and electricity in a CHP plant are influenced by a wide range of factors: plant size, site selection, technological substantiation, market conditions, and emission control etc. Typical investment cost for CHP plants ranges from 500-1500 USD/kW for those using conventional technologies to over 2000 USD/kW or even closing 5000 USD/kW for plants based on microturbines or fuel cells.

It should be noted that although CHP plants running on fossil fuels are generally not considered renewable energy resources, their relatively low emission rates and high energy efficiencies in comparison to traditional large thermal plants still make them environmentally favourable and thus they are not excluded from DER category as long as such advantages of them exist. As for CHP plants that utilizes bio-based or waste-based fuel sources, their CO_2 emissions can be viewed as environmentally

equivalent to the amount of CO_2 produced by the natural decomposition processes that would otherwise happen if the materials were not utilized by CHP plants; therefore such CHP plants should be defined as strictly renewable as wind- or solar-based applications.

2.4 Location-restricted Technologies

Some DER technologies have very strict requirements on geographical or climatic conditions in order to be utilized; among them the most frequently used are small hydro, geothermal, and solar thermal technologies. A brief introduction to these alternatives is given in this section.

2.4.1 Small Hydro

In comparison to large-scale hydro power plants with water storage capacity, small river power plants are usually interconnected to distribution grid due to limitations of their location and capacity. Both induction and synchronous generators are used in Small Hydro Plants (SHP), and the power rating of a SHP can range from several hundred kilowatts to 30MW [6].

Per-kW installation cost of a SHP generally decreases with rising size and head (difference of water level before and after a hydro turbine)—a SGP with a rating of more than 1MW and a head larger than 15 meters will cost around 1400 Euro/kW [6]. With low maintenance cost (0.8-1.9 Eurocent/kWh) and relatively long life duration (50 years), SHP provides a rather economic solution in comparison to other DER technologies, costing 10-25 Eurocent/kWh [3].

However, since water resources are not always available or suitable for exploitation, the applicability of hydro power plants is limited to regions with fast flowing river or distinctive altitude profiles. The utilization of hydro power in countries like Switzerland has almost reached its boundary, and very few chances for new SGP installations are available [2].

Finally, DG units making use of wave or tide energy can sometimes also be considered as a SHP, although they are actually designed in quite different fashions from each other.

2.4.2 Geothermal

Geothermal power technology utilizes the thermal energy stored within earth to generate electricity; two major types of geothermal usage are identified at the moment: high-temperature hydrothermal systems and Hot-Dry-Rock systems.

High-temperature hydrothermal systems are located in regions where the temperature of underground water reaches over 100 ^{o}C, thus making it possible to drive turbines and generators directly from this heated water. Iceland, for example, is extremely rich of hydrothermal resources and produces currently 17% of its electricity and 99% of its heat demand from geothermal CHP units [2].

The Hot-Dry-Rock (HDR) method, on the other hand, is applied when no natural hydrothermal resources are available. A HDR system normally consists of a deep-drilled hole several kilometres deep under earth and a hydraulic pumping cycle that

sends water deep down for heating and retrieves it back for co-generation purposes [3].

A geothermal system is normally rated from 3MW to 50MW (HDR systems are mostly above 20MW), and its generated electricity costs 7-15 Eurocent/kWh while generated heat costs 2-6 Eurocent/kWh [3].

2.4.3 Solar Thermal

Solar thermal power plants first collect the energy of solar irradiation in a thermal form, and then produce steam from it to generate electricity through a turbine or engine. Since solar thermal technologies mostly work only under direct sunlight, irradiation-rich regions—such as Mediterranean countries—are most suited for such applications [2].

Modern solar thermal technologies generally require a sun-tracking mirror to reflect solar irradiation to a focal point, where temperature is raised high enough to evaporate water or thermal oil to generate steams. Currently the following four solar thermal technologies are available in market or laboratory:

1. *Parabolic Trough Collectors*:
   Parabolic mirrors of up to 6 meters across and 100 meters long are used to achieve a concentrated temperature of 400 ^{o}C, thus steam from thermal oil is produced for a conventional steam turbine.

2. *Solar Tower Receivers*:
   A series of tracking mirrors (heliostats) mounted on top of tower collects solar radiation and delivers the thermal energy to an absorber with a temperature possibly higher than 1000 ^{o}C, a heat-transfer medium then delivers this power to a conventional power plant.

3. *Dish-Stirling Systems*:
   A parabolic sun-tracking mirror concentrates solar energy directly to a suspended absorber, which heats helium or air up to 900 ^{o}C to drive a Stirling engine. This configuration is especially suitable for DER applications.

4. Solar Chimney Power Plants:
   Air under a large collector roof is first heated by solar radiation, and then flows to a chimney located in middle of the collector roof, where it ascends and drives the wind turbine installed at the basement of the chimney [3].

The rating of a solar thermal power plant can range from 10kW in a small parabolic dish system to 200MW in tower or trough applications. And the price of generated electricity is 9-16 Eurocent/kWh for purely solar applications and 3-8 Eurocent/kWh for hybrid systems [3].

2.5 Storage Technologies for DER

For distribution networks penetrated with a large amount of DER units, traditional network devices and structures are likely to be found unable to handle all potential operating conditions caused by the stochastic nature of DER-supplied energy—especially when a large proportion of DER units adopt weather-dependent

technologies such as wind turbines and photovoltaic arrays. In the mean time, allocation of DER units to distribution stage of energy supply considerably challenges the original technical and economical designs of the distribution grid, which will likely bring about drastic changes on daily network operation. In order to meet these new requirements posed by DER penetration, various storage options have been proposed, for which some common concepts are briefly introduced in this section.

Storage devices for electrical energy have long been applied to transmission and distribution networks before the advent of DER technology, but they are traditionally used as balancing reservoirs or peak shaving devices. Introduction of DER units with intermittent generation characteristics (e.g. wind turbines and photovoltaic arrays) to electrical networks, however, poses a significantly higher demand on energy storage capacity and induces the development of a wide range of emerging technologies. Nowadays, storage options for DER complementation include battery, flywheel, pumped storage, supercapacitor, Superconducting Magnetic Energy Storage (SMES), Compressed Air Energy Storage (CAES), and hydrogen systems [2]. The first three options are currently most widely adopted in energy systems, thus brief introductions of them are given below:

2.5.1 Battery

With a long history of technical evolution, battery storage systems today have been basically commercialized for a majority of applications. For energy storage in utility-scale, lead-acid, nickel-cadmium, nickel-metal hydride, lithium-ion, lithium polymer, sodium sulphur, and red-ox (flow) batteries [2] [6] are normally available for selection. Depending on type of technology, cost for battery storage systems could range between 150 Euro/kWh and 750 Euro/kWh, while power and energy density respectively fall into ranges of 35 Wh/kg—120 Wh/kg and 50 W/kg—500 W/kg [10]. The typical size of battery installations generally amounts to several megawatts in terms of power rating [6], while charge-holding time could vary from seconds to hours [2]. Currently, the largest problem faced by battery storage systems is short service life caused by the limitation of charging cycles, as most battery applications can only achieve deep-charging between 500 and 2000 times [10].

2.5.2 Flywheel

Flywheels are energy storage devices that convert electrical energy into mechanical form during charging and perform a reversed process during discharge. A flywheel basically consists of an electric motor, a rotating mass, a generator, and a set of power electronic devices that are serially connected [2] [6]. During charging process, energy is passed on from motor to rotating mass; while during discharge, stored kinetic energy will be released from the rotating mass to the generator. Modern flywheel applications cost around 300 Euro/kWh—1000 Euro/kWh with available system sizes ranging between several kilowatts and several megawatts [6]. Depending on material used for the rotating mass, energy density of a flywheel unit could vary between 50 Wh/kg and 900 Wh/kg as rotating speed of the unit ranges between 10000 and 60000 revolutions per minute. Flywheels installations are generally placed underground or in sealed rooms due to safety considerations.

2.5.3 Pumped Storage

Pumped storage system is generally recognized as the most effective and economic option for long-term storage of a large amount of energy [2]. During daily operation,

pumped storage utilizes excess electric energy from grid to pump water from a lower reservoir to a higher one, and release the water in higher reservoir down to drive a hydraulic turbine during peak loading hours. General efficiency of pumped storage systems ranges between 70% and 80%, which can be seen as a relatively low performance when compared with other technology options; however, the relatively low costs of installation and operation for pumped storage systems practically reduce the influence of this disadvantage on investment decisions to a very large extent. Installed capacity of pumped storage systems falls into a range of 10MW—30000MW for most applications, which is comparably larger than any other technology options available today. However, like hydro power plant, pumped storage system is heavily dependent on geography and is not always applicable to a given region.

Chapter 3 Probability Distribution Functions

Probably distribution functions in this appendix are perceived as continuous in nature and defined by its characterizing parameters as well as its power density function (PDF) and cumulative distribution function (CDF). These two functions can be respectively described as:

(1) PDF (Probability Density Function) $f(x_0)$ determines the probability density of x_0 as a given value of x, which means the probability of x taking on a value in an infinitely small interval of $[x_0, x_0+dx]$ is $f(x_0)dx$, thus leading to:

$$f(x_0) = P(x_0 < x < x_0 + dx)/dx \qquad \textit{Equation B-3-1}$$

(2) CDF (Cumulative Distribution Function) $F(x_0)$, on the other hand, represents the probability of x taking on a value smaller than or equal to x_0, which means:

$$F(x_0) = P(x \le x_0) \qquad \textit{Equation B-3-2}$$

The correlation between PDF and CDF of a probability distribution can be then described as:

$$F(b) - F(a) = \int_a^b f(x)dx = P(a \le x \le b) \qquad \textit{Equation B-3-3}$$

In addition, the average values E and standard deviations V of all discussed distribution functions will be expressed in terms of characterizing parameters. For a given series $x_1, x_2, \ldots, x_n$ of random variable x, these two values can be expressed as:

$$E = \frac{\sum_{i=1}^{n} x_i}{n}, \qquad V = \sqrt{\frac{\sum_{i=1}^{n} (x_i - E(x))^2}{n-1}} \qquad \textit{Equation B-3-4}$$

Considering the fact that most applications in this report have to deal with data sets with unknown characterizing parameters, it is extremely useful to have direct or indirect formulas that could help obtain characterizing parameters from visible average values and standard deviations.

3.1 Uniform Distribution

Uniform distribution describes a random variable that has a constant probability over a given interval (*a, b*). Mathematically it can be expressed in the following form:

1. Characterizing Parameters: x ~ U (a, b)

a: lower limit (real)

b: upper limit (real)

2. PDF and CDF expressions and plots:

$$f(x)=\begin{cases}\dfrac{1}{b-a}, & a\le x\le b\\ 0, & x<a\cup x>b\end{cases}$$

Equation B-3-5

$$F(x)=\begin{cases}\dfrac{x-a}{b-a}, & a\le x<b\\ 0, & x<a\\ 1, & x\ge b\end{cases}$$

Equation B-3-6

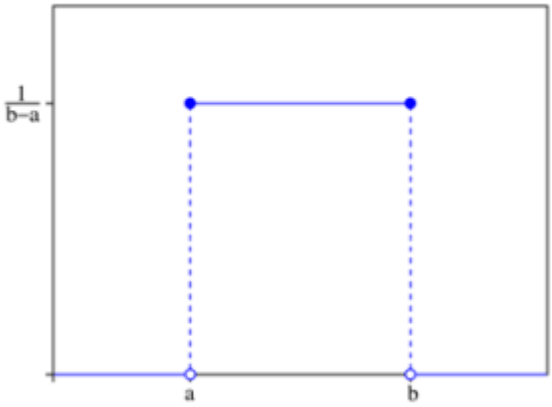

Figure B-1 PDF of Uniform Distribution

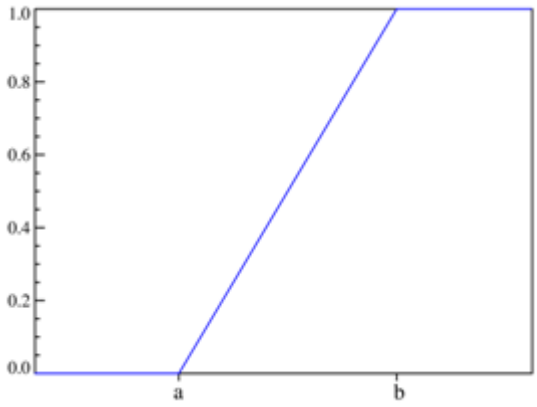

Figure B-2 CDF of Uniform Distribution

3. Average E and Standard Deviation V:

(1) Deduction of *E, V* from *a, b*

$$E=\frac{a+b}{2},\quad V=\frac{(b-a)}{2\sqrt{3}}$$

Equation B-3-7

(2) Deduction of *a, b* from *E, V*

$$a=E-\sqrt{3}V,\quad b=E+\sqrt{3}V$$

Equation B-3-8

4. Generation Algorithm

By strict definition, the closest approximation of 'truly' random variables can be found only in physical processes, but for simulation and other computational purposes the so-called 'pseudo random number generator' is normally used instead. Although the sequence of numbers generated by a pseudo random number generator is not truly 'random' in the sense that certain patterns will repeat over a relatively large sample size, by careful planning of confidence level the generated numbers can be sufficiently random to be used for the test application.

The most common form of computational pseudo random number generator gives out a floating point number *x* that is uniformly distributed over *(0, 1)*—namely, *x ~ U (0, 1)*. This programming command can be found under most application platforms and can be easily transplanted from one environment to another. Thus the random numbers generated from this *(0, 1)* interval can be used as a basis to be converted into random variables that fit into other probability distribution functions.

3.2 Normal (Gaussian) Distribution

Normal distribution, also called Gaussian distribution, is undoubtedly the most widely used distribution function. It can be described by a location parameter *μ*, and a scale parameter *σ*, which respectively equals the average and standard deviation in statistical sense.

1. Characterizing Parameters: x ~ N (μ, σ)

- *μ*: location parameter (real)
- *σ*: scale parameter (σ>0, real)

If *μ* = 0 and *σ* = 1, the distribution is defined as 'standard normal distribution'.

2. PDF and CDF expressions and plots:

$$f(x)=\frac{1}{\sigma\sqrt{2\pi}}\exp\left[-\frac{1}{2}\left(\frac{x-\mu}{\sigma}\right)^2\right]$$

Equation B-3-9

$$F(x)=\frac{1}{2}\left[1+erf\left(\frac{x-\mu}{\sqrt{2}\sigma}\right)\right]$$

Equation B-3-10

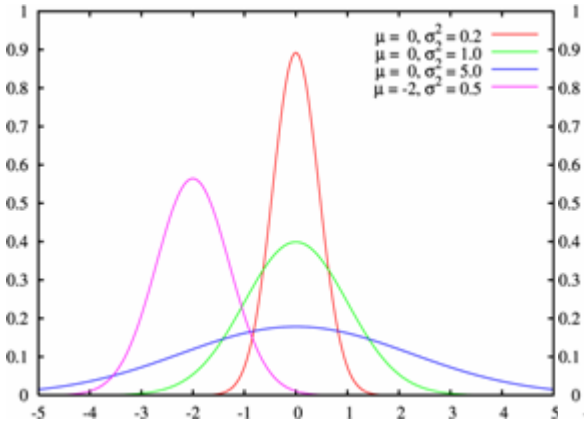

Figure B-3 PDF of Normal Distribution

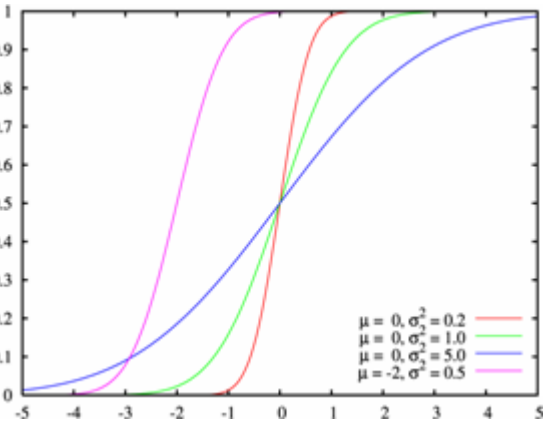

Figure B-4 CDF of Normal Distribution

3. Average E and Standard Deviation V:

(1) Deduction of *E, V* from *μ*, *σ*

$$E=\mu,\quad V=\sigma$$

Equation B-3-11

(2) Deduction of μ, σ from E, V

$$\mu = E, \quad \sigma = V$$ *Equation B-3-12*

4. Generation Algorithm

Box-Muller transformation method can be used to generate two groups of standard normally distributed random variables *x1, x2 ~ N (0, 1)* from two groups of uniformly distributed variables *u1, u2*. Two forms of this method are applicable:

(1) The Polar Form: *u1, u2 ~ U (0, 1)*

$$x1 = \sqrt{-2\ln(u1)}\cos(2\pi \cdot u2)$$
$$x2 = \sqrt{-2\ln(u1)}\sin(2\pi \cdot u2)$$ *Equation B-3-13*

(2) The Cartesian From: *u1, u2 ~ U (-1, 1)*

$$\text{For any u1, u2 satisfying R} = (\text{u1}^2 + u2^2) \in (0,1]:$$
$$x1 = u1 \cdot \sqrt{\frac{-2\ln R}{R}}$$ *Equation B-3-14*
$$x2 = u2 \cdot \sqrt{\frac{-2\ln R}{R}}$$

If the test normal distribution is characterized by *y ~ N (μ, σ)*, then it can be simply obtained from either *x1* or *x2* through the following conversion:

$$y = \sigma \cdot x1 + \mu \text{ or } y = \sigma \cdot x2 + \mu$$ *Equation B-3-15*

3.3 Truncated Standard Normal Distribution

The truncated standard normal (TSN) distribution is a modification to the standard from of normal distribution; it presumes that the data series can only be observed in a certain interval of [*a, b*]. Consequently, *a* is defined as 'left truncation point', while b is defined as 'right truncation point'.

1. Characterizing Parameters: t ~ TSN (a, b)

- *a*: left truncation point (real)
- *b*: right truncation point (real)

If *b* −> +∞, the distribution is a 'left-truncated standard normal distribution' (LTSN);
If *a* −> −∞, the distribution is a 'right-truncated standard normal distribution' (RTSN).

2. PDF and CDF expressions and plots:

$$f(x)=\begin{cases}\dfrac{f_{SN}(x)}{F_{SN}(\dfrac{b}{\sigma})-F_{SN}(\dfrac{a}{\sigma})}, & \mathrm{x}\in[a,b]\\ 0, & \mathrm{x}<\mathrm{a}\cup\mathrm{x}>\mathrm{b}\end{cases}$$

Equation B-3-16

$$F(x)=\begin{cases}\dfrac{\dfrac{1}{2}\left[1+erf\left(\dfrac{x}{\sqrt{2}}\right)\right]}{F_{SN}(\dfrac{b}{\sigma})-F_{SN}(\dfrac{a}{\sigma})}, & \mathrm{x}\in[a,b]\\ 0, & \mathrm{x}<\mathrm{a}\cup\mathrm{x}>\mathrm{b}\end{cases}$$

Equation B-3-17

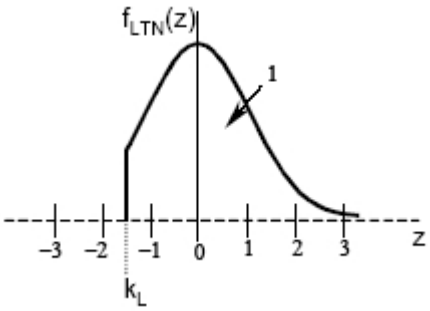

Figure B-5 PDF of a LTSN Distribution

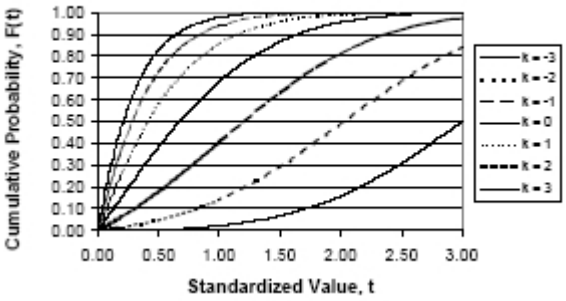

Figure B-6 CDF of a LTSN Distribution

3. Average E and Standard Deviation V:

(1) Deduction of *E, V* from *a*, *b*

$$E=-\frac{f_{SN}(b)-f_{SN}(a)}{F_{SN}(b)-F_{SN}(a)},\quad V=\sqrt{1-\frac{b\cdot f_{SN}(b)-a\cdot f_{SN}(a)}{F_{SN}(b)-F_{SN}(a)}-\left[\frac{f_{SN}(b)-f_{SN}(a)}{F_{SN}(b)-F_{SN}(a)}\right]^2}$$

Equation B-3-18

(2) Estimation of *a* from *E, V*

It can be seen that direct deduction of left or right truncation points from the values of mean and standard deviation is not feasible due to the complexity of equations. Thus in order to minimize calculation time, it is advisable to estimate the value of *a* or *b* from measured values of *E* and *V*.

For most applications in this report, translated left-truncated normal (TLTN) distribution, which assumes *b* −> +∞ and has been translated entirely into positive axis, is more frequently used to model non-negative physical values such as the active power of a load. Thus a variable *y* following TLTN distribution can be defined as the following variation of a LTSN distribution variable *x*:

$$If\ x \in LTSN\ (a), m \in R, y\ can\ be\ defined\ as:$$
$$y = m \cdot (x - a), \quad y \in TLTN\ (a, m)$$

$$The\ correlation\ between\ E\ and\ V\ values\ of\ x\ and\ y\ can\ be\ seen\ as:$$
$$E_y = m \cdot (E_x - a)$$
$$V_y = m \cdot V_x$$

Equation B-3-19

Thus the value of left truncation point *a* for variable *x* can be estimated from E_y and V_y using an approximation function *appx_f1* (detailed in Appendix):

$$a = appx\_f1\,(CoV) = appx\_f1\,(\frac{V_y}{E_y}), \quad CoV = \frac{V_y}{E_y}$$ *Equation B-3-20*

CoV stands for 'coefficient of variance'; it is the ratio of V_y over E_y, and notably independent from the value of *m*, which makes it ideal for estimation purposes.

4. Generation Algorithm

The currently adopted method to generate truncated normal distribution variables is to slightly modify the Box-Muller algorithm so that any generated value that falls out of the specified truncation range will be tossed out. This algorithm might, however, lead to an excessively large amount of wasted computations when heavy truncation is required—for example, when a standard normal distribution is left-truncated at 0, half of generated random variables will be tossed away; and when the truncation point moves to 1, 2, 3, and 4, respectively 84.13%, 97.73%, 99.87%, and 99.997% of generated random variables will be simply wasted over the course.

This phenomenon not only causes radical decrease of computational efficiency, but also leads to relatively large errors when the left-truncation point is taking a positive value. Consequently this truncation method is generally not recommended for truncation points beyond 2—namely, estimation efforts with CoV values greater than 0.906 might yield much less accurate results than expected.

3.5 Weibull Distribution

Weibull distribution features a continuous, nonnegative random variable distributed over [0, +∞]; it is defined by a nonnegative shape factor *k* and a nonnegative scale factor *λ*.

1. Characterizing Parameters: x ~ W (k, λ)

- *k*: shape parameter (*k*>0, real)
- *λ*: scale parameter (*λ* >0, real)

If *k* = 1, *x* will behave like an exponential distribution variable;
If *k* = 3, *x* will appear similar to a normal distribution variable.

2. PDF and CDF expressions and plots:

$$f(x)=\frac{k}{\lambda}\left(\frac{x}{\lambda}\right)^{k-1}\exp\left[-\left(\frac{x}{\lambda}\right)^{k}\right] \qquad F(x)=1-\exp\left[-\left(\frac{x}{\lambda}\right)^{k}\right]$$

Equation B-3-21 *Equation B-3-22*

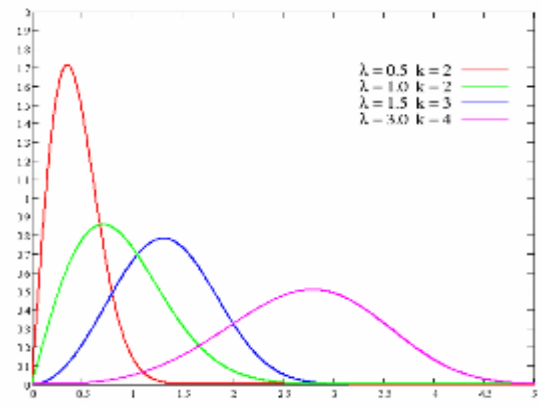

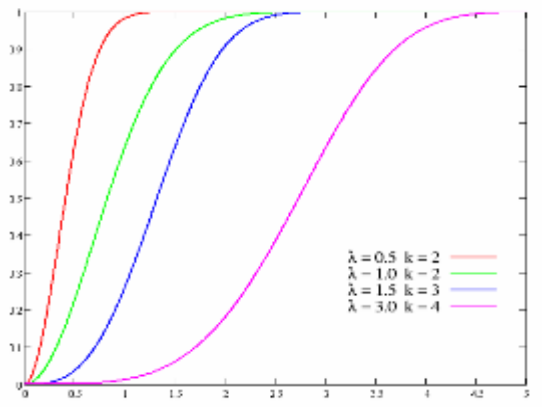

Figure B-7 PDF of Weibull Distribution Figure B-8 CDF of Weibull Distribution

3. Average E and Standard Deviation V:

(1) Deduction of *E, V* from *k*, *λ*

$$E=\lambda\cdot\Gamma(1+\frac{1}{k}),\quad V=\lambda\cdot\sqrt{\Gamma(1+\frac{2}{k})-\Gamma^{2}(1+\frac{1}{k})}$$

Equation B-3-23

(2) Estimation of *k*, *λ* from *E, V* (when 1 ≤ *k* ≤ 3)

Combination of the previous two formulas will lead to the following equations:

$$\begin{cases}E^{2}=\lambda^{2}\cdot\Gamma^{2}(1+\frac{1}{k})\\ E^{2}+V^{2}=\Gamma(1+\frac{2}{k})\end{cases}\Rightarrow\frac{\Gamma(1+\frac{2}{k})}{\Gamma^{2}(1+\frac{1}{k})}=1+(\frac{V}{E})^{2}=1+CoV^{2}$$

Equation B-3-24

Similar to the case of the TLTN distribution, direct calculation of the value of *k* from *CoV* might prove too complicated to be used effectively. Thus another approximation function *appx_f2* (detailed in Appendix) is adopted to speed up calculations:

$$k=appx\_f2\,(CoV)=appx\_f2\,(\frac{V}{E}),\quad if\ 1\le k\le 3$$

$$\Rightarrow\quad\lambda=\frac{E}{\Gamma(1+\frac{1}{k})}$$

Equation B-3-25

4. Generation Algorithm

A very simple generation algorithm is available by utilizing the CDF expression of Weibull distribution, which means a Weibull random variable *x ~ W (k, λ)* can be converted from a uniform random variable *u ~ U (0, 1)* through the following equation:

$$x = \lambda \cdot \left[-\ln(u)\right]^{\frac{1}{k}} \qquad \textit{Equation B-3-26}$$

3.6 Gamma Distribution

Like Weibull distribution, a Gamma distribution variable is also distributed over [0, +∞]; and it is also defined by a nonnegative shape factor *k* and a nonnegative scale factor *θ*.

1. Characterizing Parameters: x ~ G (k, θ)

- *k*: shape parameter (*k*>0, real)
- *θ*: scale parameter (*θ* >0, real)

If *k* is an integer, the distribution is also named as Erlang Distribution.

2. PDF and CDF expressions and plots:

$$f(x) = (x)^{k-1} \frac{\exp(-\frac{x}{\theta})}{\theta^k \cdot \Gamma(k)} \qquad \textit{Equation B-3-27}$$

$$F(x) = \frac{\gamma(k, \frac{x}{\theta})}{\Gamma(k)} \qquad \textit{Equation B-3-28}$$

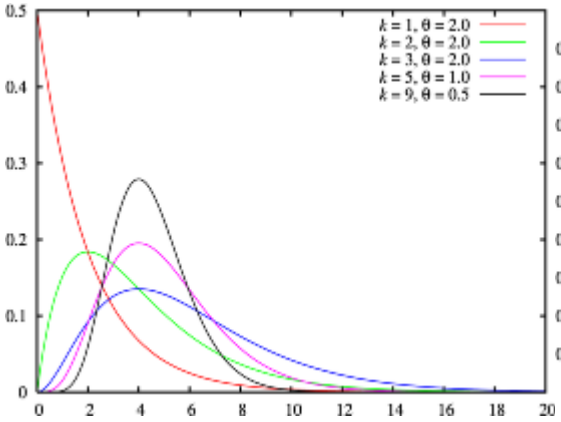

Figure B-9 PDF of Gamma Distribution

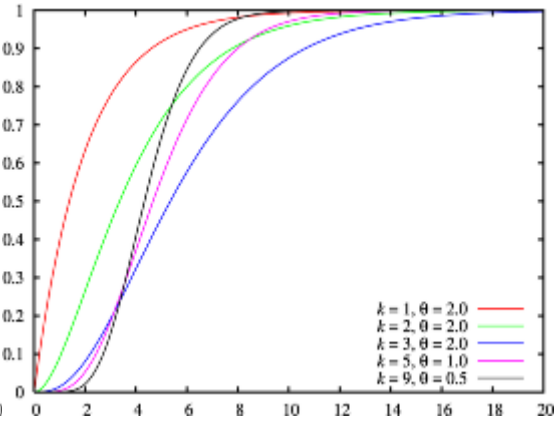

Figure B-10 CDF of Gamma Distribution

3. Average E and Standard Deviation V:

(1) Deduction of *E, V* from *k, θ*

$$E = k \cdot \theta, \quad V = \sqrt{k} \cdot \theta \qquad \textit{Equation B-3-29}$$

(2) Deduction of *k, θ* from *E, V*

$$k = \left(\frac{E}{V}\right)^2, \quad \theta = \frac{V^2}{E} \qquad \textit{Equation B-3-30}$$

4. Generation Algorithm

Two basic properties of Gamma distribution are utilized for generation of random Gamma variables—first, it is generally known that:

$$If \quad x \in G(k,1), \quad \Rightarrow \quad (x \cdot \theta) \in G(k,\theta) \qquad \textit{Equation B-3-31}$$

Secondly, if a parameter *k* consists of both integral part *Int_k* and decimal part *Dec_k*, then it is known that:

$$Let \quad \begin{cases} u \in G(Int\_k, \theta), \\ v \in G(Dec\_k, \theta), \\ x = u + v \end{cases} \qquad \textit{Equation B-3-32}$$

$$\Rightarrow \quad x \in G(k,\theta)$$

Therefore the algorithm for generating a series of random variables $x_1, x_2, \ldots, x_N$ that satisfies $x \sim G(k, \theta)$ is shown in Fig B-11.

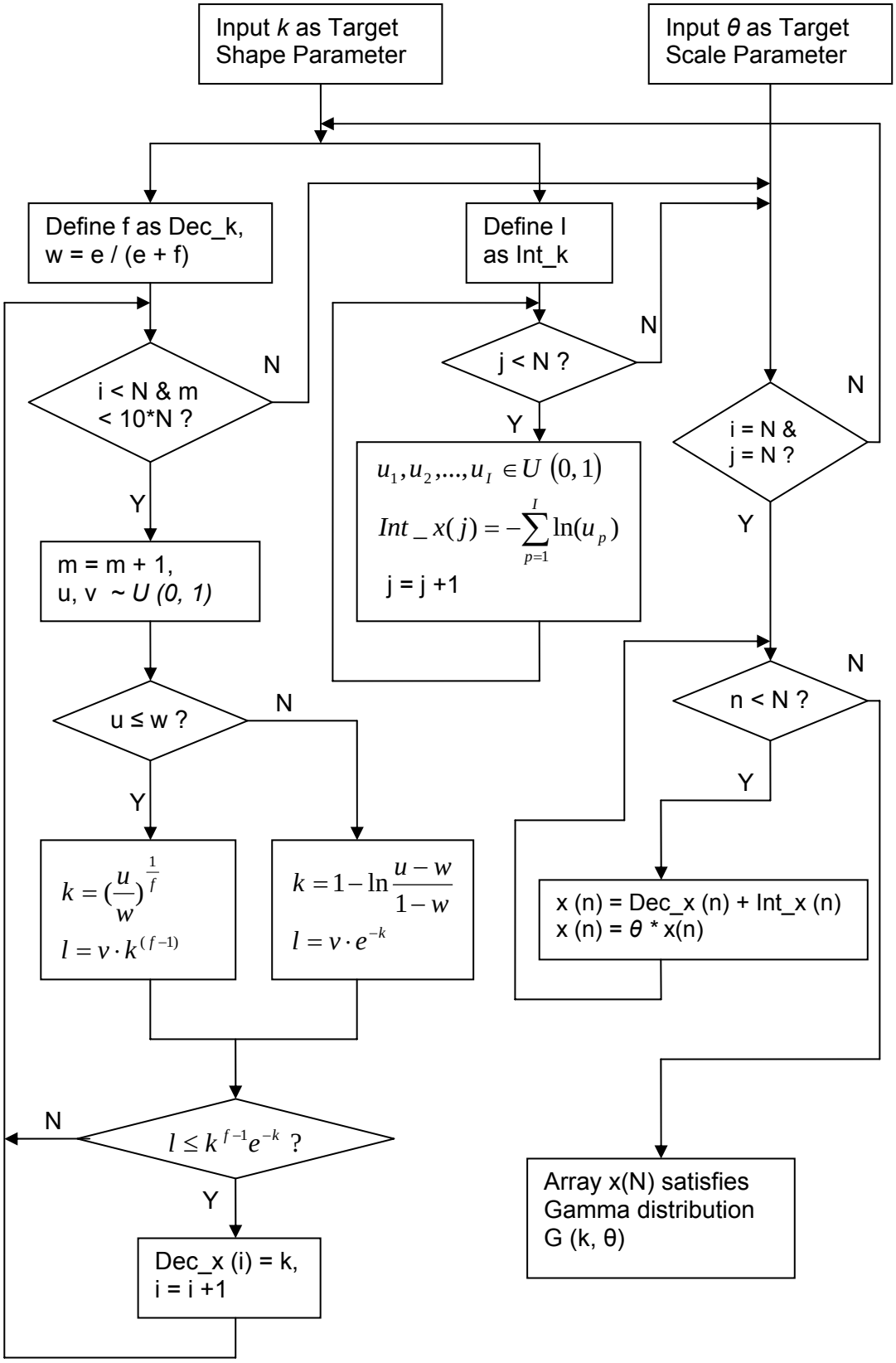

Figure B-11 Gamma Distribution Variable Generation Process

3.7 Beta Distribution

Gamma distribution variables are distributed over an interval of [0, 1]; and Gamma distribution is characterized by two nonnegative shape factors: *α* and *β*.

1. Characterizing Parameters: x ~ B (α, β)

- *α*: shape parameter (*α*>0, real)
- *β*: shape parameter (*β* >0, real)

If *α* = 1 and *β* = 1, Beta distribution will become a standard uniform distribution.

2. PDF and CDF expressions and plots:

$$f(x)=\frac{x^{\alpha-1}(1-x)^{\beta-1}}{B(\alpha,\beta)} \qquad F(x)=\frac{B_x(\alpha,\beta)}{B(\alpha,\beta)}=I(\alpha,\beta)$$

Equation B-3-33 *Equation B-3-34*

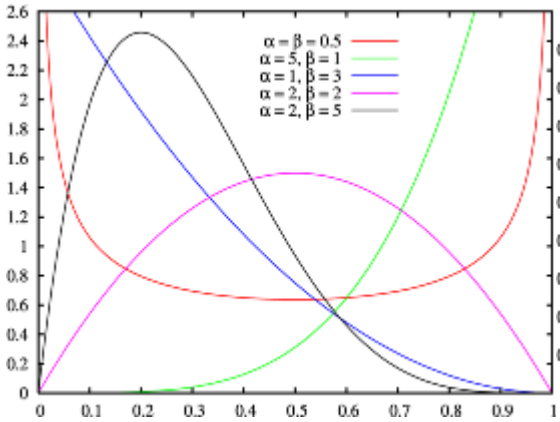

Figure B-12 PDF of Beta Distribution

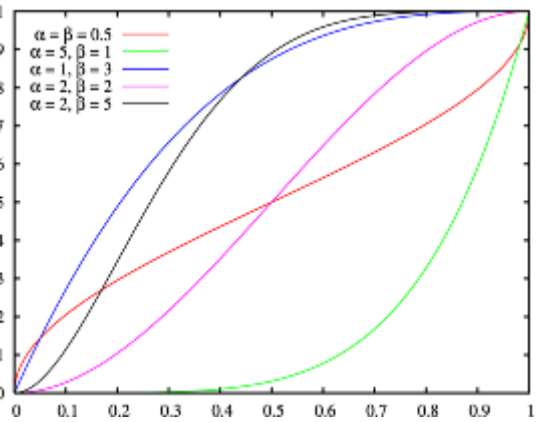

Figure B-13 CDF of Beta Distribution

3. Average E and Standard Deviation V:

(1) Deduction of *E, V* from *α, β*

$$E=\frac{\alpha}{\alpha+\beta},\qquad V=\frac{\alpha\beta}{(\alpha+\beta)^2(\alpha+\beta+1)}$$

Equation B-3-35

(2) Deduction of *α, β* from *E, V*

$$\alpha=E\left(\frac{E(1-E)}{V^2}-1\right),\qquad \beta=(1-E)\left(\frac{E(1-E)}{V^2}-1\right)$$

Equation B-3-36

4. Generation Algorithm

In order to get a Beta distribution variable *x ~ B (α, β)*, two independent Gamma distribution variables *g1 ~ G (α, θ), g2 ~ G (β, θ)* can be used as a basis for conversion:

$$x = \frac{g1}{g1 + g2}$$ *Equation B-3-37*

References

[1] Thomas Ackermann, Gören Andersson, Lennart Söder, *Distributed Generation: a Definition*, Electric Power Systems Research 57 (2001) 154-204

[2] Gaudenz Keoppel, *Distributed Generation—Literature Review and Outline of the Swiss Situation*, EEH ETH Internal Report, November 2003

[3] W. Dürrschmidt, G. Zimmermann, *Renewable Energies—Innovation for the Future*, (German) Federal Ministry for the Environment, Nature Reservation and Nuclear Safety (BMU) Brochure, April 2006

[4] Robert Priddle, *Distributed Generation in Liberalised Electricity Market*, Organisation for Economic Co-operation and Development (OECD) / International Energy Agency (IEA) 2002 ISBN 92-64-19802-4

[5] Ward Jewell, *Evaluation of Distributed Energy Storage and Generation*, Power Systems Engineering Research Centre (PSERC), Final Project Report, July 2004

[6] A. Fernández, I. Cobelo, *Library of Models, EU-DEEP Internal Report*, WP2, Sub-task 2.2.1.0.2, June 2005

[7] Gary L. Johnson, *Wind Energy Systems*, December 2001

[8] European Commision, *Energy for the Future: Renewable Sources of Energy, White Paper for a Community Strategy and Action Plan*, November 1997

[9] Karl M. Maribu, *Modeling the Economics and Market Adoption of Distributed Power Generation*, Department of Electrical Power Engineering, Norwegian University of Science and Technology, Doctoral Thesis, June 2006

[10] Jürgen Garche, *Elektrochemische Energiespeicher: Stand, Probleme, Perspektiven*, Energiewirtschaftliche Tagesfragen, 10-2006, pp. 61—66.

[11] B. Blažic, U. Kerin, I.Papic, *Techniques for DER Integration and Active Networks Management Phase I*, SOLID-DER Work Package II, Deliverable number D 2.1, Task 2.2, October 2006

[12] Sébastien Grenard, Danny Pudjianto, Coran Strbac, *Benifits of Active Management of Distribution Network in UK*, CIRED 18th International Conference on Electricity Distribution, Turin 6-9 June 2005

[13] G. Celli, E. Ghiani, S. Mocci, F. Pilo, *Distributed Generation and Intentional Islanding: Effects on Reliability in Active Networks*, CIRED 18th International Conference on Electricity Distribution, Turin 6-9 June 2005

[14] Constantin, Surdu, Leaonardo-Geo Manescu, et al, *On the Interest of the Virtual Power Plant Concept in the Distribution Networks*, CIGRE 2006

[15] Christine Schwaegerl, Alex Baitch, *Demand Side Management and Response with Distributed Energy Resources—Chances and First Experience*, CIGRE 2006

[16] BORKOWSKA, B., *Probabilistic Load Flow*, IEEE Trans., 1974, PAS-93, (3). pp. 752-759

[17] Chun-Lien Su, *Distribution Probabilistic Load Flow Solution Considering Network Reconfiguration and Voltage Control Devices*, 15th PSCC, Liege, 22-26 August 2005, Session 10, Paper 3, Page 1

[18] G.Papaefthymiou, P.H.Schavemaker, L. van der Sluis et al, *Integration of Stochastic Generation in Power Systems*, 15th PSCC, Liege, 22-26 August 2005, Session 42, Paper 1, Page 1

[19] N.D. Hatziargyriou, T.S. Karakatsanis, M. Papadopoulos, *Probabilistic Load Flow in Distribution Systems Containing Dispersed Wind Power Generation*, IEEE Transactions on Power Systems, Vol. 8, No. 1, February 1993

[20] Zechun Hu, Xifan Wang, *A Probabilistic Load Flow Method Considering Branch Outages*, IEEE Transactions on Power Systems, Vol. 21, No. 2, May 2006, pp. 507-514

[21] Leite da Silva. A.M., Arienti, V.L., Allan, R.N., *Probabilistic Load Flow Considering Dependence Between Input Nodal Powers*, IEEE Trans., 1984, PAS-103, (6), pp. 1524-1530

[22] Micheal C. Caramanis, Richard D. Tabors et al, *The Introduction of Non-Dispatchable Technologies as Decision Variables in Long-term Generation Expansion Models*, IEEE Transactions on Power Apparatus and System, Vol. PAS-101, No.8, August 1982, pp. 2658-2667

[23] Jeremy A. Bloom, *Probabilistic Production Costing with Dependent Generating Sources*, IEEE Transactions on Power Apparatus and System, Vol. PAS-104, No.8, August 1985, pp. 2064-2071

[24] Pei Zhang, Stephen T. Lee, *Probabilistic Load Flow Computation Using the Method of Combined Cumulants and Gram-Charlier Expansion*, IEEE Transactions on Power Systems, Vol. 19, No. 1, February 2004, pp. 676-682

[25] Charles M. Grinstead and J. Laurie Snell, *Introduction to Probability*, American Mathematical Society, Swarthmore College and Dartmouth College;

[26] Arvid C. Johnson and Nick T. Thomopoulos, *Characteristics and Tables of the Left-Truncated Normal Distribution*, Dominican University and Illinois Institute of Technology;

[27] Brian A'Hearn and John Komlos, *Improvements in Maximum Likelihood Estimators of Truncated Normal Samples with Prior Knowledge of σ*, Ludwig-Maximilians-Universität München, July 2003

[28] André Berchtold and Adrian Raftery, *The Mixture Transition Distribution (MTD) Model for Higher-Order Markov Chains and Non-Gaussian Time Series*, University of Washington, August 1999;

[29] Jukka V. Paatero and Peter D. Lund, *A Model for Generating Household Electricity Load Profiles*, International Journal of Energy Research Vol. 30:5;

[30] Anssi Seppälä, *Load Research and Load Estimation in Electricity Distribution*, Doctoral Dissertation, VTT Energy Nov 1996

[31] Suleiman Abu-Sharkh, *Microgrids: Distributed On-site Generation*, Tyndall Centre for Climate Change Research, March 2005

[32] John Geweke, *Efficient Simulation from the Multivariate Normal and Student-t Distributions Subject to Linear Constraints and the Evaluation of Constraint Probabilities*, Computing Science and Statistics: the Twenty-Third Symposium on the Interface, Seattle, April 22-24, 1991

[33] George Marsaglia, Wai Wan Tsang, *A Simple Method for Generating Gamma Variables*, ACM Transactions on Mathematical Software, Vol. 26, No. 3, September 2000, Pages 363-372

[34] S.A. Herman, *Probabilistic Cost Model for Analysis of Offshore Wind Energy Costs and Potential*, ECN May 2002

[35] Sami Repo, Hannu Laaksonen and Pertti Järventausta, *New Methods and Requirements for Planning of Medium Voltage Network Due to Distributed Generation*, Tampere University of Technology, Finland

[36] H. NFAOUI, H. ESSIARAB and A. SAYIGH, *A Stochastic Markov Chain Model for Simulating Wind Speed Time Series at Tangiers*, Morocco, FIER 2002;

[37] Elizabeth Stoltzfus*, Stochastic Approaches to Modeling Alternative Energy Systems*, University of California, Berkeley

[38] Francesco GROPPI, *Grid-Connected Photovoltaic Power Systems: Power Value and Capacity Value of PV Systems*, 2000

[39] P. Denholm and R. Margolis, *Very Large-Scale Deployment of Grid-Connected Solar Photovoltaics in the United States: Challenges and Opportunities*, Solar 2006 Denver, Colorado July 2006

[40] Charlotte Sprndergren, Hans F. Raxn, *A Method to Perform Probabilistic Production Simulation Involving Combined Heat and Power Units*, IEEE Transactions on Power Systems, Vol. 11, No. 2, May 1996

[41] Giancarlo Ferrari-Trecate, Eduardo Gallestey et al, *Modeling and Control of Co-generation Power Plants: A Hybrid System Approach*, ETH - Eidgenössische Technische Hochschule Zürich, Jan 2002

[42] Erik Dotzauer, *Algorithms for Short-Term Production-Planning of Cogeneration Plants, Linköping Studies in Science and Technology*, Thesis No. 644, 1997

[43] C. Randy Hudson, *ORNL CHP Capacity Optimizer User's Manual*, Oak Ridge National Laboratory 2005

[44] Univ.-Prof. Dr.-Ing. Hans Jürgen Haubrich: *Elektrische Energieversorgungs-systeme*. Aachen: Institut für Elektrische Anlagen und Energiewirtschaft – Forschungsgesellschaft Energie an der RWTH Aachen 2001

[45] *SINCAL™* Help File on Load Flow 2006

[46] N.D.Hatziargyriou, T.S. Karakatsanis, *Distribution System Voltage and Reactive Power Control Based on Probabilistic Load Flow Analysis*, IEEE Proc.—Gener. Transm. Distrib. Vol. 144, No. 4, July 1997

[47] Carol Cheng and Dariush Shirmohammadi, *A three-phase power flow method for real-time distribution system analysis*, IEEE Transactions on Power Systems, Vol. 10, No. 2, pp. 671-679, May 1995

[48] Antonino Augugliaro, Luigi Dusonchet, *A New Model of PV Nodes in Distribution Networks Backward/Forward Analysis*, Dipartimento di Ingegneria Elettrica Università di Palermo, Italy

[49] Chen G.J., Li K.K., Chung T.S., Tang G.Q., *An Efficient Two-stage Load Flow Method for Meshed Distribution Networks*, IEEE International Conference on Advances in Power System Control, Operation and Management (APSCOM), 2000.

[50] Ray D. Zimmerman, Hsiao-Dong Chiang, *Fast Decoupled Power Flow for Unbalanced Radial Distribution Systems*, School of Electrical Engineering, Cornell University, USA